POLITECNICO DI TORINO

Corso di Laurea Magistrale in Ingegneria Civile

Tesi di Laurea Magistrale

Numerical analysis of the behaviour of gas pipes buried into sand

Relatori:

Politecnico di Torino

Prof. Daniele Costanzo

Université Grenoble Alpes

Dott. Christophe Dano

Prof. Fabrice Emeriault

Dott.ssa Orianne Jenck

Ing. Antoine Mertz

Candidata:

Anna Berardo

Anno Accademico 2020/2021

March 2021

Abstract

In daily life, society needs to obtain usable energy at the lowest possible cost. Natural gas is one of the main energy sources with oil and coal. Natural gas is a gas mixture composed almost entirely of methane to which very small amounts of other gases are added, and is used daily in many households. It has many uses and this type of energy source has many advantages. One of these advantages is transportation, because gas is easily transported through underground pipelines and can be used for various purposes.

This research project is dedicated to understanding the impact of surface loads on underground pipes buried into sand, using finite element models. These models study the issues through several aspects: first, consider a complex soil model to simulate soil/structure interactions that are more faithful to the real sand behavior.

Three main analyses were performed. The first analysis consists in modelling the problem on a small and large scale in order to obtain, once normalised, comparable results. The second type of analysis involves studying the behavior of small-scale models during loading and unloading cycles to highlight the effects of nonlinear soil behavior. Ultimately, the influence of pipe thickness on the overall behavior of the soil/pipe structure was studied.

Performing this numerical analysis is to support future experimental activities. The experimental campaign will include small-scale laboratory tests in a sand tank equipped with strain gauges and miniaturised stress transducers.

Table of contents

List of figures

List of tables

1. Introduction

In the distribution of essential services such as gas and water, buried pipes play a key role. They represent almost the entire distribution network, from extraction to the end user, allowing transport over long distances. Buried pipes are advantageous because they allow the transport of raw materials at low cost. Many types of pipes are used in practice, with a wide range of materials, burial depth, or diameters, the choice being done accordingly to the type of network (gas transportation, crude oil, sewers…).

This kind of network obviously has to interact with other structures, such as roads, railways or embankments creating additional loading on the pipe. It is to be noted that in many cases, the surface loading is applied after the construction of the pipeline (sometime decades), implying that the original design of the pipe didn't take into account this secondary loading (the first type loading being the inner pressure of the transported gas, up to 6.7MPa). Protecting the pipe from the effect of surface loading (by using reinforced concrete slabs) is an expensive practice, and should therefore be avoided when possible; creating a need for more advanced tools of design and verifications (some currently exists, but with strong assumptions, such as linear elastic behaviour of the soil with Boussinesq distribution of the load).

In France, natural gas is used as a source of energy for heat and electricity production, and the transportation is mainly done (~70%) using buried steel pipes with a network of total cumulated length of more than 32.000km, capable of transporting more than 600TWh a year. (GRTgaz, 2018)

In Italy almost 70% of the electricity produced comes from thermoelectric power plants, which use methane as fuel. Natural gas is also the only source of heat for most Italian homes (Voronin, 2016).

This research project is part of a PhD project funded by GRTgaz. GRTgaz owns and operates the longest high-pressure natural gas transmission network in Europe.

It is involved in the management of networks in Germany. In Europe and worldwide, it provides assessment and consulting services in the field of gas transmission. GRTgaz performs three main roles:

- It transports natural gas on behalf of its customers, ensuring optimum safety, cost and reliability.

- It delivers gas to recipients directly connected to the transmission network: major industrial users, power plants that use natural gas to produce electricity, public distribution networks and neighbouring transmission networks.
- It expands its transmission capacity in order to meet market demand and enhance security of supply for France and Europe. (Source: http://www.grtgaz.com/)

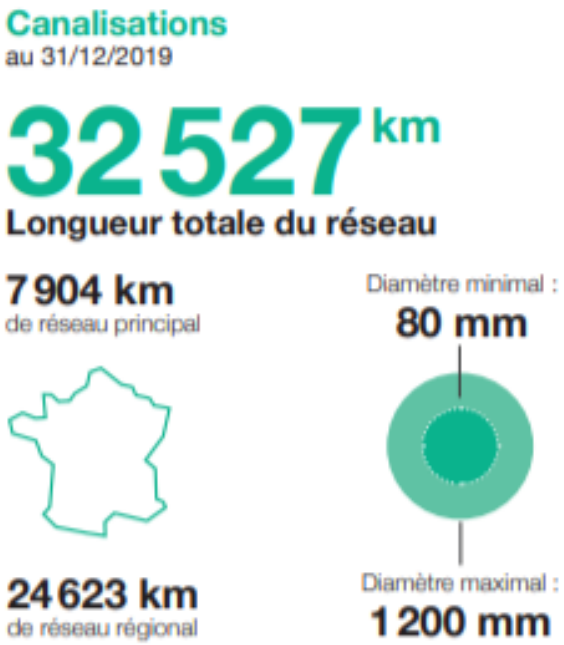

Figure 1.1: Some data about GRTgaz network (Essentiel GRTgaz, 2020)

As said before there are some tools for design and verifications of the network. GRTgaz uses a software called RAMCES PLEIADE. This software is both a tool for calculating the stresses generated on fluid transmission pipelines by different external stresses, a decision support tool for work in the vicinity of buried transmission pipelines and a tool to assist in the design of buried transmission pipelines. It thus provides decision support for the operator by enabling him to determine whether or not a load is acceptable for a pipeline. (RICE GRTgaz, 2018) This software, as many others, has some limitation (linear elastic soil model, etc) so the idea behind this research project is to provide data from numerical analysis in order to better understand the soil/pipe interactions under surface loading and improve the existing engineering practices.

This work was carried out at the 3SR laboratory of the Université Grenoble Alpes (France) in collaboration with GRTgaz.

2. Bibliography research

2.1. Literature

The problem of traffic or operational loads on buried pipes has been studied in different configurations. One of the major problems that can be encountered with buried pipes is that the soil pressure above pipes is influenced by the vertical settlement ratio between the pipe and the adjacent soil. If the pipe is a rigid element, and its stiffness is higher than the stiffness of the soil, a differential settlement would be created, since the lateral soil would be more compressible. The generation of this settlement leads to a downward shear force acting along the sides of the soil and so the load on the pipe becomes larger than the weight of the soil prism (negative arching effect). This concept was first faced by Marston and Anderson (1913). They proposed the Marston's earth pressure theory to calculate the vertical earth load on buried rigid pipes and culverts (Figure 2.1). However, this closed-form solution doesn't consider the effect of the subsidence of the soil on both sides of culvert, and the variation law of earth pressure coefficient is different from the real one (Marston, 1930).

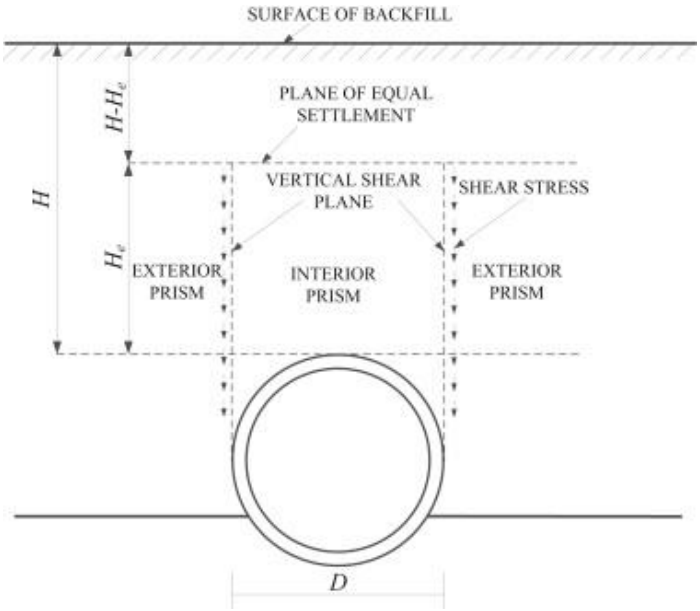

Figure 2.1: Marston's model (Tian et al.2015)

Also Terzaghi (1943) investigated the arching effect with the trapdoor experiment and he proposed a theoretical approach for aching problems in sand under plane strain conditions. Terzaghi applied this theory to tunnels and his approach is still widely used also in the case of pipelines, even if it has some

limitations. First, the vertical stresses are assumed to be uniform and secondly the trapdoor is assumed rigid.

After these initial studies, many researchers, like Spangler (1941), Heog (1968), Adams (1989) and others, improved and developed formulae for the vertical earth load on rigid pipes.

Another important feature investigated is the burial depth of the pipe, in order to analyse the effect that the depth, and so the soil, is the behaviour of the pipe. Moore (1987) studied the influence of the depth of burial, but in this case, he especially considered the critical hoop forces into the pipe. Different analytical solutions were proposed to investigate the elastic stability of shallow buried tubes: subgrade reaction theory, elastic continuum theory and finite element solution. A comparison between the methods was made and then a parametric study was performed. An important conclusion of this study is that a shallow burial depth influences the stability of the tube, in fact it will increase the risk of failure by buckling in the pipe. In this study the ratio between the stiffness of the pipe and the stiffness of the soil goes from 10^{-5} to 10^{2}. Considering the catalogue from GRTgaz, the cases that will be illustrated in this work have a stiffness ratio around 10^{-2}, so they fell in the ratio considered by Moore.

Fernando and Carter (1998) investigated the problem of buried pipes under surface patch loading. This type of surcharge is used to approximate vehicular loading. They performed a parametric study to assess the behaviour of buried pipes and to do this analysis they used an integral transformation technique (Fourier transform).

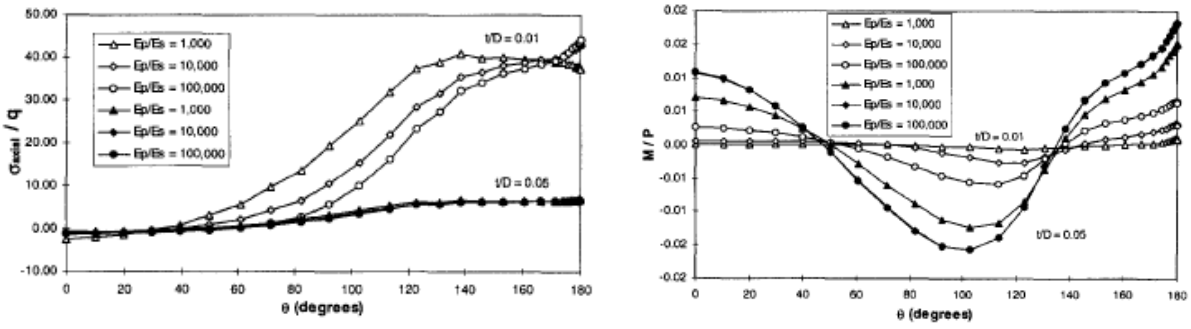

Figure 2.2: Typical in-plane forces and moments (Fernando and Carter, 1998)

The soil was idealized as a homogeneous linear elastic continuum and the buried pipe had a linear elastic plate bending element. Three assumptions were made, first the soil was well compacted, second no slip between pipe and soil, and third the soil is homogeneous (they omitted the stiffer pavement). Different cases were considered and in conclusion they could say that the relative thickness of the annular pipe has an important influence on the magnitude of forces and moments. The stiffness is also relevant when we consider the ratio between stiffness of the pipe over stiffness of the soil because it influences the magnitude of forces and moments (Figure 2.2).

More recent studies have been conducted comparing experimental and numerical investigations. Mosadegh and Nikraz (2017) studied the changes in pipe deflection, soil surface settlement and increase on earth pressure on pipe. The experimental tests were conducted in a rigid steel tank and two types of soil were used, a trench soil and a granular soil (Figure 2.3). This particular configuration is different from the one used in the experiments already performed in the 3SR lab, because, as it will be shown in the following chapter, in these experiments just one type of soil was used.

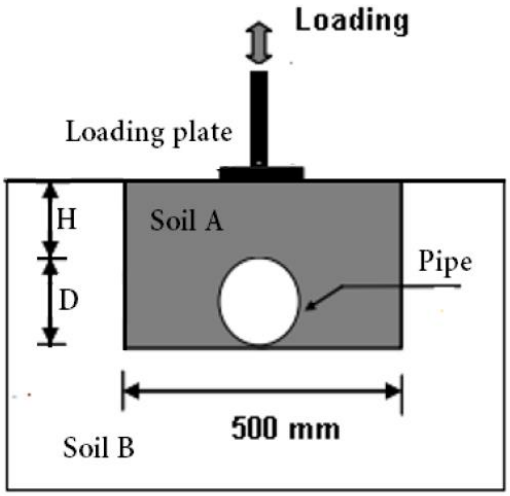

Figure 2.3: Schematic representation of the test setup. (Mosadegh and Nikraz, 2017)

The pipe used by Mosadegh and Nikraz was a polyethylene pipe with a thickness of 6.8mm and a diameter of 110mm. To record the pipe deflection and the pressure on the pipe strain gauges and pressure cells were used, attached to the pipe, and also a LVDT was placed on top of the plate to monitor the settlement. Numerical simulations were conducted, and a FE model based on the laboratory setup was built (Figure 2.4). The mesh has been refined around the pipe and the boundary

conditions were fixed in one direction on the sidewalls. The soil model used was the Drucker-Prager failure criterion and for the pipe a linear elastic behaviour was used.

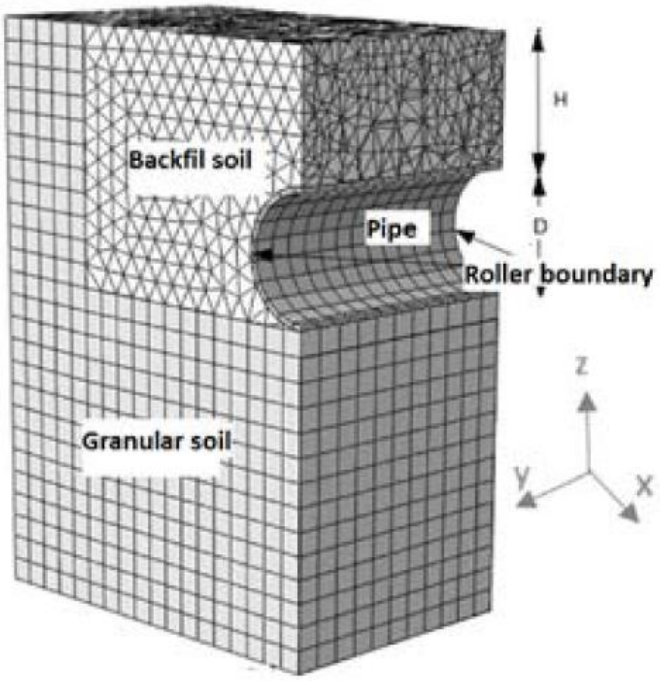

Figure 2.4: Finite element discretization (Mosadegh and Nikraz, 2017)

The ultimate bearing capacity of soil and traffic load simulations were tested. They noticed a good agreement between numerical simulation and experimental results, for example the bearing capacity is similar in both tests. Traffic test results reveal that pipe burial depth has a significant effect on surface settlement. Also increasing the surface pressure has a significant impact on increasing pipe deflection, soil surface settlement and pressure on pipe as expected.

Apart from the burial depth, it is also interesting to analyse the influence of soil saturation on the behaviour of buried pipes since it can vary a lot during the life of a pipe. Even if this issue will not be investigated in the following work, it is important to know the effect of soil saturation in order to make the correct assumption to be in safety conditions during the analyses. Randeniya et al. (2020) were interested in this subject and they performed large-scale experiments and numerical simulations. For the experiments they used a box with plywood steel to support the soil fill and to apply the load (internally and externally). A manual pressure pump and a hydraulic loading jack were used. The traffic load was applied as a static one. An interesting difference from the previous study analysed is the internal water pressure applied in this case in order to simulate a uniform pressure inside the pipe.

To record the strain evolution, on and in the pipe, 12 strain gauges were used as well as some sensors pads placed on the pipe. The pipe used for the experiments was a cast iron one with a diameter of 122 mm and a thickness of 11 mm. The soil was a lean clay with gravel. They performed 20 direct shear tests to characterize the soil with different saturation levels. Also, numerical simulations of the experimental setup were carried out with a FE software. The soil model used in this case was a modified elastoplastic model with Mohr-Coulomb failure criterion that consider strain softening at high strain. The most interesting conclusion of this study is that 20% and 85% of water saturation degree conditions can cause larger pipe deformations compared to 65% of saturation degree under simulated traffic loads (Figure 2.5).

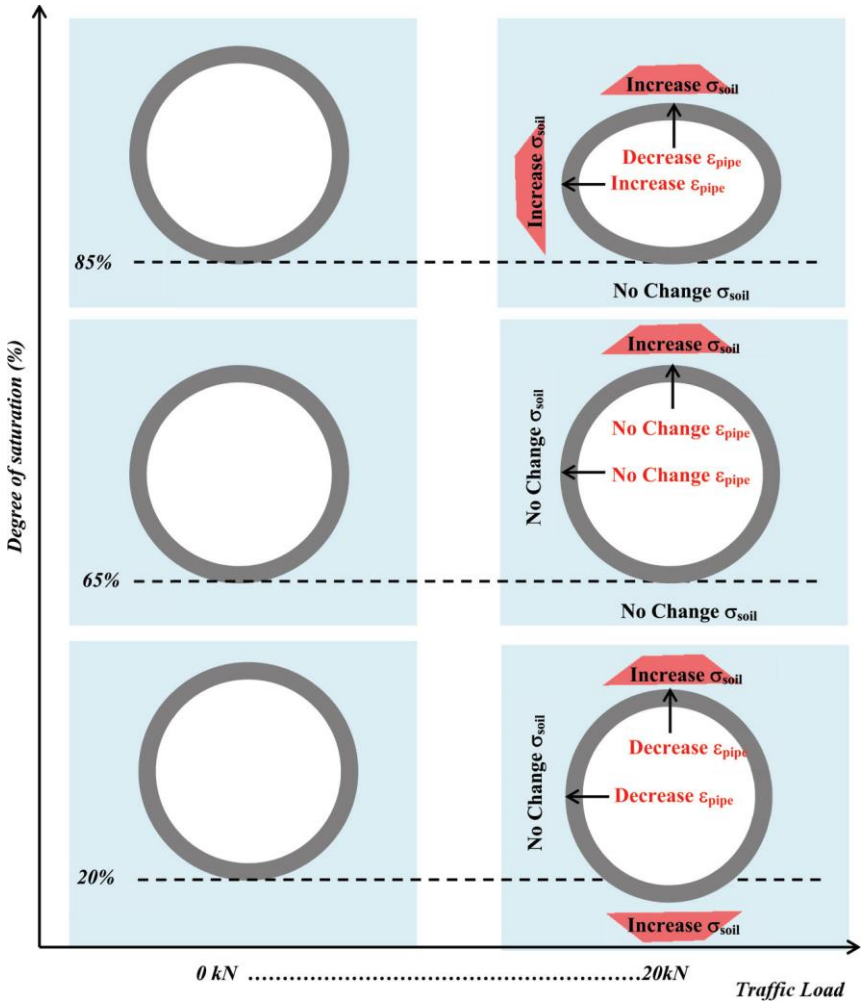

Figure 2.5: Deformation mechanism of pipe under traffic load (Randeniya et al., 2020)

It indicates that an intermediate degree of saturation of the soil can be favourable for the pipeline: since in real conditions, this value is not likely to be known precisely (and there are no guarantees that it will be sustained), considering what happen at more extreme values is at the safe side. With this conclusion in mind the following work is conducted with a dry soil.

2.1.1. GIPIPE

The GIPIPE research project investigates the mechanical behaviour and structural integrity of buried steel pipelines, subjected to severe ground-induced permanent action – including tectonic (quasi-static) effects, slope movements, and liquefaction-induced displacements – using advanced experimental techniques and high-performance numerical simulations. (European commission, 2015)

This study was carried out in pursuit of the objective of drawing up a comprehensive set of guidelines for the design of underground pipelines. Another important objective of the EU commission was to develop a list of operational recommendations for underground pipelines. As mentioned above, the areas of analysis are areas where ground induced actions are very likely to occur.

The study was divided into three phases. The first phase consisted of an introductory work where existing and previously used methodologies were analysed. Also, in this phase, models were analysed to represent the soil in the models created to study the soil-pipe interaction under permanent ground-induced actions. In the second phase, experimental studies were carried out to investigate the soil-pipe interaction combined with finite element models. In the last phase of this study, the results of the previous phases were collected to draw up guidelines for pipeline design.

The GIPIPE research project therefore studies the mechanical behaviour and structural integrity of buried steel pipelines subjected to severe permanent soil-induced actions, using advanced experimental techniques and high-performance numerical simulations.

The main result of this study is certainly to have drafted the set of guidelines researched, but in addition important conclusions have been obtained. First of all, it was found that a very good overlap can be obtained between results obtained from experiments and those obtained from numerical models, even in the case of simplified models. With regard to pipelines, the tests indicated that the formation of local buckling can lead to premature fracture and loss of pipe containment.

This study was very relevant at European level as it allowed the drafting of guidelines for the design of buried pipelines, and although it is of relative interest to our field of analysis, as we do not deal

with pipelines subject to severe ground-induced permanent action, it was interesting to analyse how they investigated the problem and compared the experimental data with the numerical once.

2.2. Work already done in 3SR

From this literature review, it can be seen that many analyses have been made concerning buried pipes, in different ways and considering different aspects of the problem. In addition to consulting the literature, this project was also based on the work previously done on this topic. In fact, an experimental and numerical campaign have been carried out in 2018 that inspired and influenced this work. They will be presented right after.

2.2.1. Experimental work

An experimental campaign (Dano, 2019) was performed in the test tank of the 3SR Laboratory, called VisuCuve. The dimensions of the tank are 2000mm*950mm*900mm, as depicted Figure 2.6. A hydraulic jack, resting on a square steel loading plate (10*10 cm^2), applies the loading and is monitored by a 20kN force transducer. A dry Fontainebleau NE34 sand was used to fill the tank. Several layers were done, each of them was compacted individually. Two different cover height (from the surface to the top part of the pipe) were used for the pipe, 45cm and 30cm. A test with a buried distributing plate was also performed. The pipe was modelled using a 6060-aluminium tube with a diameter of 100mm and a thickness of 2mm.

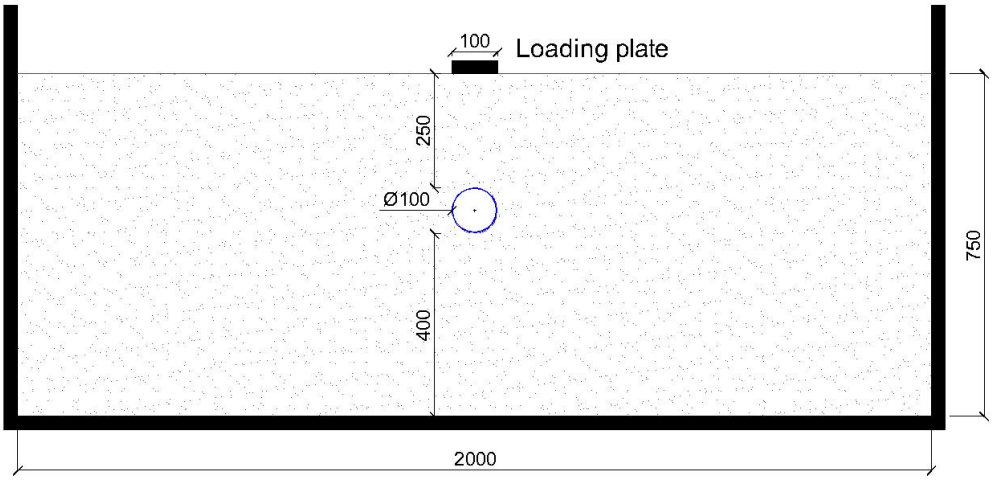

Figure 2.6: Visucuve scheme (dimensions in mm)

This experiment was made at small (model) scale, with a similitude ratio of 3. This configuration is the basis for the numerical models that will be presented in this report. Therefore, the reflexion about this scaling laws will be discussed in the following chapter. The pipe was instrumented with 4 pairs of strain gauges, placed on the outer surface of the pipe. The nature of the deformation measured by each strain gauge is different, axial stain for odd numbers (J1, J3 J5, J7) and hoop strain for even number (J2, J4, J6, J8) (Figure 2.7). Three trials were performed with two different cover heights and in the third case by also adding a distribution plate. As in the studies illustrated before, the experiments showed that a cover of 45cm induces a small amount of deformations on the pipe (Figure 2.7), so the cover of 30cm was more relevant in order to measure and draw conclusions.

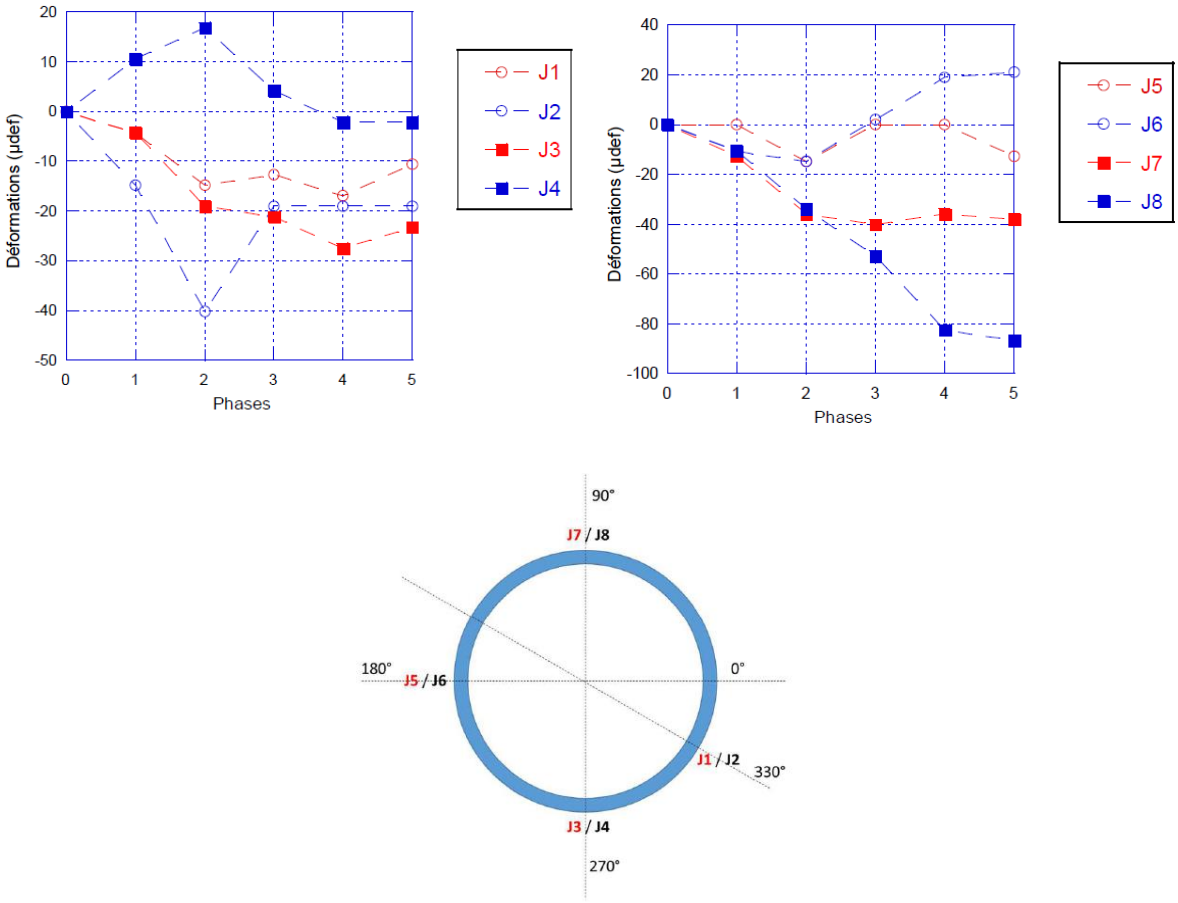

Figure 2.7: Evolution of deformation during loading (First trial with 45 cm cover) (Dano, 2019)

At 30cm of cover, the strain gauges showed that a flexion of the pipe due to the concentrated load was involved, at the same time as the expected ovalisation of the pipe. This bending is a 3D

phenomenon, so in this following 2D study it was not possible to capture completely this behaviour. The last test performed with a distributing plate under the loading showed a limited impact of it: for a given amount of surface stress, the plate does not change the amount of stress on the pipe but it seems to have a “delaying” effect (Figures 2.8-2.9).

This experimental campaign was useful to set the basis of the upcoming work that need to be done, such as an analysis of the pipe behaviour using FEM, or more experimental work using in-soil stress transducers and adding an internal pressure in the pipe. The latter experimental part will be carried out during a PhD project.

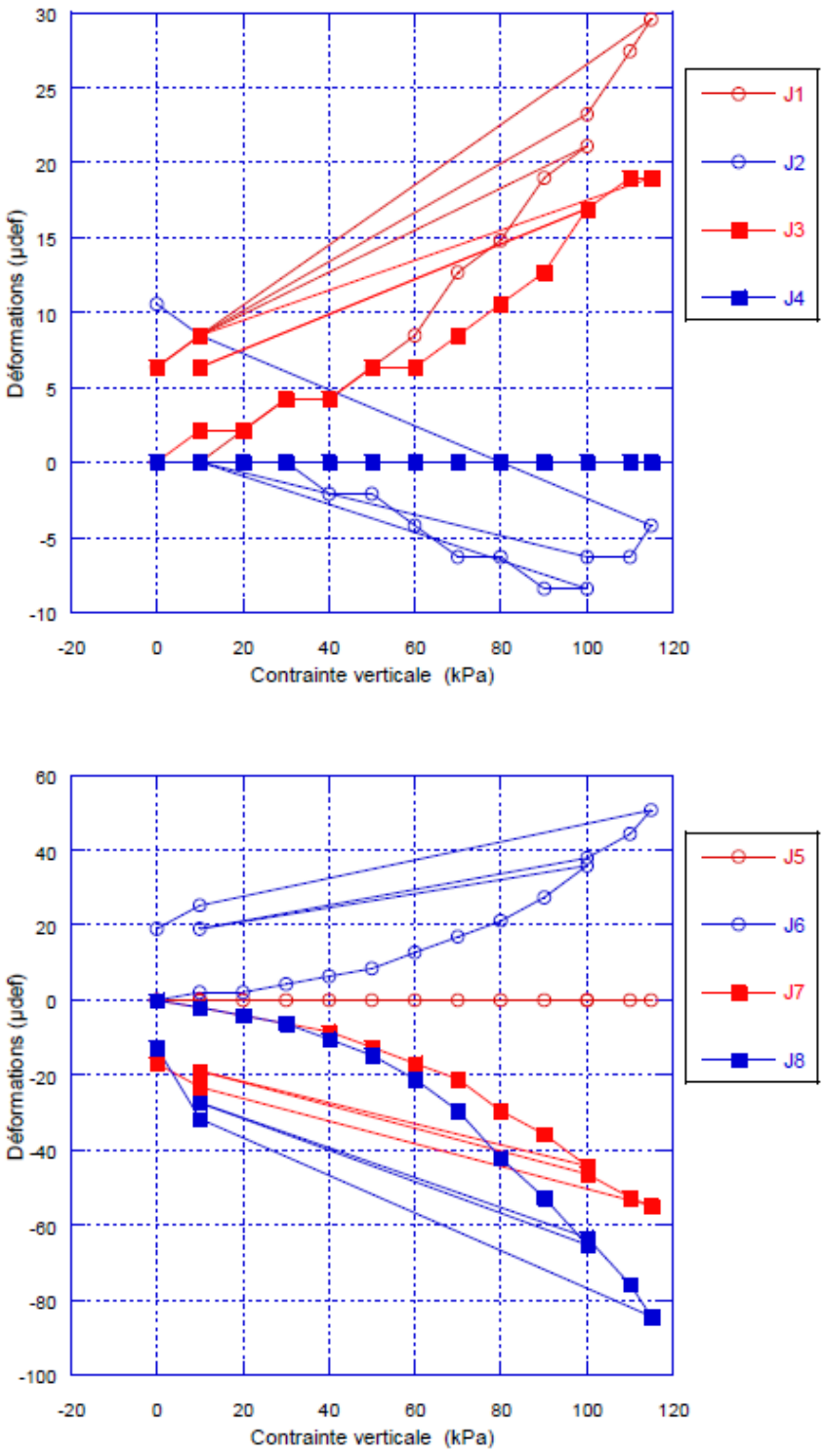

Figure 2.8: Pipe deformation according to surface vertical applied stress second trial (cover height of 30 cm) (Dano, 2019)

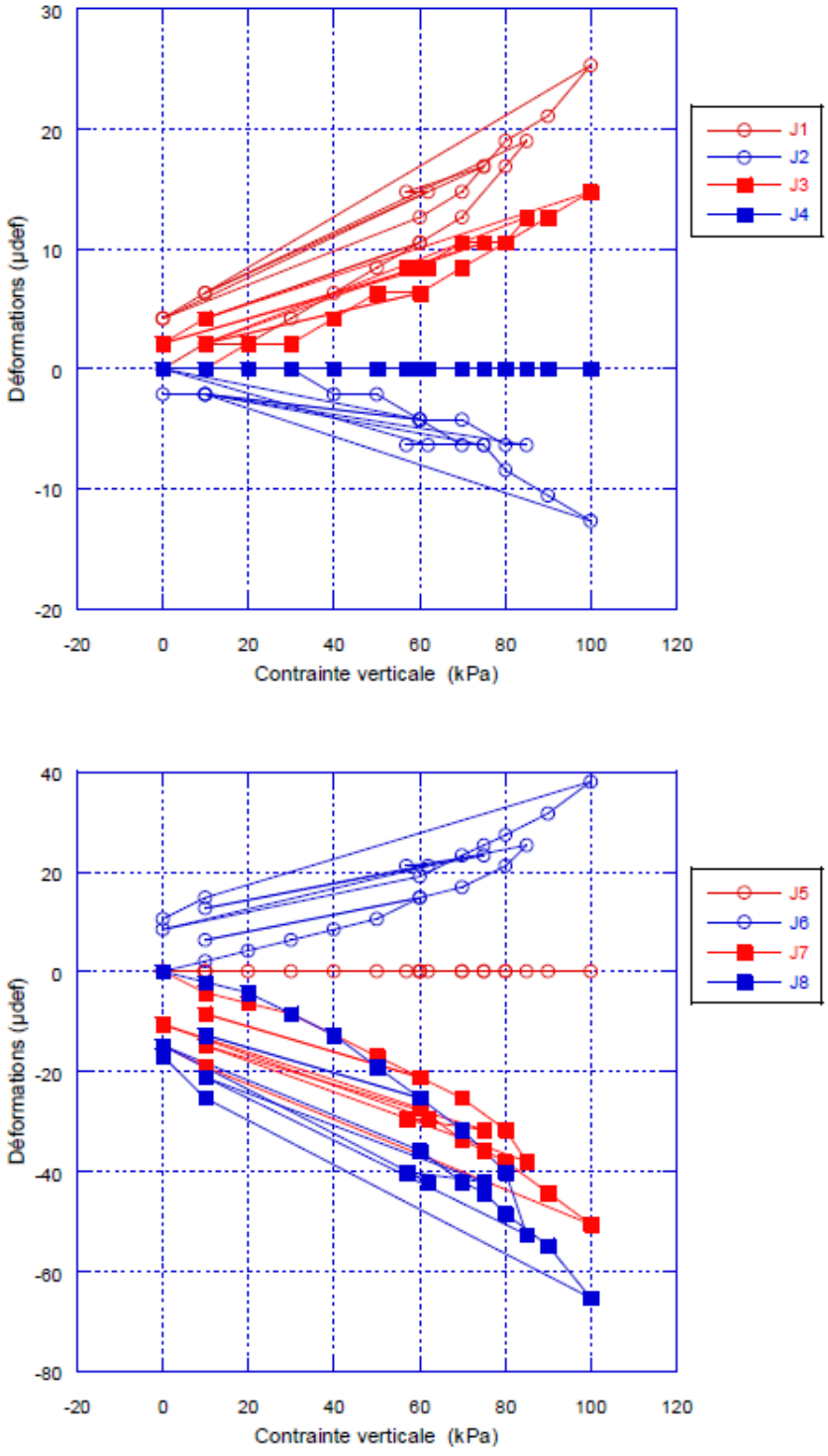

Figure 2.9: Pipe deformation according to surface vertical applied stress third trial (with distribution plate) (Dano, 2019)

2.2.2. Numerical work

A numerical campaign was also carried out and the software used was PLAXIS 2D (Boulon, 2018). The calculations concern again a reduced model of a tank filled with sand in which a pipe is buried (Figure 2.10). The soil/structure model is supposed to operate under plane strain conditions, and it is loaded with a vertical force on the axis of a steel rigid plate. The scaling laws that links the prototype scale and the model scale chosen for this study was based on a geometrical scale, under the normal gravity field, in this case 1/10.

Since the problem is symmetrical, just half of the tank and half of the pipe are modelled. The vertical side are fixed for horizontal sliding and the bottom is totally fixed. The pipe model is based on an aluminium pipe with a diameter of 50 mm and thickness of 0.5 mm, the behaviour of this material was considered elastic (with a Young modulus E=69 GPa).

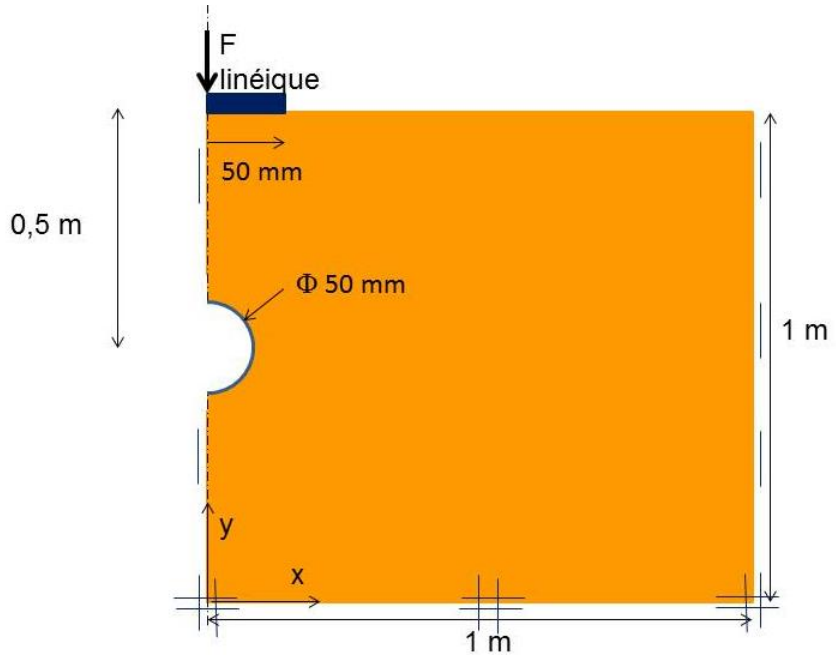

Figure 2.10: Tank model including a buried pipe and loading through a metal plate (Boulon, 2018)

A dense Fontainebleau sand was used for the soil model, but the mechanical properties are strongly dependent on the local level of average stress. The elasto-plastic Mohr-Coulomb model with constant Young's modulus was chosen for this study. The parameters used are reported below, as well as the interface friction angle between the soil and the pipe (δ):

$$\gamma = 16\ kN/m^3,\ E = 2901\ kPa,\ \nu = 0.3,\ c = 0.1\ kPa,\ \phi = 40°,\ \psi = 5°,$$

$$K_0 = 0.3926,\ \tan(\delta) = 2/3,\ \tan(\Phi) = 0{,}559 \rightarrow \delta = 29°$$

To have a more realistic simulation of the real behaviour of the sand in the following work a different constitutive model will be used. The maximum load reached was 3.09 kN/m and the loading process was divided in 82 steps.

- Phase 2 (ph2) = initial phase, put in place of the model
- Phase 3 (ph3) = laying of the distribution plate on the bed of sand
- Phase 4 (ph4) = loading up to 2kN/m
- Phase 5 (ph5) = limit loading up to 3.09 kN/m (Figure 2.11)

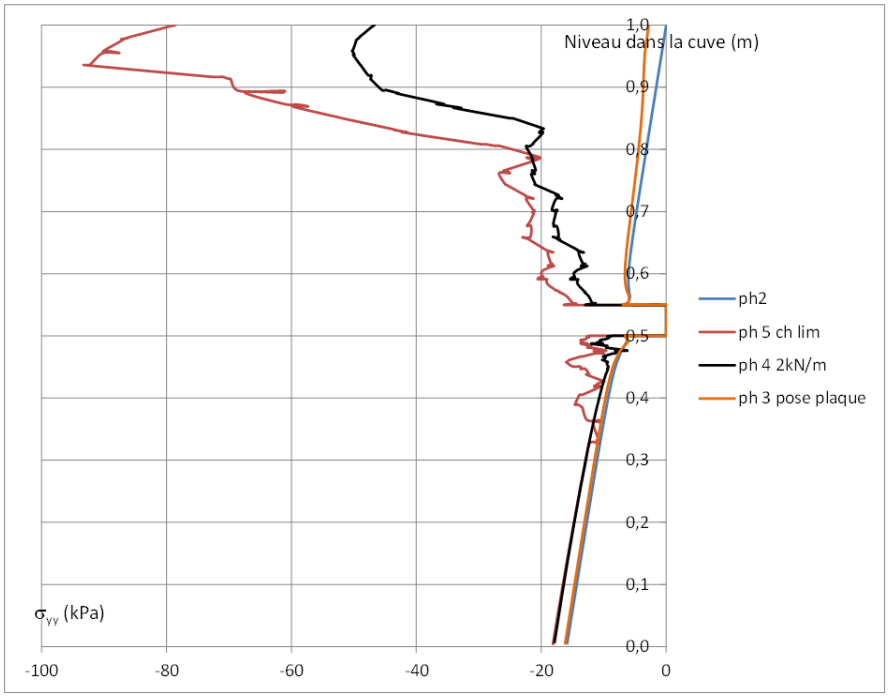

Figure 2.11:Vertical stress profile below the load axis at several loading stages (Boulon, 2018)

By analysing the vertical stress, it was found that the pipe acts as a diffuser of this solicitation, whereas, by considering the vertical displacement, it clearly appears that the pipe was compressed along its vertical axis (Figure 2.11).

Considering the distribution of horizontal stresses, it was noted that the installation of the surface plate has a great influence on horizontal stresses leading to an increase of almost double at the borders. An increase in horizontal stresses around the pipe has also been noted. In the horizontal direction there is an outward displacement which increases as the loading increases. It can be also seen that the deformation of the pipe under the effect of loading, including initial gravity, is not symmetrical with respect to the horizontal direction (Figures 2.12-2.13).

The resulting tube ovalisation at the end of loading reaches a maximum shortening of 1.17% in vertical direction, while the maximum lengthening is around 1.25% in vertical direction, instead the diameters oriented in the range (50°, 55°) remain invariant. Regarding the stress in the pipe, the main conclusion was that the influence of the normal force is marginal to that of the bending moment. Boulon suggested that it could not be the case if the pipe was under internal pressure (but this is not the most critical configuration in terms of pipe deformation.

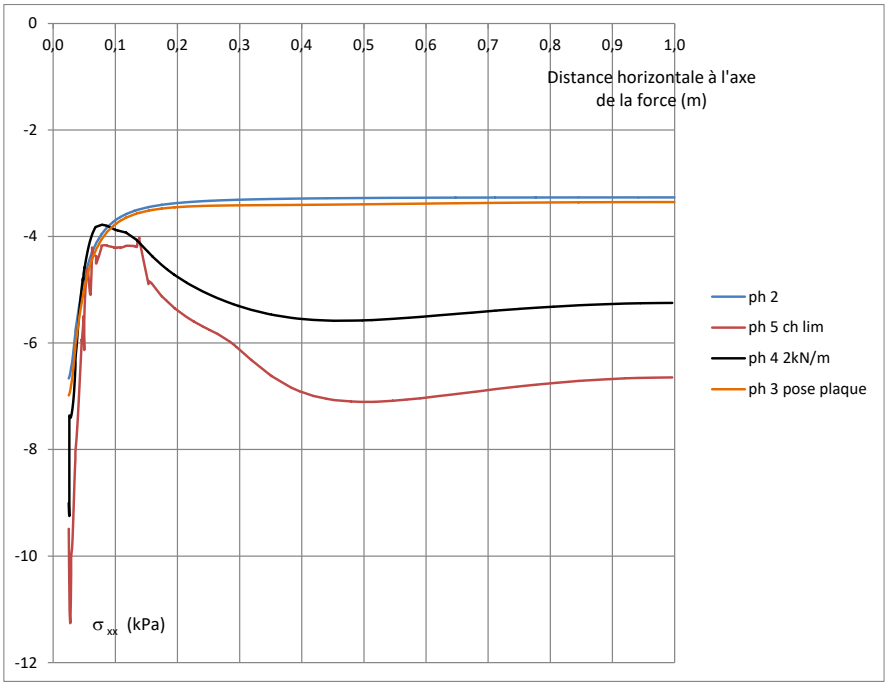

Figure 2.12: Profile of the horizontal stress at several loading stages (Boulon, 2018)

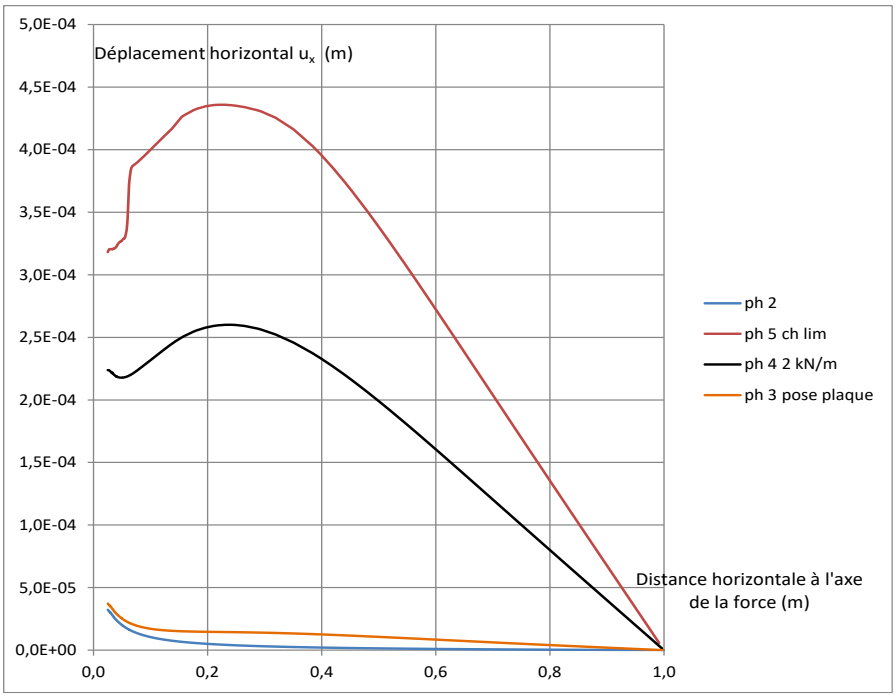

Figure 2.13: Profile of the horizontal displacement along the horizontal axis of the pipe at several loading stages (Boulon, 2018)

3. Context of the work

The general objective of this work is to investigate the behaviour of gas pipes buried in sand in order to have results, still preliminary at this stage, which will be used for future PhD work. The ultimate aim of this project will be to have an in-depth analysis of the behaviour of the pipes in order to improve the design approach now used by GRTgaz. The Master research project was supposed to provide data from both experiments and numerical analysis, but unfortunately due to 2020 special circumstances, only the numerical analysis and a small portion of preliminary experimental work were carried out.

3.1. Small scale laboratory model

The laboratory model on which the numerical analyses are based is presented here.

3.1.1. Presentation of the experimental setup

The experimental setup that was intended to be used is the same as the experimental campaign previously illustrated (Dano, 2019) with some modifications and additions. The new experimental campaign will be carried out during the PhD project. The new experimental setup that will be used and on which the numerical models are based is illustrated thereafter.

The tank to be used is the VisuCuve in which the small-scale tests will be performed respecting the similitude conditions with a scale factor $\lambda = 1/3$. In the following section, more details on the scaling laws will be given. The characteristics of this tank have already been presented. The load is applied with a hydraulic jack, this condition will not be respected in the FE models since in reality traffic loads are imposing directly a load on the soil (or pavement) and not imposing a displacement. The pipe and the soil intended to be used are the same ones as in previous experiments.

In addition to the strain gauges glued on the pipe to measure the deformation and deduce the stresses acting on the pipe, it was decided to use 20 miniature stress sensors, to be placed in the soil mass, in order to detect the evolution of the stresses in the sand during the loading phases.

These stress sensors are extremely sensible to many factors like the cell installation and the consequent ‘cell action’. This behaviour happens because there is a difference between the effective stiffness of the cell and the one of the soils. So, to be able to use these sensors, they must be calibrated

and the procedure that was used is illustrated in a study (Zhu et al., 2009) then adapted to this specific work. To perform the calibration, the same soil as in the experiments, must be used and particular attention must be paid to the boundary conditions because it is important to try to minimize the effect of these on stress- non-uniformity in the sensor placement area.

A "tall oedometer" was used to perform the sensor calibration in different steps:

1. Connect the sensor to the signal
2. Fill the Oedometer with sand and compact it manually to reach a target density around the one used in the VisuCuve in the experiments illustrated by Dano (2019). The density effect on the calibration will be then studied.
3. Place the cell and continue to fill the sand
4. Apply pressure changes under automatic control to increase or decrease the vertical stress

From different tests found in literature (Zhu et al., 2009) it was shown that a standard depth of 90mm was sufficiently deep to eliminate loading plate effects and allow cell action to develop fully avoiding excessive wall friction losses.

3.1.2. Scaling laws

In some cases, it can be necessary to perform experiments at small scale, maybe because of size limitation of the model, as in this case. So, there is the necessity to transpose the results obtained on scale models into full-scale results (or prototype). In order to use the data obtained, care must be taken to respect the conditions of similitude. If these conditions are not fulfilled, a distortion called scale effect is generated. This can lead to errors in the interpretation of the results, so it is really important to control and minimize this scale effect

In the field of geotechnical engineering, different tools have been developed to avoid the consequences of scale effects, although it is not always possible to eliminate them completely. The most common instruments used in the field of geotechnics are for example geotechnical centrifuges, calibration chambers or hydraulic gradient models. When using a geotechnical centrifuge, the literature on the laws of scale is very extensive, there are in fact many different scale factors depending on the physical mechanism involved. (Dano, 2018)

A different approach has been chosen for this study; in fact, all the scaling laws, also called similitude conditions, are based on the dimensional analysis. This theory is also called Pi-Theorem and was

introduced by Buckingham (1914) among others and it states that given a physical process described by an equation even indefinite (in its analytical form), the problem can be expressed with adimensional terms. It is based on the use of π-terms relationship which describes the performance of a system (physical variables), the prototype.

$$\pi_1 = f\ (\pi_2, \pi_3, \pi_4, \ldots, \pi_{s)}$$

Every π-term is dimensionless, is independent from the other and represent primary quantities. The same equation can be written for the model since it describes the same phenomena as the prototype. So, if the fundamental quantities of these n π-terms are k (for example, mass, length, time in a purely mechanical problem), then the problem can be expressed as a function of n-k adimensional groups. The corresponding π-terms groups provide a set of design conditions in order to create the model.

So, Pi-theorem finally affirms: "If there are n variables in a problem and these variables contain m primary dimensions (for example M, L, T) the equation relating all the variables will have (n-m) dimensionless groups." (Buckingham, 1914)

Given the similitude of behaviour, the model and prototype imply that there are constant relationships (Scale factors):

λ= model property /prototype property

The relationships between these scale factors would then be the basis on which the conditions of similitude between the two scales are based.

In this study, therefore, the fundamental quantities involved are:

- The length L.
- The time T.
- The mass M.

The geometric scale factor is $\lambda_L = \frac{L_{\text{mod}}}{L_{prot}}$ and following that, it is also possible to say that the scale factor on deformation λ_ε is 1. All the experiments are conducted in a normal gravity field so, the scale factor for gravity is 1 also. Following these considerations, all the other scale factors are derived and here is reported a table (Table 3.1) with the list of the most important ones regarding a 2D case (plane strain).

Table 3.1: Scale factors (Dano, 2018)

Property	Symbol	Scale factor
Mass	λ_M	λ_L^3
Volumetric mass	λ_γ	1
Time	λ_T	$\lambda_L^{1/2}$
Stress	λ_σ	λ_L
Elastic modulus	λ_E	variable
Moment of inertia	λ_I	λ_L^3
Linear force	λ_F	λ_L^2

For this study, the geometrical scale factor adopted is 1/3. The reason behind this decision lays in the Young modulus of aluminium, in fact the ratio between the modulus of aluminium and the modulus of steel (material used in reality) is exactly 1/3. This is a condition that it was important to fulfil for the purpose of the investigation that is being done. Also, from the experimental point of view, with this scale factor, a good range of pipes can be investigated.

In the next section, the scale factors applied to the various elements of the study under review are presented with their dimensions and considerations.

- VisuCuve Characteristics: The cuve is at the “model” scale, so for numerical calculation, we had to consider a “prototype” cuve as follows:
  It is to be noted that the prototype dimensions will only be used for numerical modelling, it doesn’t correspond to a physical experiment.

Table 3.2: Scale factors for the VisuCuve

Characteristic	Theoretical ratio	Model characteristic	Ideal prototype	Actual prototype	Actual ratio
Length [mm]	$\frac{1}{\lambda}$	2000	6000	6000	$\frac{1}{3}$
Width [mm]	$\frac{1}{\lambda}$	1950	5850	5850	$\frac{1}{3}$
Depth [mm]	$\frac{1}{\lambda}$	900	2700	2700	$\frac{1}{3}$

– Pipe characteristics: The prototype considered was a steel pipe of 300mm outer diameter and 6mm thickness, that correspond roughly to a DN250, cat.C pipe used by GRTgaz (273mm diameter and 6.5mm of thickness). Hereby, it was proposed to use an aluminium pipe of 100mm outer diameter and 2mm thickness, which lead us to consider the following parameters:

Table 3.3: Scale factors for the pipe

Characteristics	Theoretical ratio	Prototype characteristic	Ideal model	Actual model	Actual ratio
Diameter [mm]	$\frac{1}{\lambda}$	300	100	100	$\frac{1}{3}$
Thickness [mm]	$\frac{1}{\lambda}$	6	2	2	$\frac{1}{3}$
Young Modulus [GPa]	$\frac{1}{\lambda}$	210	70	69.5	$\approx \frac{1}{3}$
Moment of Inertia $[m^4/m]$	$\frac{1}{\lambda^3}$	1.8×10^{-8}	6.67×10^{-10}	4.67×10^{-10}	$\approx \frac{1}{27}$

Characteristics	Theoretical ratio	Prototype characteristic	Ideal model	Actual model	Actual ratio
Flexural rigidity EI [kN.m²/m]	$\frac{1}{\lambda^4}$	3.78	4.67×10^{-2}	4.63×10^{-2}	$\approx \frac{1}{81}$
Normal rigidity EA [kN/m]	$\frac{1}{\lambda^2}$	1.26×10^6	1.40×10^5	1.39×10^5	$\approx \frac{1}{9}$

The "ideal model" correspond to what would be the "perfect" dimensions and characteristics for the model pipe in respect to the scaling laws. The "actual model" correspond to the dimensions and characteristics of the model pipe that have been used in reality (which could be different, due to a various range of limitations). The theoretical ratio has been determined accordingly to the recommendations made by Boulon and Dano (2018)

The agreement between the theoretical ratio and the actual ratio is really good, mainly due to the fact that the aimed ratio of 3 allows to use a pipe of aluminium 6060 for the model pipe (while the prototype one is in steel), which greatly helps to respect the similitude condition on the flexural and normal rigidity, and to have a correct estimation of the hoop stress acting on the pipe.

– Loading characteristics: The loading is also affected by the scaling of the problem. The numerical model is piloted through a uniformly distributed loading, applied on a stiff pressure plate. The pressure plate, as a geometrical object, will be affected by the geometrical scaling conditions, as follows:

Table 3.4: Scale factor for the loading plate

Characteristic	Theoretical ratio	Prototype characteristic	Ideal model	Actual model	Actual ratio
Length [mm]	$\frac{1}{\lambda}$	30	10	10	$\frac{1}{3}$
Width [mm]	$\frac{1}{\lambda}$	30	10	10	$\frac{1}{3}$

Characteristic	Theoretical ratio	Prototype characteristic	Ideal model	Actual model	Actual ratio
Thickness [mm]	$\frac{1}{\lambda}$	2.82	0.94	0.94	$\frac{1}{3}$

We know from Boulon and Dano (2018) that the scaling factor, in 2D plain strain, for a distributed load is $\frac{1}{\lambda^2}$. In our case, the load is distributed on a plate, with dimension that has been affected by the scaling, so in order to respect the condition for the stress under the plate (the scale factor for the stresses is $\frac{1}{\lambda}$), we need to use instead the factor $\frac{1}{\lambda}$ for the loading, otherwise, the resulting stress would be λ time too small.

We will see further on that this condition is not always fulfilled, especially when it comes to failure.

- Soil: The soil should also be modified in regard to the geometrical scaling of the model, since its properties are affected. The main effect is on the stiffness, since it depends heavily on the stress level acting in the media, stress level affected at the first order by the scaling. Since the soil used at both scales remain the same, it realistically introduces a bias, that should be quantified, to see if it remains acceptable.

3.2. Aim of numerical modelling

The aim of this project, in the beginning, was intended to use numerical models as a reference to interpret the results obtained from the experiments conducted in parallel. However, considering that it was not possible to perform experiments during this work, it was decided to expand the numerical modelling campaign. The models thus realized are based on the experiments carried out in the previous experimental campaign (Dano, 2019). The main objectives of this numerical study are first of all to have access to a wide range of data that can be used as references for future campaign of experiments. These results should cover the soil but also the tube and the interaction between the two for different soil conditions. Another important result to be obtained is the influence of similarity conditions on the results.

4. Numerical model

In this section the numerical models are described. They were obtained using a FE software called PLAXIS and they are all 2D plane strain models.

4.1. General presentation of the numerical model

4.1.1. Presentation of the software

PLAXIS (Plane strain and axial symmetry, indicating the geometric types handled in the original code) is a powerful and user-friendly finite element software, used all around the world for geotechnical engineering and design. This program is developed for the analysis of deformation, stability and groundwater flow in geotechnical field and rock mechanics (PLAXIS manual, 2019).

This software is intended to provide a tool for practical analysis to be used by geotechnical engineers. The problems that often arises with finite element programs are the long computational time and the complexity in the usage. But PLAXIS is developed to be easy to use since its interface is logical and friendly for designing robust models.

PLAXIS proposes advanced constitutive models for the simulation of non-linear, time dependent and anisotropic behaviour of soil and/or rocks. In particular for this project, it was used PLAXIS 2D which is a package intended for two-dimensional analysis in many applications range from excavations, embankment and foundations to tunnelling mining and reservoir geomechanics. PLAXIS 2D abilities can be extended with three additional modules: Dynamics, Plaxflow and Thermal, but in this project, these extensions were not necessary.

4.1.2. Geometry of the model

The aim of this study, as explained in detail before, is to show preliminary results about the behaviour of a model pipeline buried into a sand bed that receives a surface loading.

In this study, different configurations have been tested. First, two different scales were considered (model and prototype); then, at model scale, three different thicknesses for the pipe were also considered. These comparisons were always made in two different soil conditions, in fact a loose

sand and a dense sand were considered. The sand in both states was used because, in the experiments, a compaction will be done but since it's not easy to have a perfect uniform compaction in the entire VisuCuve, considering also the presence of the pipe, there will probably be both sand states in the same model. For this reason, it was decided to explore the behaviour of the Fontainebleau sand in both conditions.

As mentioned above, sand in two different states of compaction was used as a reference, they will be referred to as loose sand and dense sand during the discussion. In reality, observing the degree of compaction, it can be seen that they are a medium dense and a dense sand. The notation has been simplified to avoid confusion. In fact, during the experiments, the sand used is never in a "loose" state, but even in the less compacted areas, such as around the pipe, it will be at least moderately dense. Since the tank is symmetric and only centred surface load is first considered, for sake of simplicity and to have faster calculations (less computation time), on PLAXIS just half of VisuCuve was represented. In Figure 4.1 are shown the half-models at model scale performed on Plaxis 2D with the two different sand conditions. The dimensions are the one of the VisuCuve but in 2D: 1m (length) x 0.75m (height).

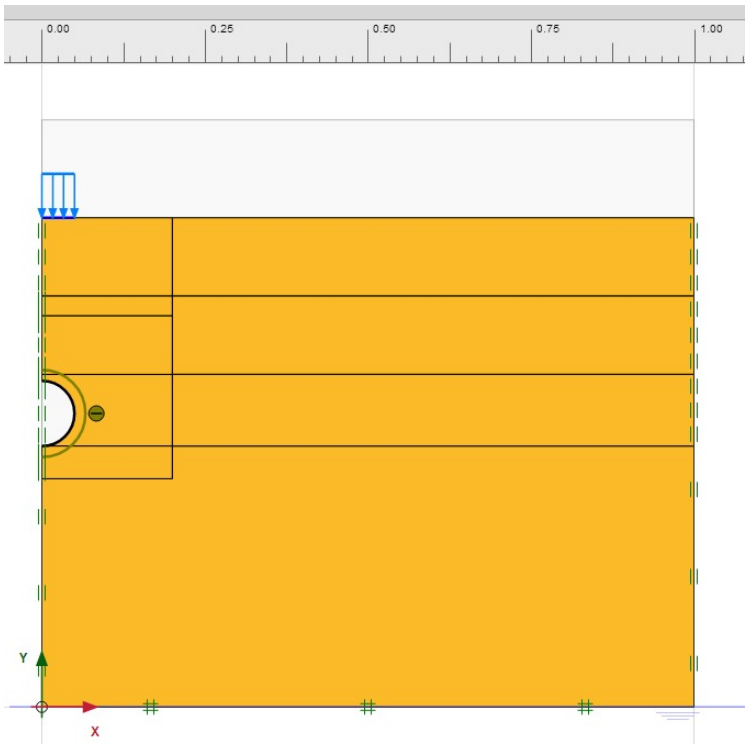

Figure 4.1: Plaxis model at model scale (dimensions in m)

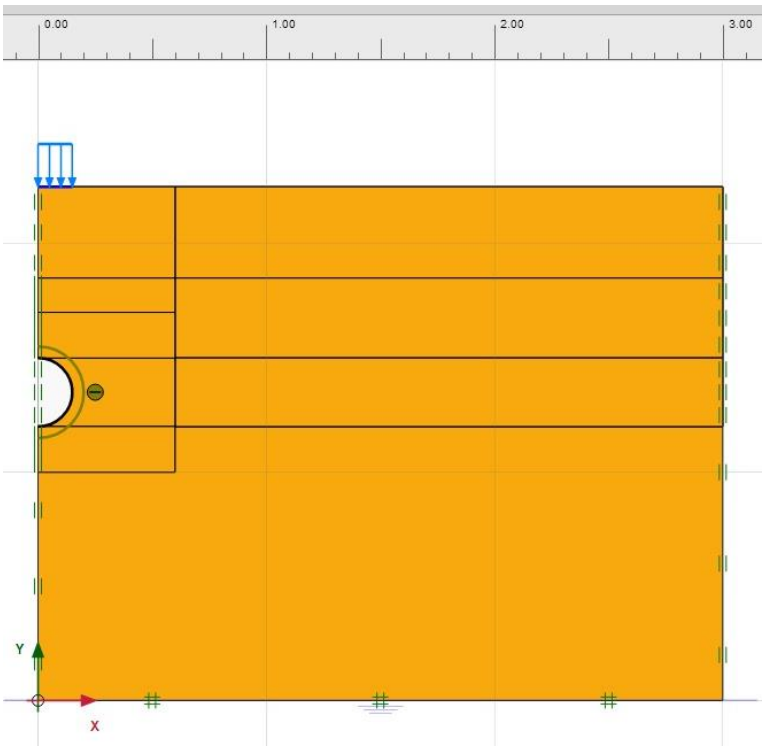

Figure 4.2: Plaxis model at prototype scale (dimensions in m)

Instead in Figure 4.2 are shown the half-models at prototype scale again with the two different sands. The dimensions of the models respect the scaling laws, the scale factor between the two representations is 1/3. So, the dimensions of the prototype model are 3m (length) x 2.25m (height).

4.1.3. Elements of the model

The models are made up of different elements of different nature. The first analysed here is the soil. In order to properly simulate the behaviour of the sand, the soil model used in this study is the Hardening Soil Model with Small Strain (HSsmall) (Benz, 2007). This model has been chosen for its capability of taking into account the complex behaviour of the soil better than other simpler model like, for example, a linear elastic and perfectly plastic model with a Mohr-Coulomb (MC) criterion. In fact, the HSsmall model considers the soil non-linear response, and complex plastic mechanism in the soil. The model also responds for the stress dependency of the different stiffness moduli. The drawback of this better prediction capability is the increase in input parameters, and the higher attention needed to evaluate the response of the model on real tests. Later in the report the parameters

calibration will be illustrated. The model walls have been assigned the following boundaries conditions:

- Bottom: totally fixed
- Lateral boundaries: Horizontally fixed

The bottom of the tank must be fixed because during the loading process, it doesn't move. Instead the lateral boundaries have to be just horizontally fixed since they are rigid, and they don't allow horizontal deformations during the phases. The pipes on PLAXIS are modelled by using a plate (structural element available in PLAXIS), considering, as reference, the catalogue from GRTgaz where are reported the dimensions of the pipes used for their gas network in France. Here the analysed ones are reported.

Table 4.1: Extracted from "Canalisations réelles et modèles" (GRTgaz)

	DN250	DN250	DN250
External diameter (mm)	273	273	273
Steel quality	TUE360	TUE360	TUE360
Young's modulus (GPa)	210	210	210
Thickness (mm)	6.5	4.3	3.6
Elastic Limit (GPa)	360	360	360
Failure Limit (GPa)	480	480	480

The first type of pipe used, as reference, at model scale is the one used in the experiments previously conducted and illustrated in the report "Expérimentation sur tube creux en cuve à sable" (Dano, 2019) which refers to the first type of pipe reported from the GRT gaz's catalogue but scaled with a scale ratio of about 1/3. The experimental pipeline used was a 6060-aluminium tube, 100mm outside diameter, with a wall thickness 2mm and length 0.935m. Its mechanical properties are: Young's modulus E = 69.5 GPa, Poisson's coefficient, $\nu = 0.33$.

The parameters used to define the material at model scale in the software are:

- EA= normal rigidity $= E * h$
- EI= annular flexural rigidity $= E * \frac{h^3}{12}$
- ν= Poisson's coefficient

where:

- A = b x h, but since we are in 2D plain strain, b does not appear in the formula
- I= $b\ x\ \frac{h^3}{12}$, but, again, since we are in 2D plain strain, b does not appear in the formula

In Figure 4.2 are presented some diagrams which present the terms associated to the pipe. These formulas are referred to view A-A which can be seen in Figure 4.3.

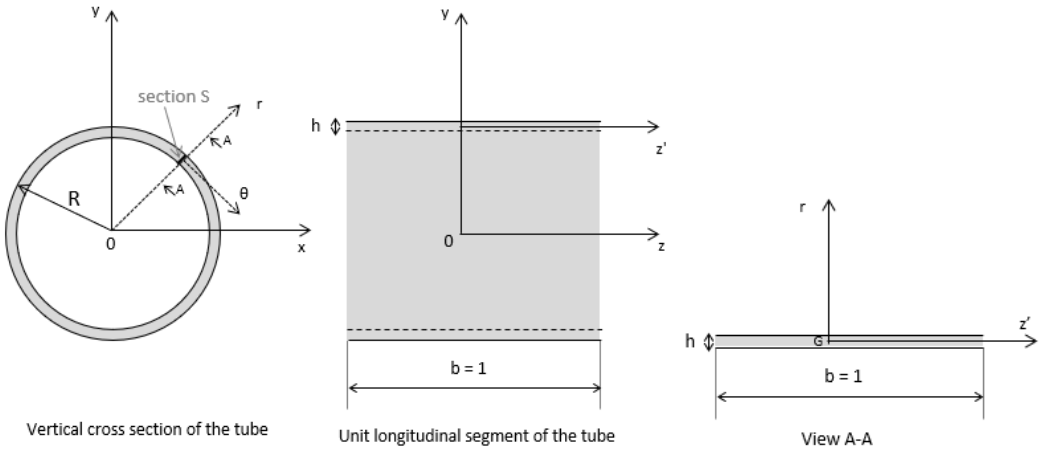

Figure 4.3: Pipe representation

Table 4.2: Characteristics of the pipe at model scale

Thickness	0.002 m
EA	$139*10^3$ kN/m
EI	0.04633 kN m^2/m
ν	0.33

Instead at prototype scale the following parameters were used:

Table 4.3: Characteristics of the pipe at prototype scale

Thickness	0.006 m
EA	$126*10^4$ kN/m
EI	3.78 kN m^2/m
ν	0.33

Two others pipe were considered in order to check the influence of the thickness on the behavior of the pipe and their characteristics are here reported:

Table 4.4: Characteristics of other pipes at model scale

Thickness	0.00133 m	Thickness	0.001 m
EA	$92.435*10^3$ kN/m	EA	$69.5*10^3$ kN/m
EI	0.01363 kN m^2/m	EI	0.00579 kN m^2/m
ν	0.33	ν	0.33

At the contact between the pipe and the soil, an interface (assumed rough) has been placed, with an interface friction angle of $\frac{2}{3}\ \varphi$, in order to materialize accurately the contact.

The load is applied on a stiff rectangular rigid plate which is modelled with an elastic plate element with high stiffness and with transverse half-length of 0.05 m.

4.1.4. Modelling

Since PLAXIS is a FE software, a mesh was created. 15-nodes triangular elements were used with a general coarseness factor, which indicates the local refinement of the mesh at the geometric entity, of 1 with a refinement to a coarseness factor of 0.25 around the pipe and under the loading plate. This mesh was used for all the models. (Figure 4.5)

The numerical model is loaded through a uniformly distributed loading, applied on the stiff plate illustrated before. It was decided to use this load control mode, instead for example the displacement control mode, because it more resembles the reality of a traffic loading.

The models, at both scales, were built and loaded by phases respecting the layer subdivision (Figure 4.4):

- Initial phase: 1st layer of sand
- 1st phase: pipe+2nd layer of sand
- 2nd phase: 3rd layer of sand
- 3rd phase: 4th layer of sand

  In these phases the sand is only subjected to the force of gravity and horizontal stresses are computed with K_0=0.5

- 4th phase: From this phase the loading procedure starts, and the actual loading is increased at every phase.

Failure occurred at different loading phases either modelling loose or dense sand, because the latter is stiffer, so higher bearing capacities were reached.

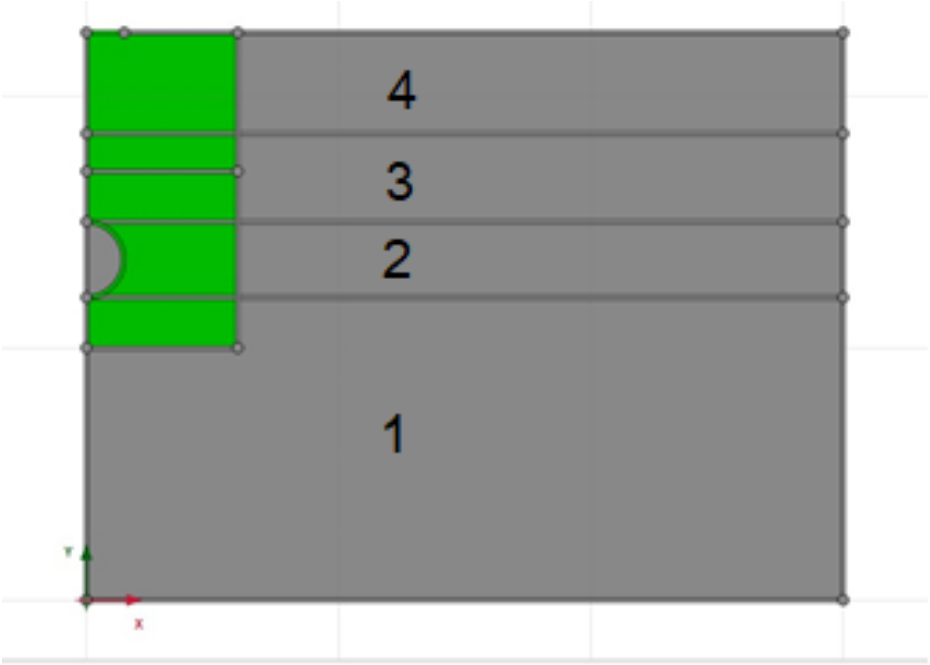

Figure 4.4: Layer subdivision

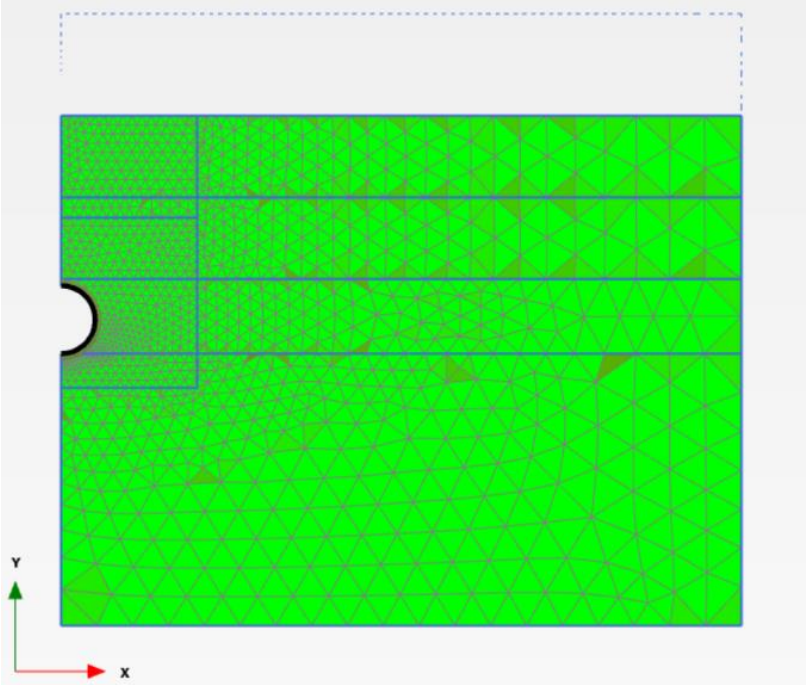

Figure 4.5: Mesh of the model

4.2. Numerical modelling of the soil behaviour

To represent the behaviour of granular media, it was proposed to use the Hardening Soil Model with small strain. HSMsmall is a model well suited to model the behaviour of granular soil such as sand, since it takes into account the effect of the plastic deformations occurring in the soil, even during the early stages of the loading, something that models using an elastic-perfectly plastic behaviour are not capable. The "small strain" variant of the HSM is designed to also take into account the fact that the soil usually has a higher stiffness at small strains, that degrades with the increase of the strain level.

In this chapter, the analysis performed, and the assumptions made that best suit the case under study are explained.

4.2.1. Hardening soil model (HSM)

To simulate the behaviour of a sandy soil, it was decided to use the Hardening Soil Model (HSM) because this model is well adapted for granular soil under monotonic and limited unloading stress path. In fact, by comparing it with other models, linear elastic and perfectly plastic model, which assume a Mohr-Coulomb (MC) criterion, it was possible to notice that the MC model has some intrinsic limitations like the bilinearity (constant E, ν), unlimited dilation, isotropy and perfect plasticity. In conclusion it can be stated that the HSM model is more appropriate since it still includes the theory of plasticity and the soil dilatancy, as MC, but it introduces a yield cap and the elastic modulus is stress dependent.

The major differences for the HSM is that the elastic domain isn't fixed, but it does change, in fact it can expand depending on the volumetric and deviatoric plastic strains and it comprises two distinct mechanisms of yielding: one in shear and one in compression. (Figure 4.6) Shear hardening is used to model irreversible strains due to primary deviatoric loading. Compression hardening is used to model irreversible plastic strains due to primary compression in oedometer loading and isotropic loading (Schanz et al., 1999).

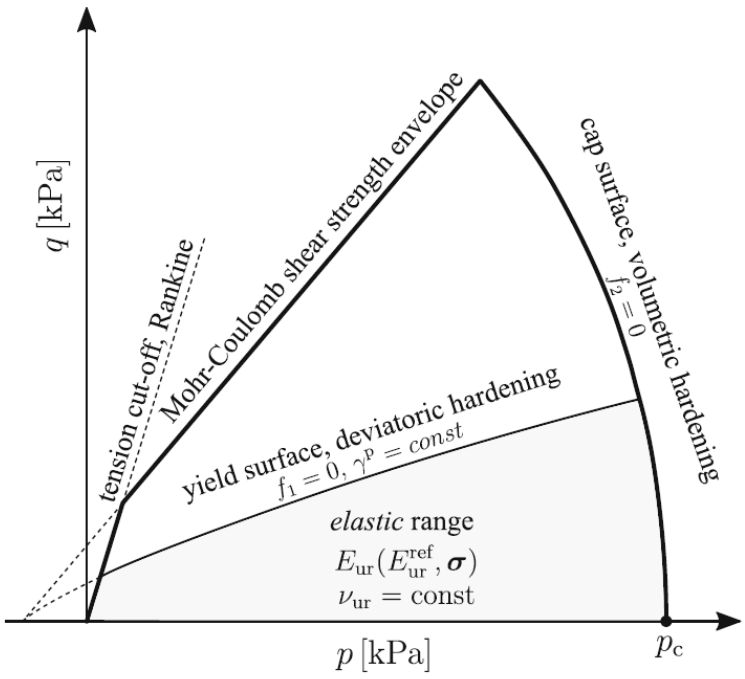

Figure 4.6: Yield surface and elastic range in the basic HS model (Cudny et al., 2020)

Another difference between the models is in the parameters, the elastic perfectly plastic Mohr-Coulomb model is based on the friction angle φ, the dilatancy angle ψ, the cohesion c, Poisson's ratio ν and the stiffness E. In the case of HSM instead, a single parameter for the stiffness is not considered but three:

- The secant stiffness in standard drained triaxial test $E_{50} = E_{50}^{ref} \left(\frac{\sigma_3 + c\ cotg\ \varphi}{p^{ref} + c\ cotg\ \varphi}\right)^m$
- The tangent stiffness for primary oedometer loading $E_{oed} = E_{oed}^{ref} \left(\frac{\sigma_1 + c\ cotg\ \varphi}{p^{ref} + c\ cotg\ \varphi}\right)^m$
- The unloading/reloading stiffness $E_{ur} = E_{ur}^{ref} \left(\frac{\sigma_3 + c\ cotg\ \varphi}{p^{ref} + c\ cotg\ \varphi}\right)^m$

Where

- m: power for stress-level dependency of stiffness
- p^{ref} : reference mean effective stress; a usual value is 100 kPa
- E_{50}^{ref}: secant stiffness in standard drained triaxial test with reference to p^{ref} (Figure 4.2)
- E_{oed}^{ref} : tangent stiffness for primary oedometer loading with reference to p^{ref}

- E_{ur}^{ref} : unloading/reloading stiffness from drained triaxial test with reference to p^{ref} (Figure 4.7)

This is because the HSM considers also the stress-dependency of stiffness moduli. In fact, it is observed that stiffnesses increase with pressure, so these three parameters are related to a reference stress. The result will be a stiffer response upon unloading/reloading compared to virgin loading since this model also takes into account the overconsolidation.

As it is possible to notice that from the previous equations, all the stiffnesses depend on the power *m* that is used to simulate a logarithmic stress dependency (Schanz et al., 1999)

In the situation under examination, the real important range of strain that we should take into account is the interval concerning the small strains

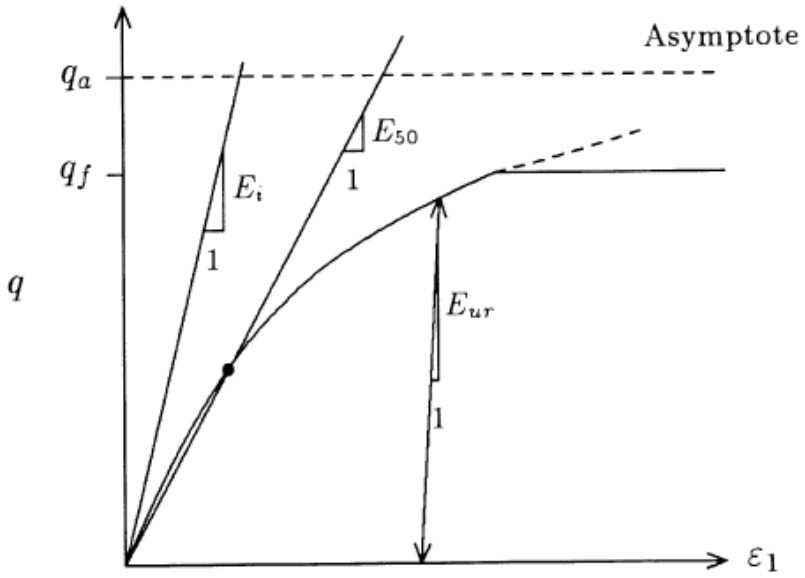

Figure 4.7: Hyperbolic stress-strain relation in primary loading for a standard drained triaxial test (Schanz et al.,1999)

4.2.2. Hardening soil model with small-strain stiffness (HSsmall)

The HSS model is a development of the previous Hardening soil model (HS), incorporating specific soil stiffness at small strains (Benz, 2007). The reason why this particular model was found necessary is because HSM during unloading and reloading considers the soil as an elastic material, but as it was said before, this is true just at small strains. If fact it is possible to notice that by plotting on a

logarithmic scale the shear strain against the soil stiffness, it is obtained a S-shaped stiffness reduction curve. (Figure 4.8)

Small-strain soil stiffness and its non-linear dependency on strain amplitude should be properly taken into account. This can be easily noticed from Figure 4.2 where it turns out that that at the smallest strain measurable with usual laboratory test soil stiffness is actually half of the initial one.

The major practical deference with this model is that it depends on two more parameters which are:

- The initial or very small-strain shear modulus G_0
- The shear strain level $\gamma_{0.7}$ at which the secant shear modulus G_s is reduced to about 70% of G_0

These parameters are influenced by many factors, but mainly by the void ratio and by the material actual state.

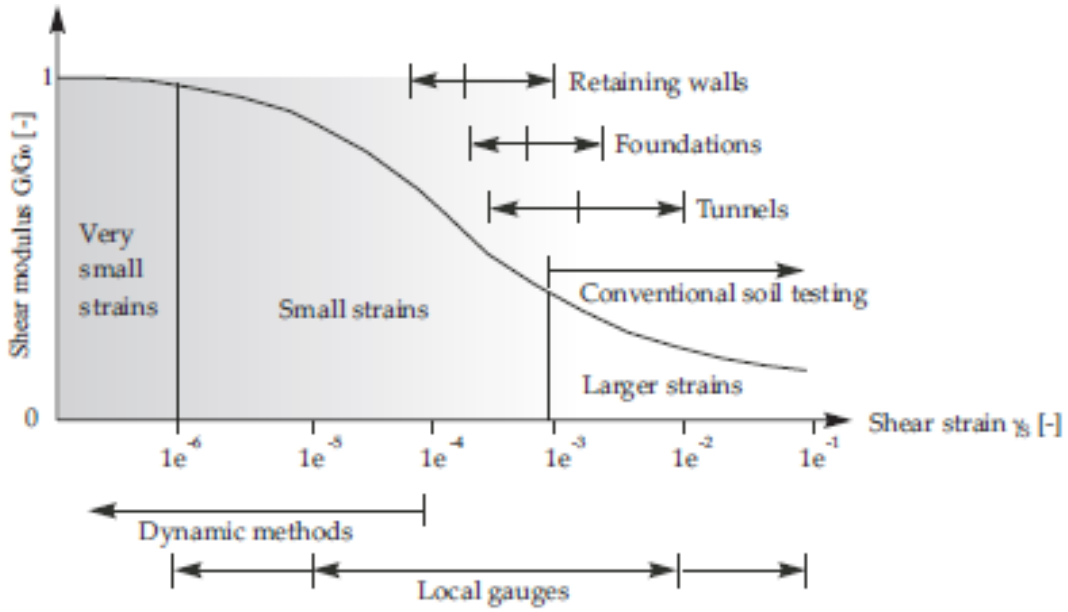

Figure 4.8: Characteristic stiffness-strain behaviour of soil typical strain ranges for laboratory tests and structures (PLAXIS manual, 2019 after Atkinson & Sallfors 1991)

4.2.3. HSsmall in the software

PLAXIS, as already illustrated in the previous chapter, is a computer programme that performs finite element analyses in the geotechnical field, which is the software that was used for the numerical

modelling of the problem under examination, because, in this software, is already implemented the HSsmall model.

In PLAXIS, when a model must be created, it is required a soil material type. In this specific section, it is possible to choose the model that better simulates the behaviour of the case under test. Practically what PLAXIS requires is a set of parameters to define the soil, and this set depends on the model chosen (MC, HSM, HSsmall, etc…).

In the case of HSsmall the required input parameters for defining the soil type are:

- m: power for stress-level dependency of stiffness
- E_{50}^{ref}: reference secant stiffness in standard drained triaxial test
- E_{oed}^{ref}: reference tangent stiffness for primary oedometer loading
- E_{ur}^{ref}: reference unloading/reloading stiffness from drained triaxial test
- ν_{ur} : Poisson's ratio for unloading/reloading
- G_0^{ref} : reference shear modulus at very small strains ($\varepsilon < 10^{-6}$)
- $\gamma_{0.7}$: threshold shear strain at which $G_s = 0.722\ G_0$ (PLAXIS manual, 2019)

The following chapter of this report will be dedicated to the model done with PLAXIS.

4.2.4. Calibration of soil model parameters

Before starting to model the soil, it was necessary to determine the parameters necessary to do so, which are the one presented in the previous section.

The sand used in the experiments is the Fontainebleau NE34 sand and to calibrate the parameters, it was considered a study "Caractérisation mécanique du sable de Fontainebleau NE34 à l'appareil triaxial sous cisaillement monotone" (Andria-Ntoanina et al., 2010). They provided a set of experimental data from triaxial tests on Fontainebleau NE34 sand.

It was considered the four sets of results which consist in two sand specimens with different densities at two different confinement pressures:

- Loose sand ρ_d=1.537 g/cm^3 σ_3=50 kPa e=0.718
- Loose sand ρ_d=1.542 g/cm^3 σ_3=100 kPa e=0.712
- Dense sand ρ_d=1.676 g/cm^3 σ_3=50 kPa e=0.573

– Dense sand ρ_d=1.672 g/cm^3 σ_3=100 kPa e=0.579

It was considered these two sets of data (50 kPa and 100 kPa) because the parameters are stress dependent so just one set wasn't enough to determine parameters that can fit even at different stress levels. This was necessary since by examining a previous study "Experimentation sur tube creux en cuve à sable" (Dano, 2019), it was assumed that in the VisuCuve, the range of confinement pressure is less than 50 kPa but it must be taken into account also the evolution of the mean stress during loading (in particular below the loading plate).

A limitation of HSM is that it is not possible to have a single set of parameters to describe the same soil at different levels of compaction. In fact, the parameters used to define the model vary with the stress but do not depend on density.

To overcome the problem in this study, two sets of parameters were considered to describe the same sand at two different levels of compaction (loose and dense). As stated in the paper "Loading tests on buried flexible pipes to validate a new design model" (Crabb et al., 1985), the compaction of the soil is a key parameter for the performance of buried pipes, and this statement is widely accepted in the literature.

By starting from the first type, we computed all the parameters needed to define the soil material on PLAXIS:

– Since E_{50}^{ref} is the secant stiffness at 50% of maximum deviatoric stress, it was necessary to determine the slope of the line passing through the exact point corresponding to half of q. First it was found, in the data from the test, the maximum deviatoric stress, then it was computed the 50% of this maximum value and so it was possible to establish the corresponding axial strain. Once that these values were fixed, it was possible to compute the slope of the line, and so the value of E_{50}^{ref}.
– For E_{oed}^{ref}, as the software manual and the literature suggest, it was used an approximate value of

$$\cong 1.5 * E_{50}^{ref}.$$

– Since in this triaxial test were performed also some unloading and reloading cycles, it was possible to compute the slope of these loading/unloading curves and an average value was considered for E_{ur}^{ref}.

– The value of G_0^{ref} was computed using the following formula

$$G_{max} * e = 4.38 * {p^{ref}}^{0.56} \text{ [MPa]}$$

Where e is the void ratio and p^{ref} is the reference mean effective stress in kPa.

Table 4.5: First trial stiffnesses computed

E_{50}^{ref}	15.9	MPa
E_{oed}^{ref}	23.85	MPa
E_{ur}^{ref}	69.3	MPa
G_0^{ref}	54.54	MPa

The first test considered in this analysis is subjected to a confinement pressure of 50 kPa, but it was decided to use $p^{ref} = 100\ kPa$, so using the formulas given before the starting values of the stiffness were computed.

Table 4.6:Stiffnesses computed with p_{ref}=100 kPa

E_{50}^{ref}	21.4	MPa
E_{oed}^{ref}	42.8	MPa
E_{ur}^{ref}	114	MPa
G_0^{ref}	80.4	MPa

Then by using the PLAXIS tool Soil test, it was simulated a triaxial test using the HSsmall model with the previous values found, other data taken from the test and instead, some of the other parameters needed were determined by consulting the literature. (Figure 4.9)

The Soil test option in PLAXIS is a convenient procedure to check the behaviour of the selected soil material model with the given material parameters. After entering the model parameters, the user can quickly simulate several standard soil lab tests and compare the results against the results from actual laboratory tests. (PLAXIS manual, 2019)

Parameter	Value
Saturated weight density, γ_{sat} (kN/m^3)	18.5
Unsaturated weight density, γ_{unsat} (kN/m^3)	16.5
Friction angle, φ' (°)	33
Dilatancy angle, ψ (°)	8
Cohesion, c' (kPa)	1.0
Coefficient of lateral earth pressure, K	0.5
Initial (small-strain) shear modulus, G_0 (MPa)	85
Shear strain corresponding to $0.7G_0$, $\gamma_{0.7}$	4×10^{-3}
Tangent oedometric stiffness, $E'_{oed}{}^{ref\,a}$ (MPa)	18
Secant stiffness in drained triaxial test, $E'_{50}{}^{ref}$ (MPa)	18
Unloading/reloading stiffness, $E'_{ur}{}^{ref}$ (MPa)	45
Unloading/reloading Poisson's ratio, ν_{ur}	0.2
Reference pressure for stiffness, p_{ref} (kPa)	100
Power for stress-level dependency of stiffness, m	0.5
Interface strength reduction factor, R_{inter}	0.9

[a] $E_{oed}{}^{ref}$ set equal to $E_{50}{}^{ref}$ in the absence of an appropriate reference.

Figure 4.9: HSsmall parameters for Fontainebleau sand from Sheil et al. 2016.

Table 4.7:Other parameters necessary in the software to model the loose sand

Friction angle	φ_{peak}	34	°
Dilatancy angle	ψ	4	°
Weight density	γ	15.5	kN/m^3
Cohesion	c	1	kPa
Unloading/reloading Poisson's ratio	ν_{ur}	0.2	-
Power law	m	0.5	-

Coefficient of earth pressure at rest	K_0	0.5	-
Shear strain threshold	$\gamma_{0.7}$	$4*10^{-3}$	-
Interface strength reduction factor	R_f	0.9	-

Where the interface strength reduction factor is defined as the failure ratio q_f/q_a (see Figure 4.7), it is not a soil property and it set by default equal to 0.9.

This procedure was performed for both loose and dense sands, in order to find a unique set of parameters that can represent the soil at both confinement pressures with a unique p^{ref} of 100 kPa. The final set of values is reported here:

Table 4.8:Final set of parameters in loose sand

E_{50}^{ref}	21	MPa
E_{oed}^{ref}	42	MPa
E_{ur}^{ref}	110	MPa
G_0^{ref}	65	MPa
ψ	4.5	°

In the following Figures 4.10 and 4.11 are reported the curves resulting from the 2 triaxial tests performed on loose sand compared with the ones obtained through the simulation done on PLAXIS with the parameters illustrated before.

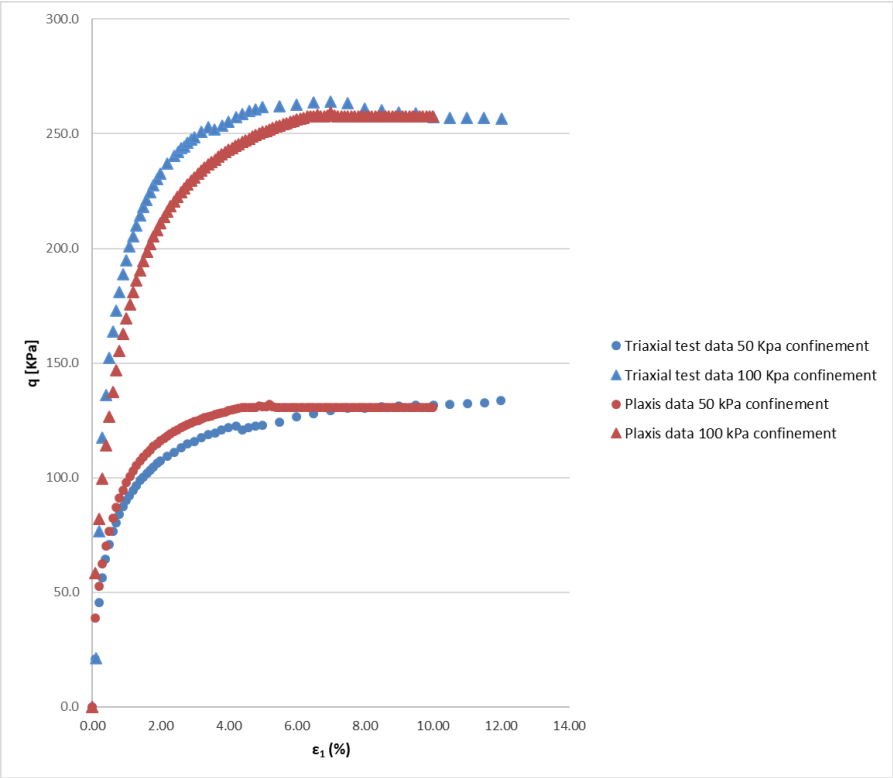

Figure 4.10: Deviatoric stress evolution curve with axial strain in loose sand

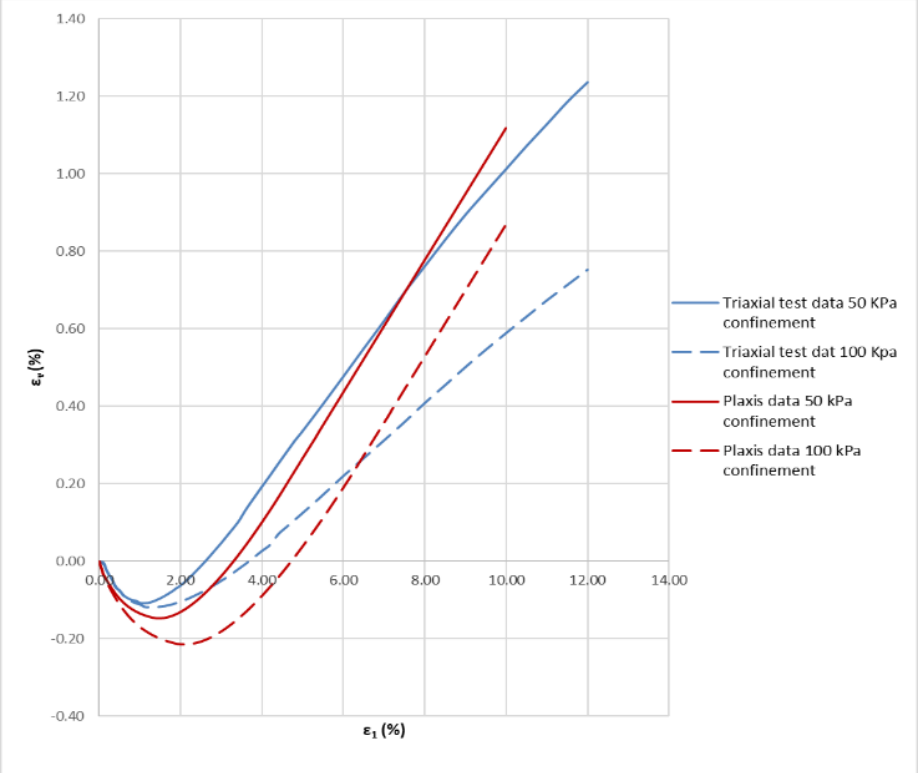

Figure 4.11: Volumetric strain evolution curve with axial strain in loose sand

By observing these graphs, it is possible to say that a good agreement was achieved, especially in the small strains range, which is the area of interest in our analysis. So, this model can simulate the stress dependency of the parameters with good approximation.

Then the parameters for the dense sands with 2 different confining stresses were examined. First the friction angle, dilatancy angle and density have been changed, related to that also G_0^{ref} had to be changed since it depends on the void ratio.

Table 4.9: Other parameters necessary in the software to model the dense sand

Friction angle	φ_{peak}	41	°
Dilatancy angle	ψ	15	°
Weight density	γ	16.5	kN/m^3
Shear modulus	G_0^{ref}	100.8	MPa

The other parameters necessary for HSsmall on PLAXIS were the same values as before. By starting from the stiffness parameters found for the loose sand, these values were adjusted to better fit the triaxial data from both tests performed on dense sand. Here are reported the final values obtained after the calibration process and the graph comparing the curves obtained from the tests and the curves obtained from the simulation on PLAXIS. (Figure 4.12-13)

Table 4.10: Final set of parameters in dense sand

E_{50}^{ref}	33	MPa
E_{oed}^{ref}	45	MPa
E_{ur}^{ref}	110	MPa
G_0^{ref}	100	MPa

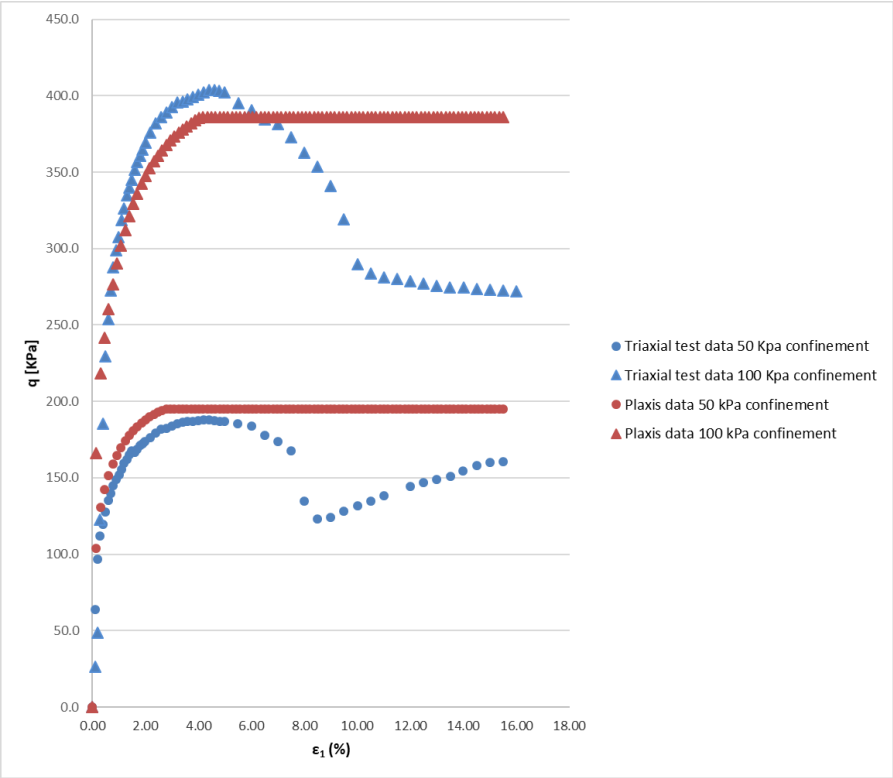

Figure 4.12: : Deviatoric stress evolution curve with axial strain in dense sand

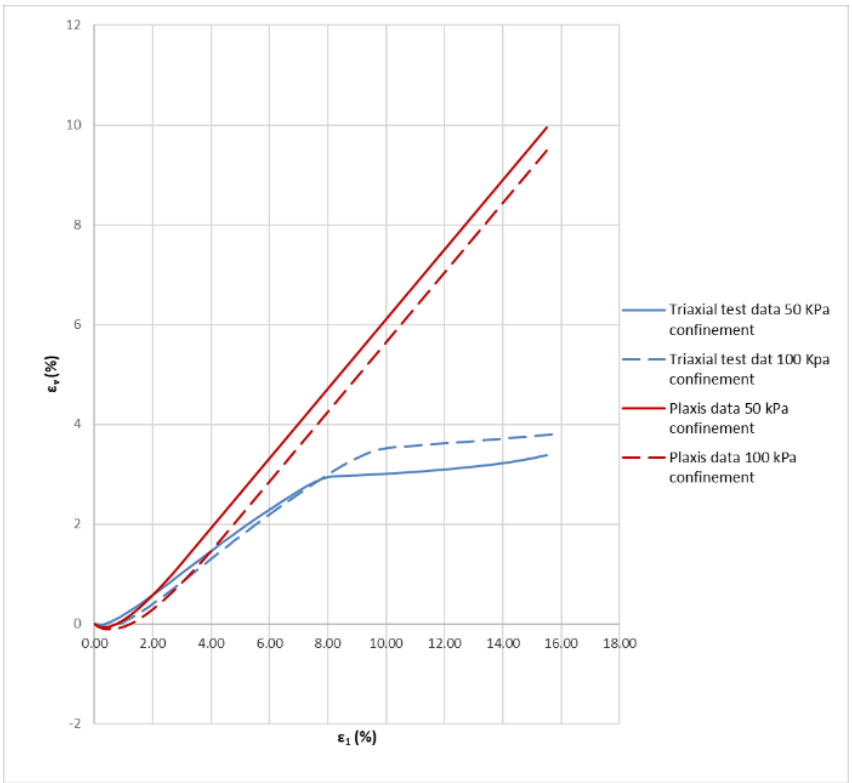

Figure 4.13 Volumetric strain evolution curve with axial strain in dense sand

In conclusion, we can say that the HSsmall model simulates the behaviour of the soil and the stress dependency of the parameters that define it but just at small strains. At larger strains, the model diverges from the real behaviour of the soil. In this problem, we are interested in small strains, so even if we don't have a perfect fit, the model was acceptable.

By observing Figure 4.12 and 4.13 as explained in the book "Geotechnical engineering" (Lancellotta, 2008) in both cases it is observed that, when sheared, the soil tends towards an ultimate (asymptotic) or stationary condition, in which shearing can continue without changes of volume or effective stresses. But in loose sand, by applying a deviatoric stress, the sand has a ductile behaviour with a direct tendency to the stationary condition. Instead in the case of the dense sand, there is a volume increase corresponding to the increase of deviatoric stress until the peak is reached. After this maximum point, in a dense sand it is observed an unstable behaviour, softening, since with the following strains there is also a reduction in the deviatoric stress until an asymptotic value is reached. This specific behaviour, found in dense sand, is not simulated on PLAXIS, that's why in Figure 4.6b the curve from the simulated model is not perfectly following the same path as the one extrapolated from the real triaxial test.

Here in table are summarized the parameters used to model the soil illustrated previously.

Table 4.11:Soil model parameters

Parameter	Symbol	Dense sand value	Loose sand value	Unit
Weight density	γ	16.5	15.5	kN/m^3
Void ratio	e	0.573	0.718	-
Friction angle	φ_{peak}	41	34	degree
Cohesion	c	1	1	kPa
Unloading/reloading Poisson's ratio	ν_{ur}	0.2	0.2	-
Power law	m	0.5	0.5	-

Parameter	Symbol	Dense sand value	Loose sand value	Unit
Coefficient of earth pressure at rest	K_0	0.5	0.5	-
Shear strain threshold	$\gamma_{0.7}$	$4*10^{-3}$	$4*10^{-3}$	-
Interface strength reduction factor	R_f	0.9	0.9	-
Reference secant stiffness in standard drained triaxial test	E_{50}^{ref}	33	21	MPa
Reference tangent stiffness for primary oedometer loading	E_{oed}^{ref}	45	42	MPa
Reference unloading/reloading stiffness from drained triaxial test	E_{ur}^{ref}	110	110	MPa
Reference shear modulus at very small strains	G_0^{ref}	100	65	MPa
Dilatancy angle	ψ	15	4.5	degree

4.3. Introduction to the numerical simulations performed

The problem under consideration has been analysed under different aspects. As already illustrated above, first of all, the effect of the scale was investigated, so two models were realized, one at full scale and one at the scale of the experiments. These initial models are of relevant importance for the future experimental campaign, but there could be possible numerical scale effect coming from the elastic moduli that are stress dependent.

In the small-scale model, it was also decided to investigate the influence of the pipe thickness on the behaviour of the tube itself under the effect of a uniformly distributed static load. The behaviour of the models at both scales undergoing a loading and unloading cycle was also investigated.

In the following chapter, different kinds of results and outputs obtainable from the numerical modelling process will be presented. The software allows to obtain different results in output at all stages of construction and loading of the model. It was therefore decided to extract the output data at specific loading (or unloading) phases, in which the amount of applied stress at both scales is respecting the scaling factor of 1/3rd, in order for the results to be comparable (example, 10kN/m model scale, 30kN/m at prototype).

Table 4.12:Loading steps selected for the analysis

Loading steps extracted in LOOSE SAND	
Model scale	Prototype scale
0 kN/m	0 kN/m
10 kN/m	30 kN/m
20 kN/m	60 kN/m
40 kN/m	
Unloading 20 kN/m	Unloading 60 kN/m
Unloading 10 kN/m	
Unloading 0 kN/m	
Loading steps extracted in DENSE SAND	
Model scale	Prototype scale
0 kN/m	0 kN/m
20 kN/m	60 kN/m
50 kN/m	150 kN/m
60 kN/m	180 kN/m
100 kN/m	

Unloading 100 kN/m	
Unloading 60 kN/m	Unloading 180 kN/m
Unloading 20 kN/m	
Unloading 0 kN/m	

In this way, the results are comparable at different scales showing at the same time the different responses of the models to the increase (or decrease) of the load. These are all the phases extracted but for the different analysis, just some of them are used. The details will be presented in the following chapters before starting the discussion about the results.

In order to compare solicitations and stresses in the pipe that are expressed at different scales (i.e., model and prototype), it was decided to normalize them. Before going in details of the normalization, it is interesting to discuss about which results that will examinated. First of all, two main solicitations normal force N_θ and bending moment M_{fz}, where were extracted. The hoop stress is the stress which is induced inside a vessel in the transverse direction (perpendicular direction of the longitudinal axis). The resulting stress, acting in the pipe, is given by the combination of the normal force and the bending moment. In case of earth load, the formula is the following:

$$\sigma_{\theta\theta} = \frac{N_s}{S} \pm \frac{M_{s,z}}{I_{g,z}} \cdot y \qquad [Hoeg, 1968;\ Moore, 2001]$$

In figure 4.14 is reported a scheme to help to understand how this solicitation are acting in the pipe and to which section they are referred.

To do the normalization, the maximum admissible solicitation of the cross section was considered. In this extent if it is the only solicitation acting, the maximum admissible solicitation is defined as being the solicitation that would induce a stress equal to the yielding stress of the material. The normal force has been normalized with regard to the maximum admissible normal force $N_r$with:

$$N_r = \sigma_k \times h$$

σ_k being the yield stress and h height of the section A-A.

- Yielding stress at model scale: 120 MPa

– Yielding stress at prototype scale: 360 MPa

The bending moment has been normalized with regard to the maximum admissible bending moment $M_{r,z}$, calculated as follows:

$$M_{r,z} = \pm \frac{\sigma_k \times I_{g,z}{}'}{y}$$

with $I_{g,z}{}'$ the quadratics moment over the z'-axis, y half the pipe thickness, and σ_k the yielding stress.

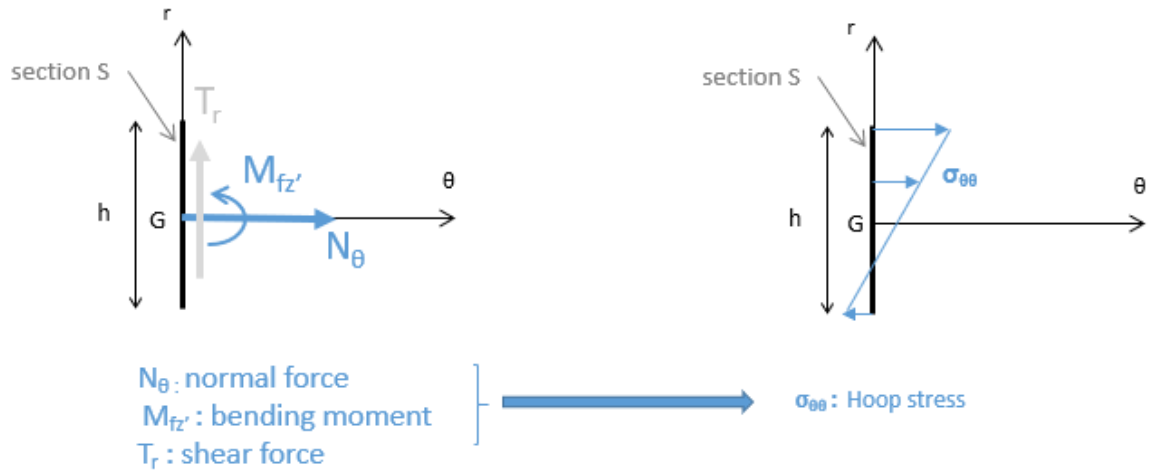

Figure 4.14: Tube internal forces and stresses

After definition of the maximum admissible solicitation, the ratio of acting and resisting solicitation will be calculated, and the ratio at prototype and model scales can be directly compared one to one, since it is an adimensional metric, freed from the similitude problematics.

Also the actions at the soil-pipe interface, normal stress and shear stress were extracted from the software. To normalize these stresses, it was decided to divide them by the value of stress acting under the loading plate for the phases considered for the comparison. So, for the case with the loose sand it was considered 20 kN/m^2 at small scale and 60 kN/m^2 at full scale. For the dense sand, 60 kN/m^2 and 180 kN/m^2 were considered at small scale and full scale respectively. In this way, adimensional stress ratios were obtained and the results at different scales are therefore comparable.

5. Comparison of the numerical study at model and prototype scale

In this part, the results about the comparison of data extracted at different scales will be presented and discussed. The goal is to discuss the match between the values at model scale and prototype scale. To do so, the normalization method explained before had been used to make the results comparable (the “raw” results are not directly comparable, since they are not at the same scale).

All the results concerning the pipe or the interface between pipe and soil are plotted with polar coordinates in order to be more readable. In order to help locating on the pipe, the following convention on angle was adopted (Figure 5.1):

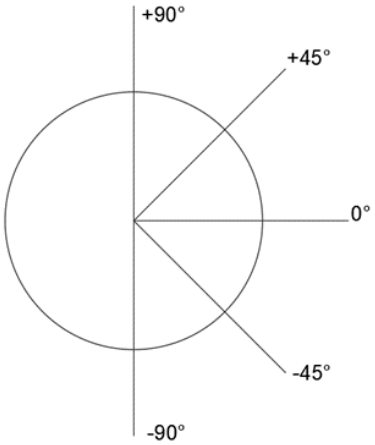

Figure 5.1:Angles convention

For the stresses, the convention of sign of continuum mechanic was assumed, with compression being negative.

In the case of perfect similitude, the results should be, after all care given to make them comparable, strictly identical. As seen in part 3.1.2, the scaling laws are not perfectly fulfilled when it comes to the soil, introducing error that need to be assessed, in order to conclude on the validity of the design choices. In the following discussion this problem will be examinated, since the effected of this bias will lead to difference between the results obtained at model scale and the ones at prototype scale.

For this section all the plots have the same colours: BLUE for model scale and RED for prototype scale. To have a more facilitated reading the same marker (*, o, +) between related loading phase has been used (for example, 20 kN/m at model scale and 60 kN/m at prototype scale, etc…)).The loading phases considered for this analysis are reported in Figure 5.2.

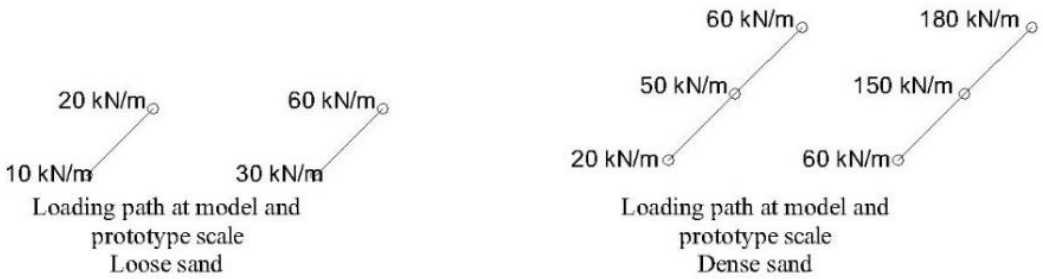

Figure 5.2: Loading path

5.1. Bearing capacity

The bearing capacity (or limit load q_{lim}) represents the maximum pressure that a foundation can transmit to the ground before it reaches rupture.

In strict respect to similitudes conditions, the maximum value of the distributed load applied to the pipe should be 3 times higher at prototype scale than at model one. Actually, failure at model scale, occurs for load that, once up scaled, is higher than the value reached at prototype scale. In the model with the loose sand, failure happens for a maximum load of 60 kN/m but at prototype scale, failure occurs at 80 kN/m, not at 180 kN/m as it should, considering the similitude conditions. The same behaviour can be found in the model with dense sand where at model scale, failure occurs at 140 kN/m and at prototype scale at 200 kN/m of loading instead of 420 kN/m.

This is most likely due to the fact that the soil remains the same at both scales, and its properties remains unchanged, the only thing that changes is the level of stress.

This is an issue inherent to the use of the same soil material at different scale, and its effect will need to be taken into account.

5.2. Solicitation and stresses in the pipe

The solicitation and the resulting stresses are probably the most important results to analyse in order to assess the validity of the model. They are the relevant information that are interesting for engineering practices, and ultimately for the design of the pipe, and compliance to regulation. It is also proposed to study the action that are related to the hoop stress, the latter resulting from the bending moment and the normal force. In order to be able to compare the results obtained at the different scales, as illustrated before (section 4.3), it has been used a "solicitation ratio", the ratio between the acting solicitation, and the pipe maximum effort/stress that the pipe is able to withstand.

5.2.1. Normal force

Under normal operating conditions, the pipes are subjected to an internal pressure caused by gas. The gas pressure is counteracting the earth pressure and opposing the deformations. Therefore, if we consider this condition, the internal pressure of the pipe has a favourable impact on its overall stability. The normal force caused by the weight of the ground and the surface load is therefore in opposition to the internal pressure, therefore unfavourable when it comes to deformations. This work focused on this situation (empty pipe) mainly because it is the most difficult to calculate (the only acting load/pressure is the soil action, that becomes marginal when the pipe is internally loaded, and the gas action is way easier to determine). Also, it is the situation where the deformations are maximum (flexural deformation vs normal deformation), that can cause damage to the pipe. Since the internal gas pressure is null, the normal force impact depends on the sign of the critical bending moment.

The acting normal force N_s has been normalized with regard to the maximum admissible normal force $N_r = \sigma_k \times h$.

- Admissible normal force at model scale= 240 [kN/m]
- Admissible normal force at prototype scale= 2160 [kN/m]

In Figure 5.3 and 5.4 are reported the results from the specific loading phases that were considered for this analysis, respecting the scale factor. The normalized normal force in the model with loose sand, at the various loading steps, is practically constant at the top and at the bottom of the pipe.

Whereas, in the dense sand, it is possible to observe that there is a difference in the solicitation ratio between the loading phases, at θ=±90°, especially between 20 kN/m and 60 kN/m. At θ=0°, in both models, there is some variability in the values of the normalized normal force between loading phases. The solicitation ratio tends to be higher (almost doubled, between the steps, for loose sand, even more for dense sand) for higher loads. It can also be noted that there is variability between the loading steps at different scales. One could therefore think that the scaled model is underestimating the effects of the normal force stress, but by analysing these graphs, the soil scale effect must be taken into account. The soil in fact remains unchanged between the two models and this affects the results. Considering therefore the maximum capacity ($N_r = 1$ failure reached), it has been found that at both scales the overall stress remains low.

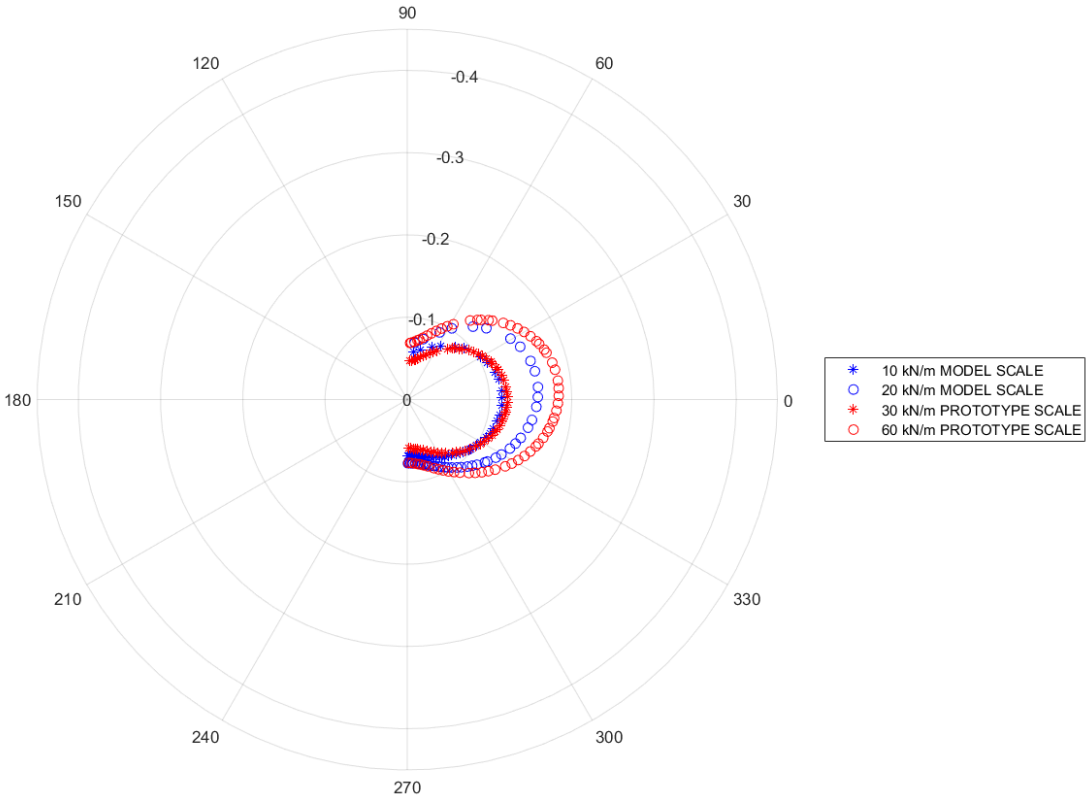

Figure 5.3: Normalized normal force (%) on the pipe in loose sand

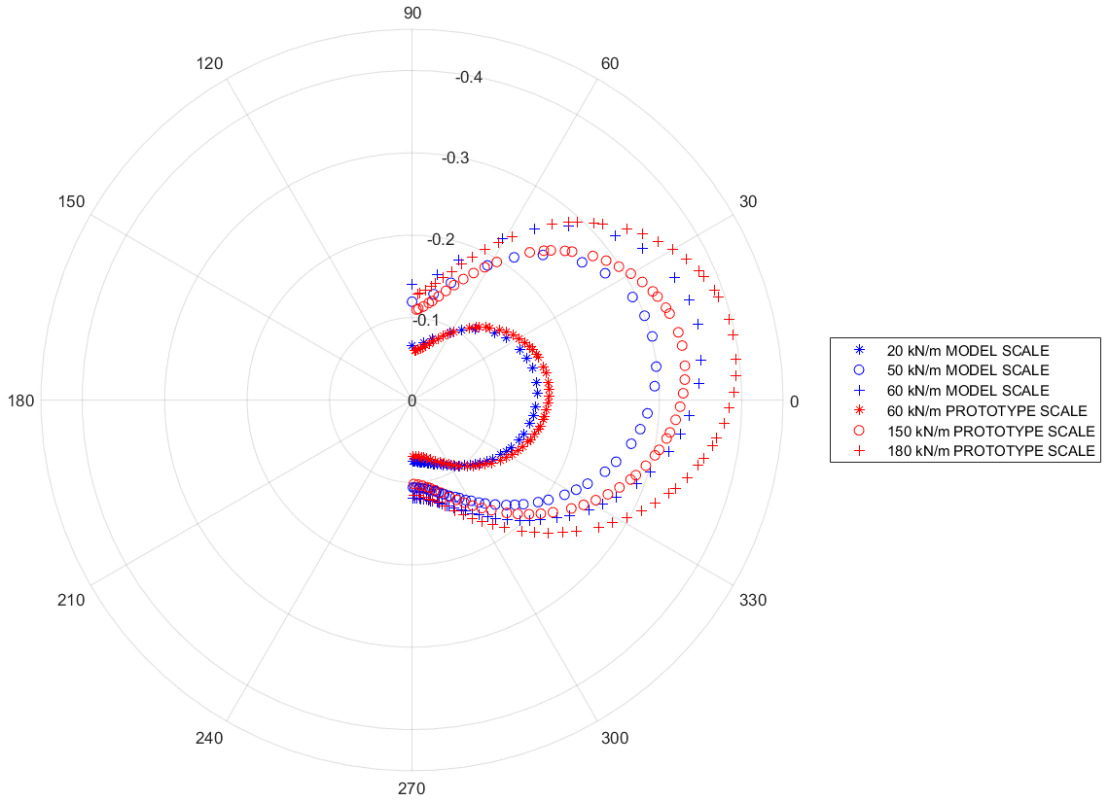

Figure 5.4: Normalized normal force (%) on the pipe in dense sand

5.2.2. Bending moment

The bending moment is the solicitation that generally creates the higher overall stress in pipeline, after the inner pressure. This solicitation is highly sensitive to the ratio between the stiffness of the pipe and the one from the soil (Moore, 1987).

The plots show the ratio between the acting bending moment M_s, and the maximal admissible bending moment $M_{r,z} = \pm \frac{\sigma_k \times I_{g,z}}{y}$.

- Admissible bending moment at model scale= 0.08 [kNm/m]
- Admissible bending moment at prototype scale= 2,16 [kNm/m]

The bending moment in the pipe around the local axis z' perpendicular to the plan of deformation is reported in Figure 5.5 and 5.6 for the models with both sands. The bending moment has negative values around θ=±90°, so at top and bottom of the pipe, with null values around θ=±45°.

The qualitative agreement between both scales is rather good, but we still see some variation between the prototype and model scale, with the same tendency already seen for the normal force. The model scale seems to underestimate (in absolute value) the intensity of the solicitation due to bending moment compared to the prototype scale.

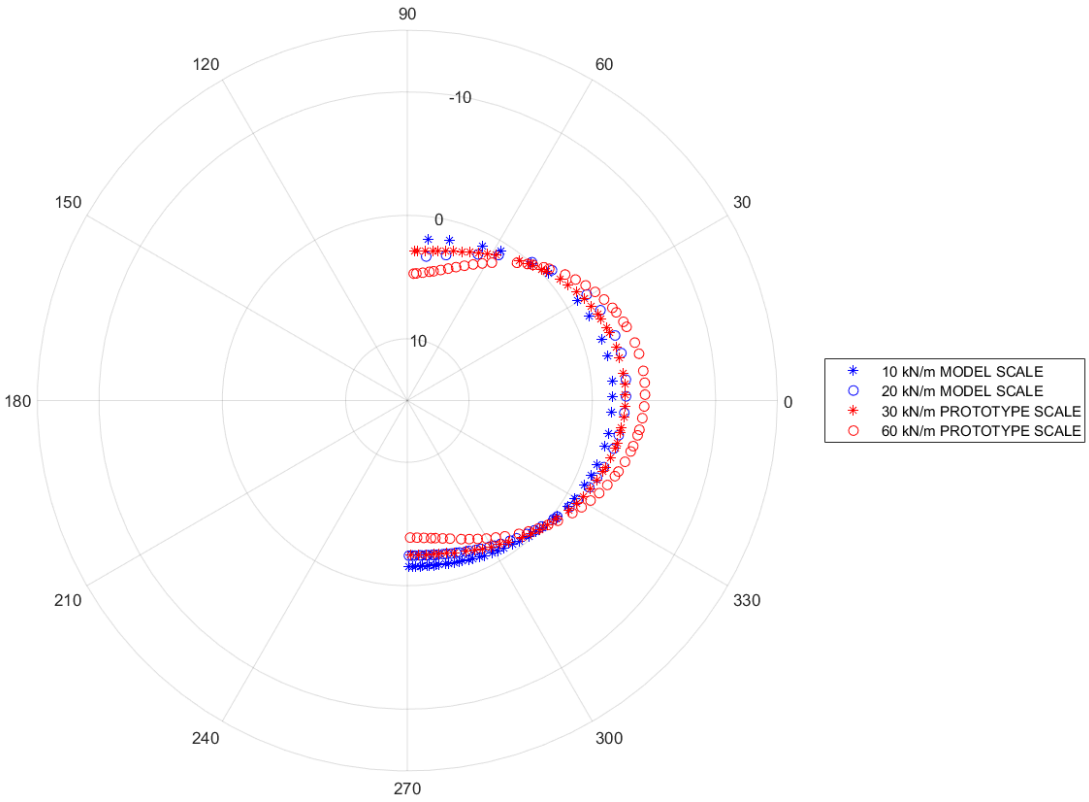

Figure 5.5: Normalized bending moment (%) on the pipe in loose sand

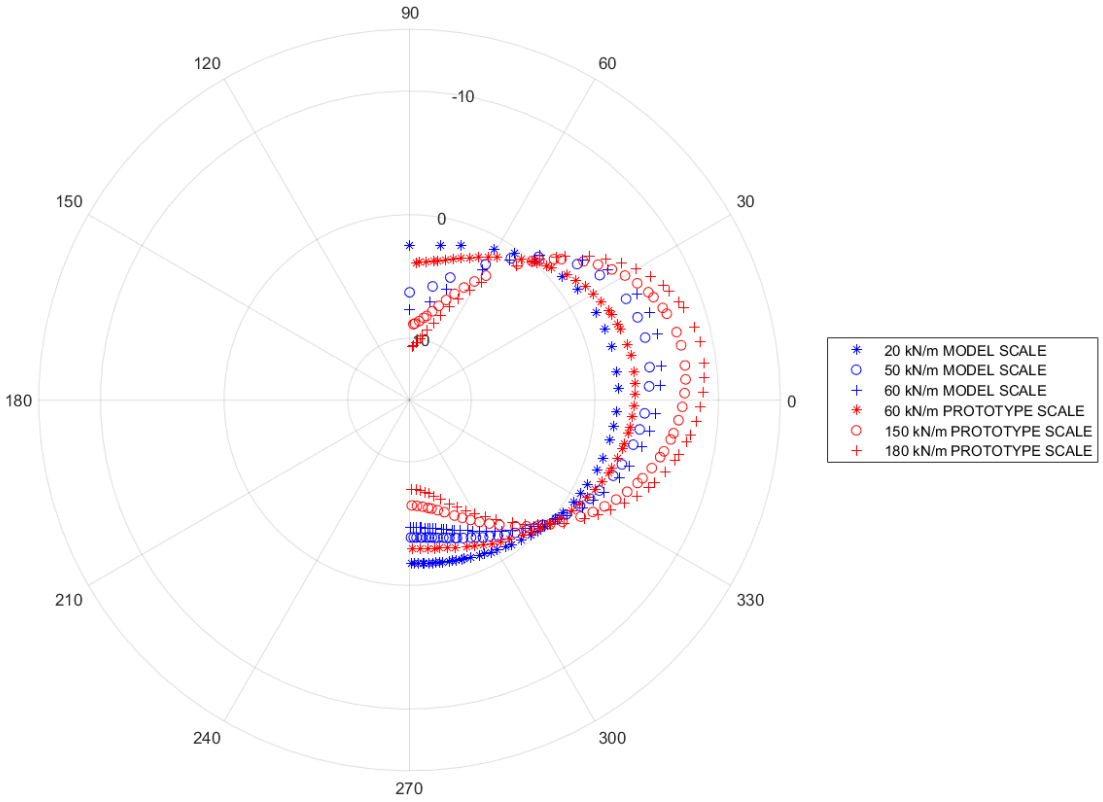

Figure 5.6: Normalized bending moment (%) on the pipe in dense sand

5.2.3. Hoop stress

The hoop stress is the final object of interest, since the regulations are formulated accordingly to this metric. It can be referred to the internal or external face of the pipe, were it reached its maximum absolute value. In this case it was decided to consider the maximum value, in absolute, of the two, since it is the most critical and interesting one. Again, the results are plotted in function of the angle θ and the results plotted refer to the loading phases indicated before. In Figure 5.7 and 5.8 are reported the results in normalized form. In this case, the values of the maximum hoop stresses are divided by the yielding stresses of the pipe material.

At both scales and with both sand densities, the pattern is the same and mirrored between top and bottom parts of the pipe. Since the normal force is always negative, the maximum resulting hoop stress will be negative, i.e. compression. Around $\theta = \pm 45°$ the values reach zero, this means that there is a switch, first the outer part of the pipe is in compression that the inner and then again the outer.

Again here the same behaviour can be found, in fact, the model scale underestimates the values from prototype scale. Again, this behaviour can be caused by the scaling effect on the soil but we can still say that the agreement seems correct, despite the lower values.

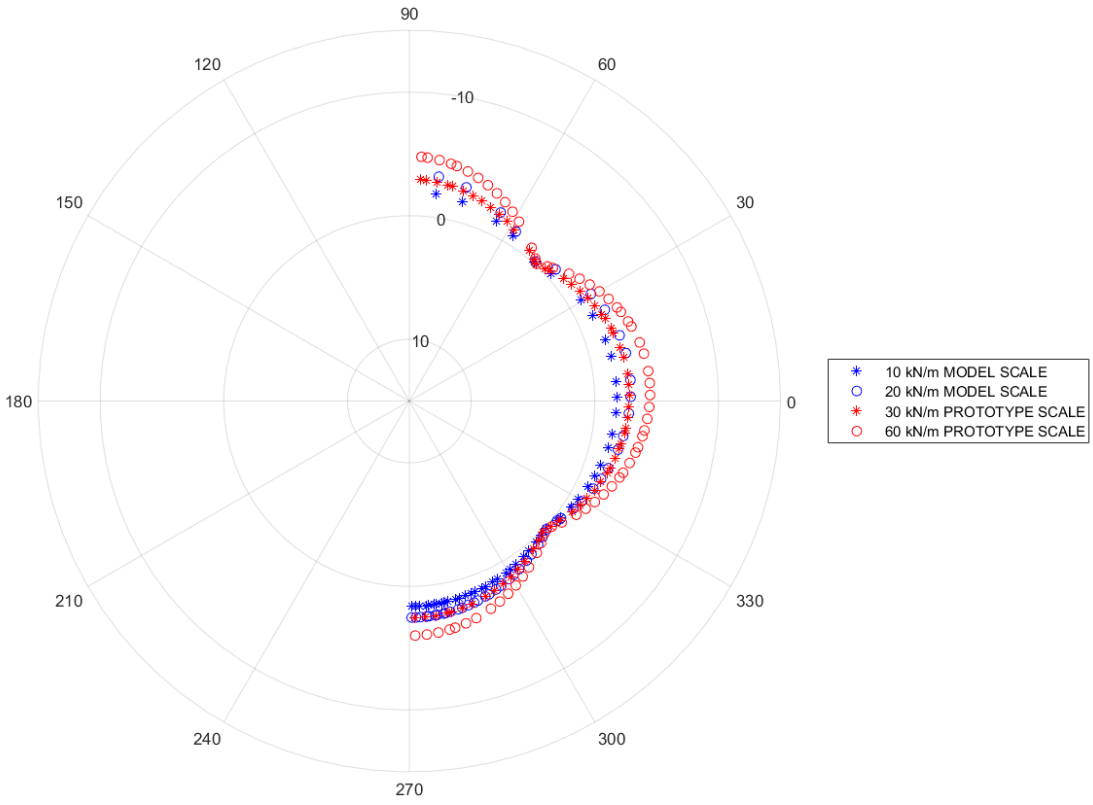

Figure 5.7: Normalized hoop stress (%) on the pipe in loose sand

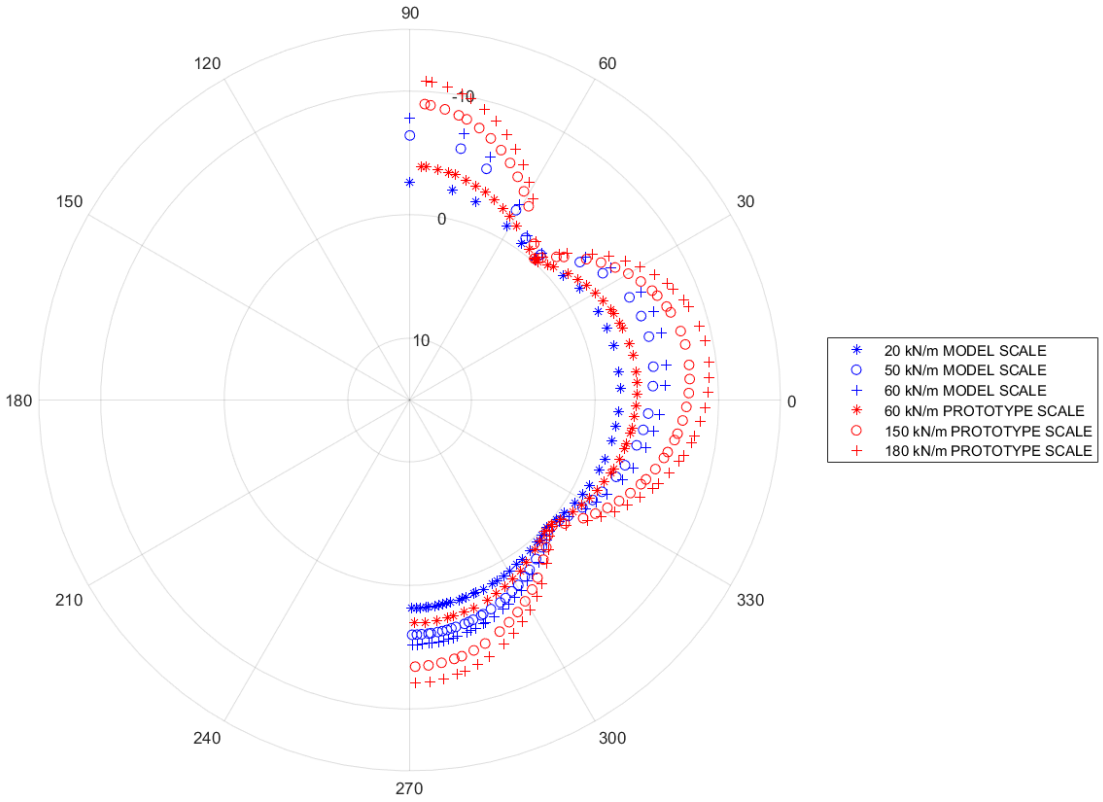

Figure 5.8: Normalized hoop stress (%) on the pipe in dense sand

5.3. Actions at the soil/pipe interface

In this section is reported the evolution of the usual actions typical of the problem of the pipe buried into sand, specially about what happens at the interface between pipe and soil. The values plotted in the following figures are normalized according to the procedure illustrated in section 4.3.

- Stress for normalization in loose sand at small scale= 20 kN/m^2
- Stress for normalization in loose sand at full scale= 60 kN/m^2
- Stress for normalization in dense sand at small scale= 60 kN/m^2
- Stress for normalization in dense sand at full scale =180 kN/m^2

5.3.1. Normal stress at interface

The normal stress in mechanics is the intensity of the net forces acting normal (perpendicular) to an infinitely small area within an object per unit area. In figure 5.9 and 5.10 is presented the normalized normal stress applied by the soil on the pipe at the different phases of loading of the model with the two sands.

It can be noted that the normalized normal stress is almost constant for low loading apart from the top and bottom of the pipe where an increase is registered. In the dense sand a change around θ=30° is registered. Around this angle in fact it can be observed a sudden decrease of the stress, which is more evident for higher loading. In the model with loose sand it can be observed that higher stresses are reached, especially at top and bottom of the pipe.

It must be taken into account that the two sands configurations are normalized by different values of stresses, as illustrated in paragraph 4.3. So, this can influence the final output.

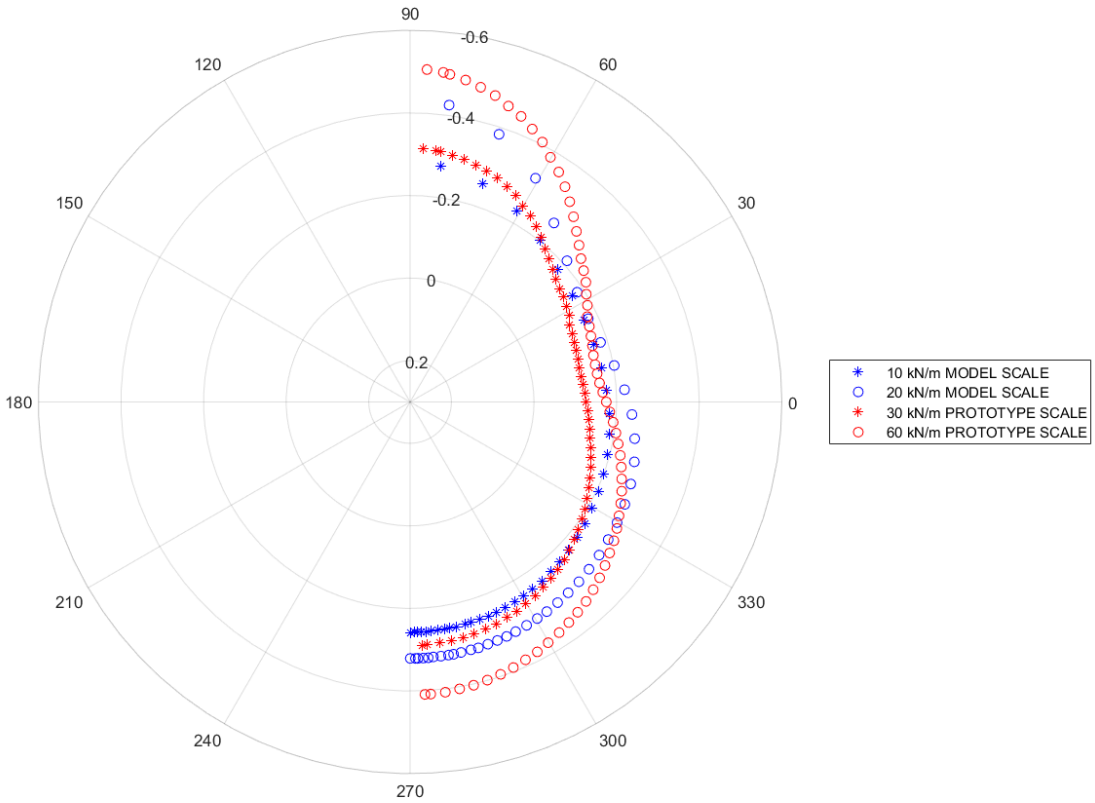

Figure 5.9: Normalized normal stress (%) at interface soil/pipe in loose sand

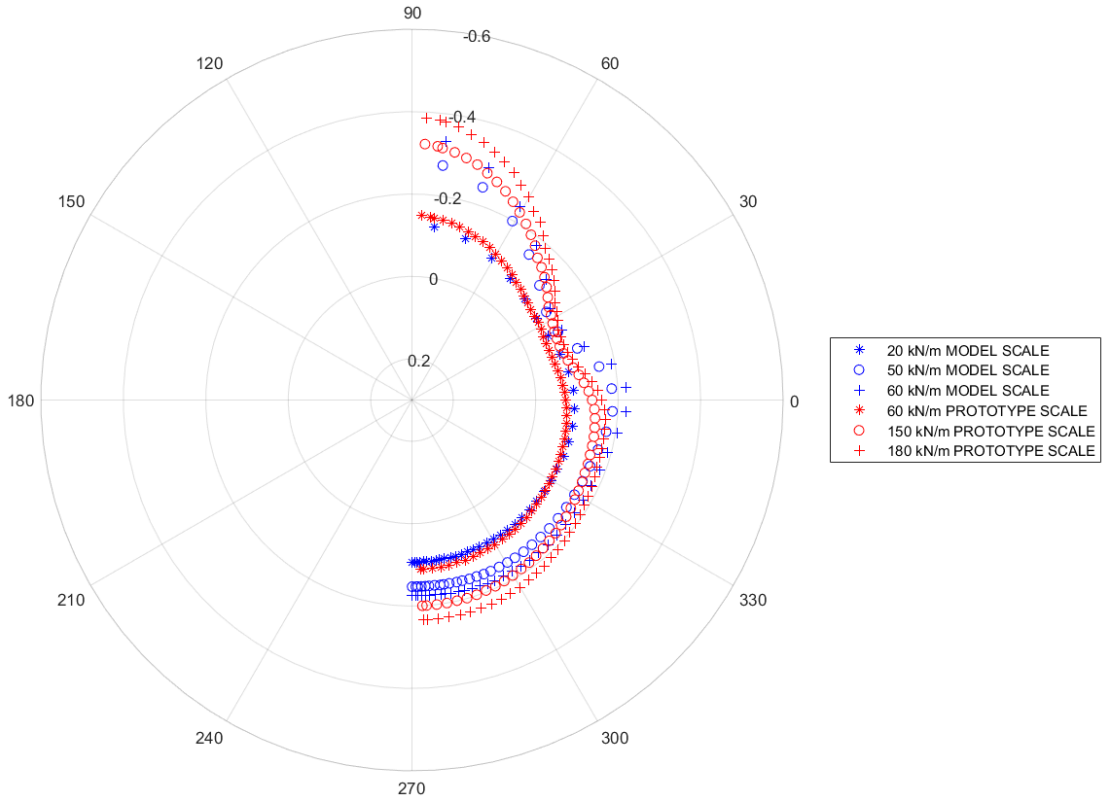

Figure 5.10: Normalized normal stress (%) at interface soil/pipe in dense sand

5.3.2. Shear stress at interface

The shear stress is the intensity of the net forces acting parallel to an infinitely small area within an object per unit area.

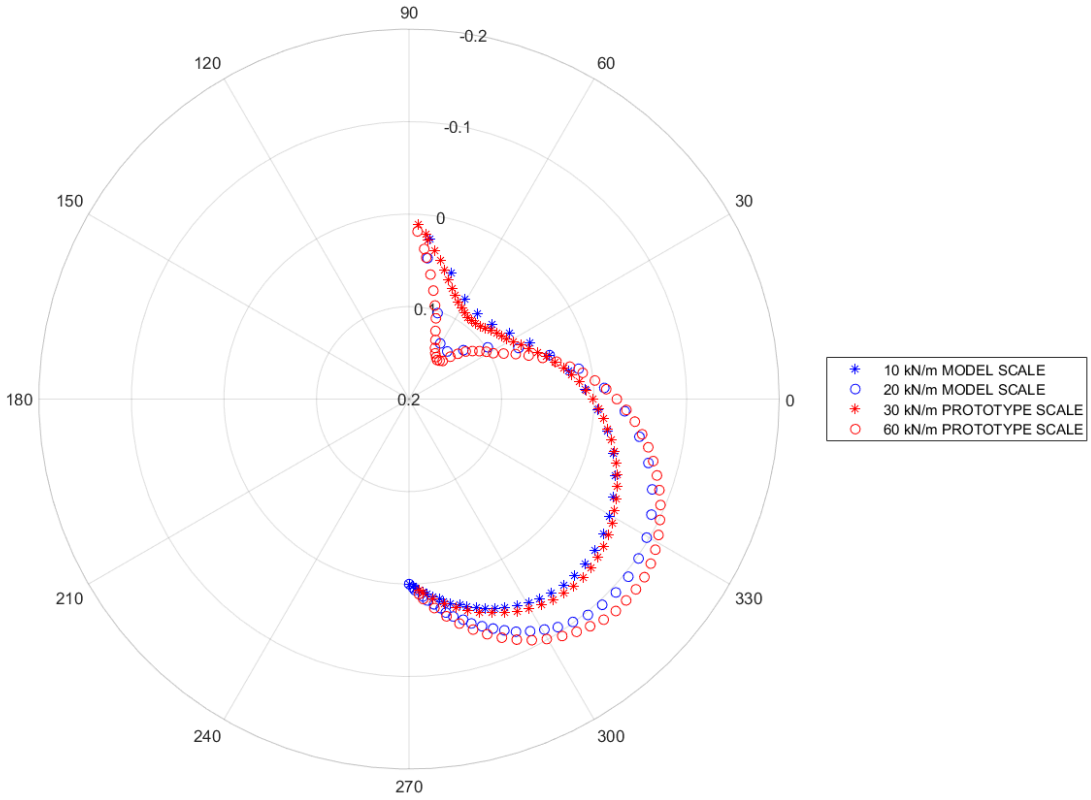

Figure 5.11: Normalized shear stress (%) at interface soil/pipe in loose sand

In figures 5.11 and 5.12 the normalized shear stress at interface is presented, and it can be observed that in both models, with different sand densities, the shear stress follows the same pattern. At higher loading phases, a sudden change is more pronounced around θ=60°, instead with lower loading, this behaviour is less visible.

As in the plot of the normalized normal stress, even the normalized shear stress in the model with loose sand, shows higher values. In this case the difference is less visible but still present, and it is again because by the different normalization between the models.

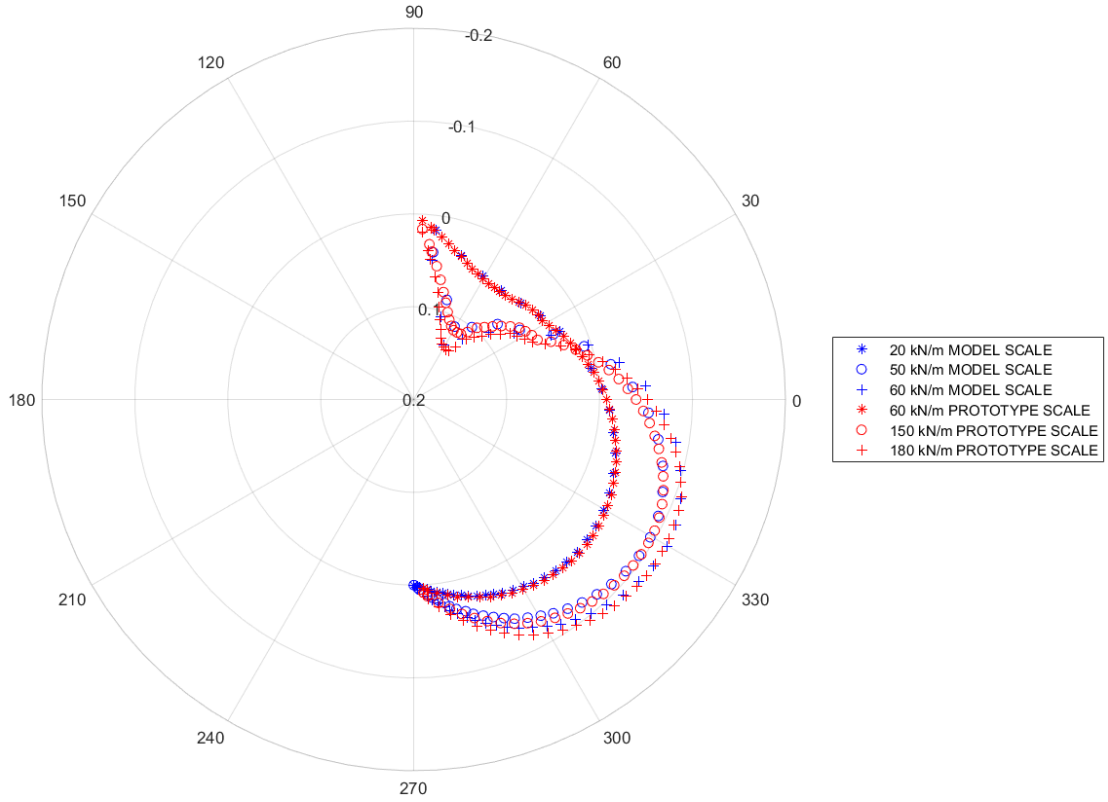

Figure 5.12: Normalized shear stress (%) at interface soil/pipe in dense sand

5.3.3. Stress ratio at interface

The stress ratio is the ratio between shear stress and normal stress. It is an interesting result because it allows to check if there is sliding between the pipe and the soil. Here is analysed the stress ratio at the soil/pipe interface.

In this case the results plotted are not normalized since the stress ratio is already adimensional.

As cohesion is almost null; the limits are given by the tangent of the interface friction angle $\left(\frac{2}{3}\varphi\right)$which is 22.67° for the loose sand and 27.33° for the dense sand.

This limit comes from the Mohr-Coulomb criteria:

$$\tau = c + \sigma_n * tan\left(\frac{2}{3}\varphi\right)$$

Since at interface the cohesion can be considered null, we can directly compare the ratio $\frac{\tau}{\sigma_n}$ with $tan\left(\frac{2}{3}\varphi\right)$. If the values of the ratio are equal to this limit, sliding would occur.

In this case (Figures 5.13-5.14) it can be observed that this behaviour occurs between θ=30° and θ=60° in both sands and also between θ=0° and θ=-60°.

There is a good agreement between the values of the stress ratio at different scales. It can be said that this ratio is not affected by the scaling effect seen before in other plots.

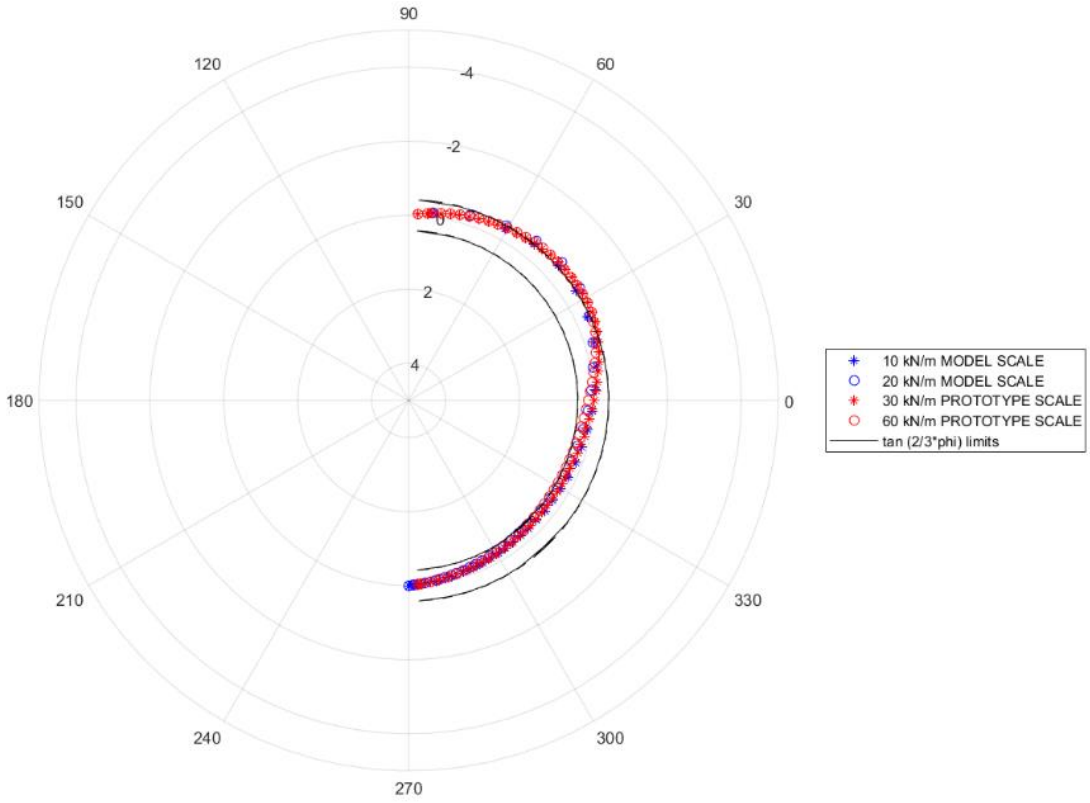

Figure 5.13: Stress ratio at interface soil/pipe in loose sand

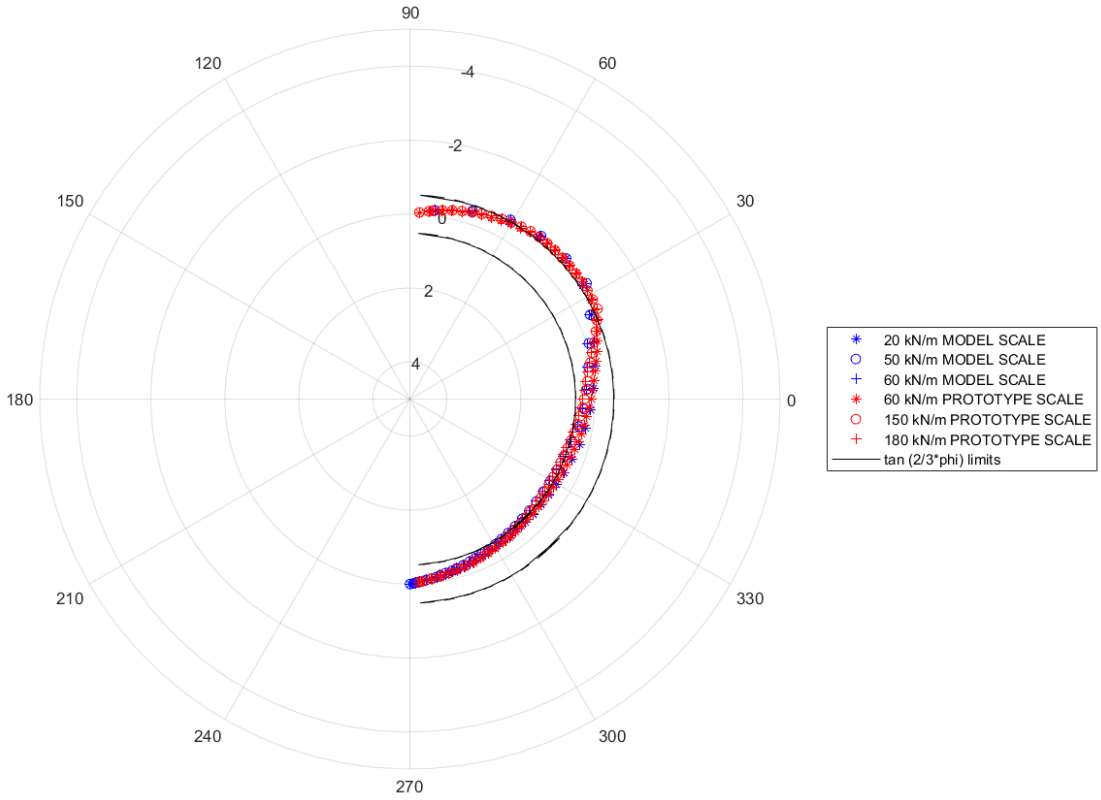

Figure 5.14: Stress ratio at interface soil/pipe in dense sand

5.4. Ovalisation of the pipe

Ovalisation is an important metric to be considered for pipeline, since a heavily deformed pipe may no longer be suitable for its use, or maintenance operations.

This behaviour occurs when the pipe is loaded, even only by the weight of the surrounding soil, it tends to be deformed in an “oval” way. The deformed shape will no longer be a perfectly circular ring. This effect becomes more important when the pipe is free from inner pressure.

The oriented ovalisation is defined as follow; such formulation allowing it to be determined for every orientation of the pipe:

$$O(\theta) = \frac{D(\theta) - D_0(\theta)}{D_0(\theta)}$$

with D_0 initial diameter and D diameter in the deformed state, at orientation.

The results are expressed in percentage of ovalisation.

The agreement between the different scales is rather good, and it is to be noted that the overall ovalisation remains low in those cases. In fact, by comparing it with the results obtained by Boulon (2018), around 1%, it can be observed that the values in this case are lower around 0.1%. (Figures 5.15-5.16)

The main hypothesis can be related to the thickness of the pipe, Boulon used a different pipe with a bigger diameter and a smaller thickness.

GRTgaz are interested in this result because it is rather important to be sure that during the life of the pipe, it won't deform too much. Some internal studies at GRTgaz research department, tend to show that RAMCES is inaccurate when it comes to ovalisation with or without the pipe.

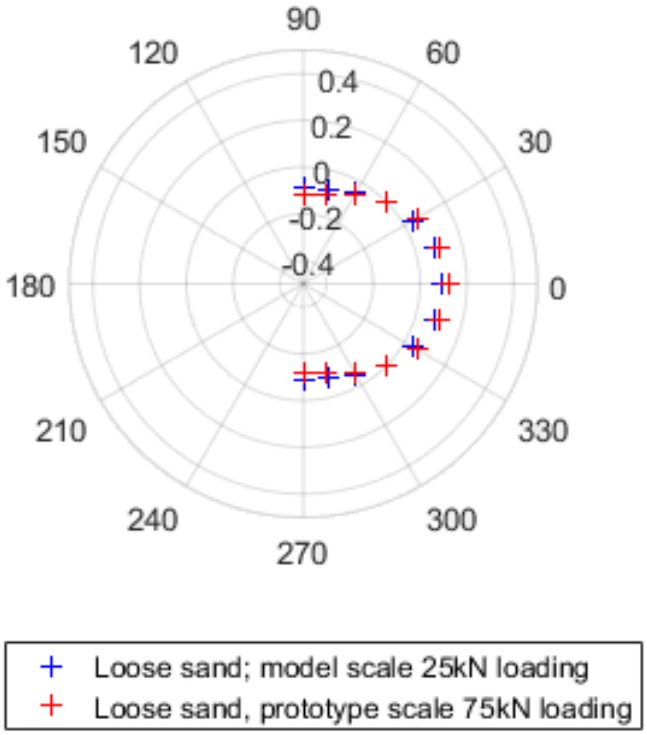

Figure 5.15: Ovalisation of the pipe (%) with loose sand

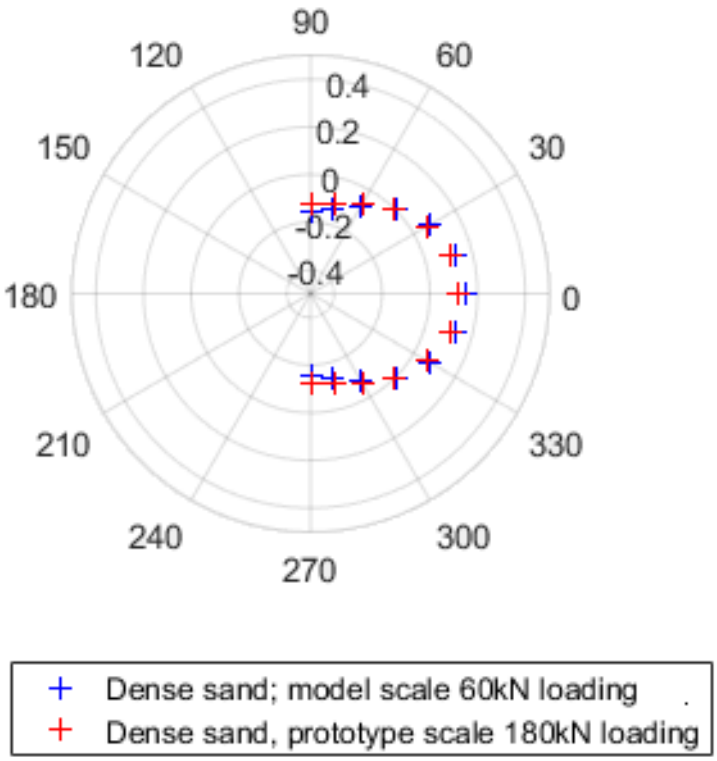

Figure 5.16: Ovalisation of the pipe (%) with dense sand

6. Analysis of the behaviour of the model under loading-unloading cycle

In this chapter are presented the results from the FEM soil/pipe model during a loading-unloading cycle.

It was decided to perform this analysis in order to investigate the nonlinear response of the soil and the influence that this behaviour has on the pipe. This situation may occur in case of a storage area where loads are first stored and then removed.

The loading steps considered for this analysis are reported in a scheme in figure 6.1

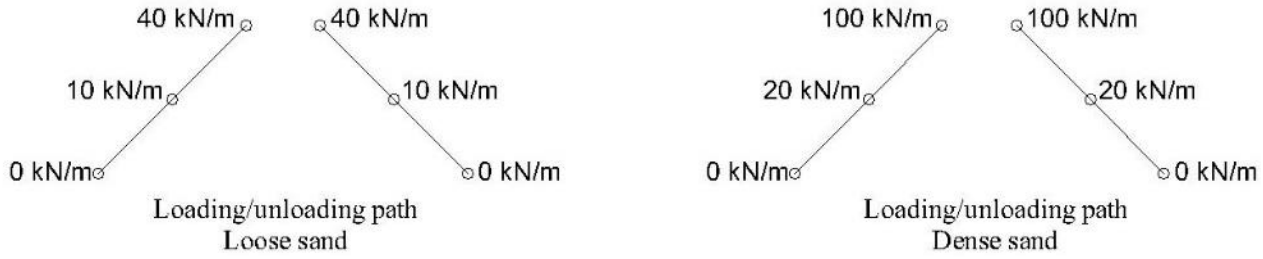

Figure 6.1:Loading-unloading scheme

6.1. Comparison at different scales

The initial idea of this analysis was to perform again a comparison at different scales. While analysing the plot for normalized bending moment (Figure 6.2-6.3) and normalized normal force (Figure 6.4-6.5), in the pipe we conclude that this analysis would be affected by biases.

Table 6.1:Failure phases

	Model scale failure phase	Prototype scale failure phase	Expected prototype scale failure phase
Loose sand	60 kN/m	80 kN/m	180 kN/m
Dense sand	140 kN/m	200 kN/m	420 kN/m

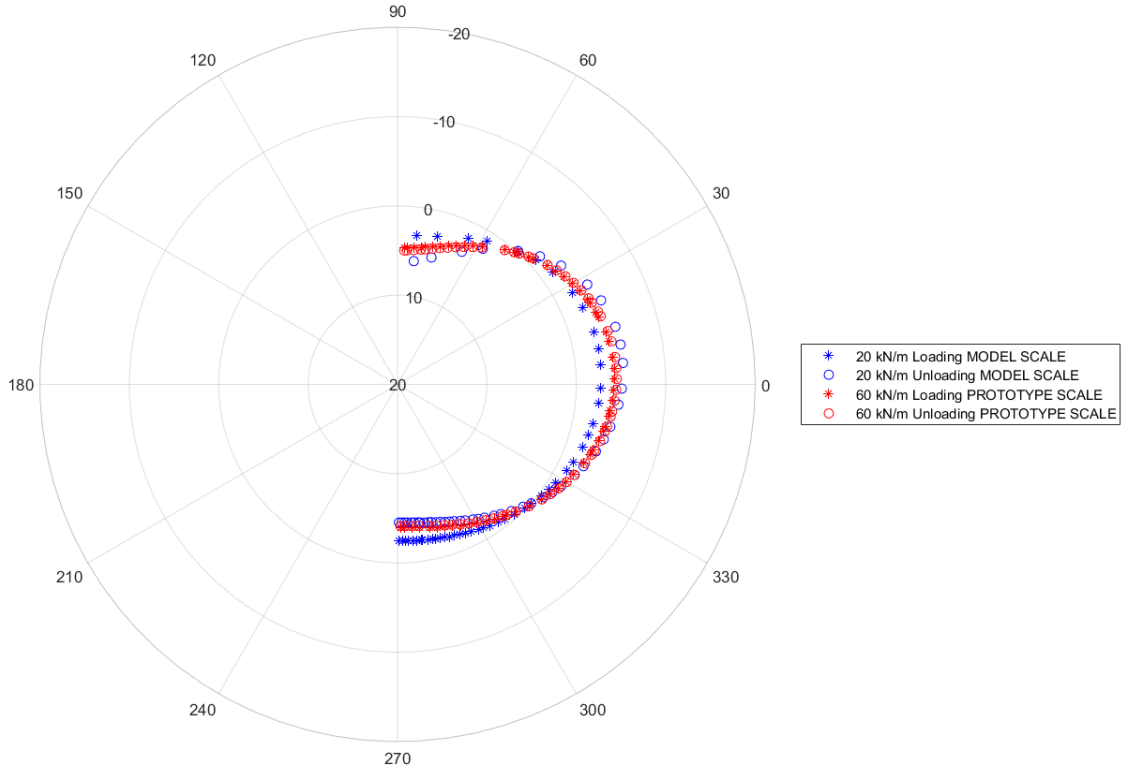

Figure 6.2:Normalized bending moment (%) in the pipe under loading-unloading cycle in loose sand

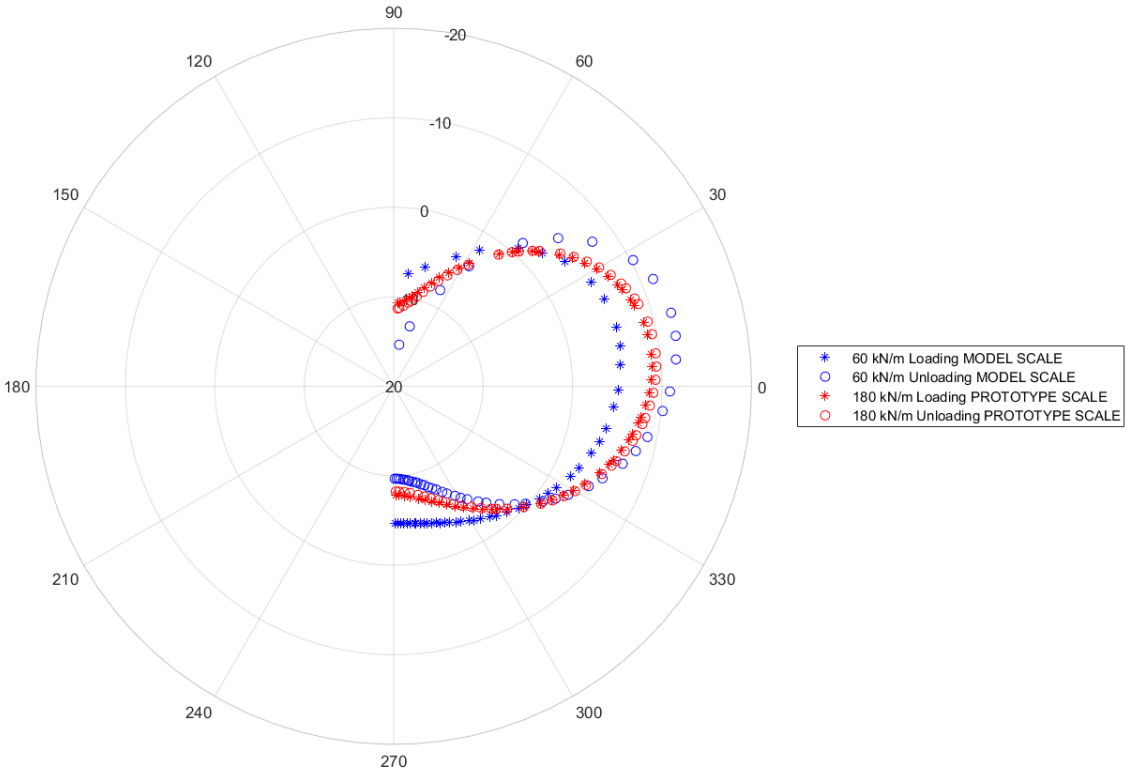

Figure 6.3: Normalized bending moment (%) in the pipe under loading-unloading cycle in dense sand

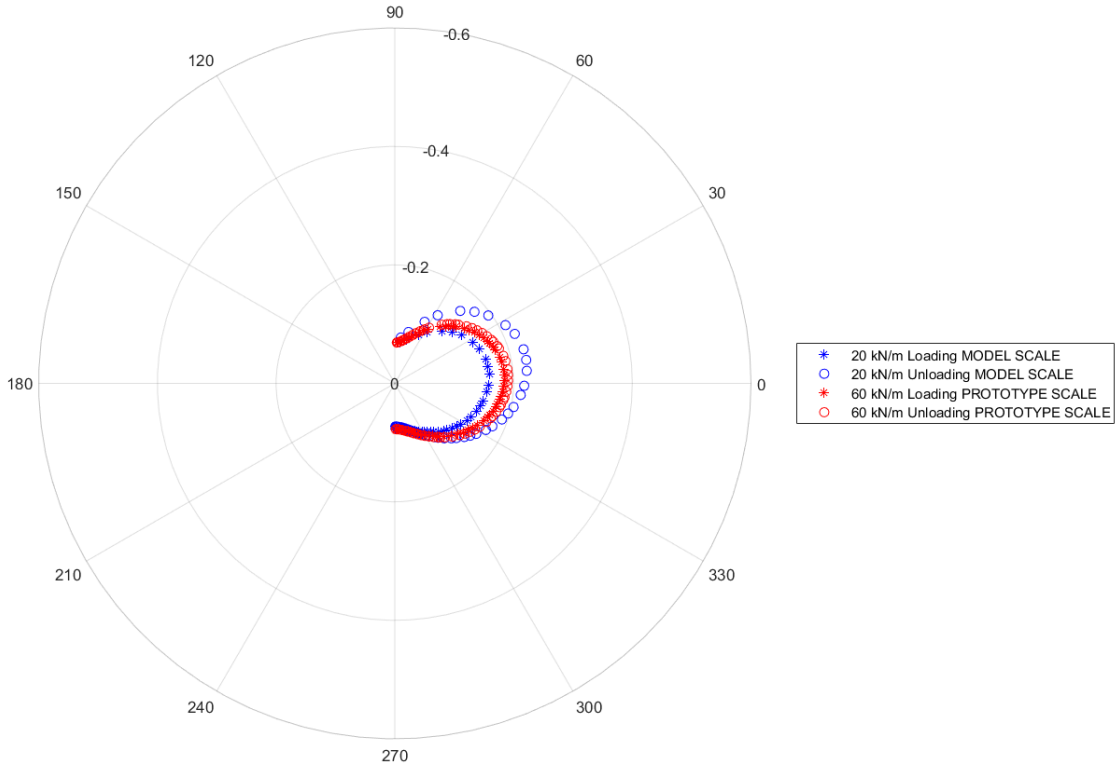

Figure 6.4: Normalized normal force (%) on the pipe under loading-unloading cycle in loose sand

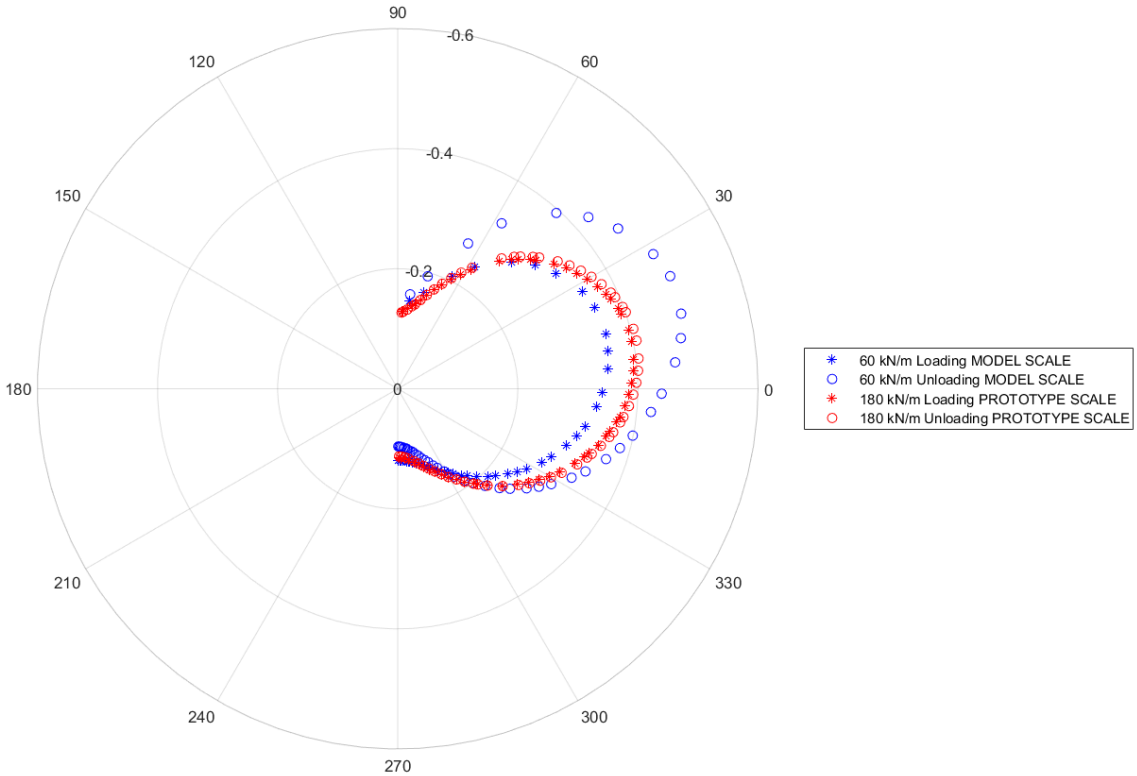

Figure 6.5: Normalized normal force (%) on the pipe under loading-unloading cycle in dense sand

These models are not directly comparable because, due to the non-linear behaviour of the sand, we have inconsistencies in the results of the bearing capacity. As we can see from the table 6.1, the load-bearing capacity does not respect the conditions of similarity and is subject to the scale effect of soil.

As it can be seen from the figures, there is a big difference between the values resulting from the loading and unloading phase at model scale. This occurs because there are other loading and unloading phases in between, while at prototype scales they are directly in succession. So, for this reason no conclusion can be extracted from this comparison. This behaviour is linked to the non-linear behaviour of the sand that later will be analysed more in details.

For the future, to solve this problem, the same loading path could be respected in order to have comparable results.

6.2. Solicitation and stresses in the pipe

The results presented in this section are just at model scale, for this reason they are "raw" data. The normalization was not necessary because no comparison with results from other scale was done.

The solicitation analysed in this section are normal force and bending moment in the pipe, because, as said before in paragraph 5.2, they are relevant information for engineering practices.

For this section, all the plots have the same colours: CYAN for loading phases and BLACK for unloading phases. To have a more facilitated reading the same marker (*, o, +) between related loading phase has been used. (for example, 20 kN/m at loading and 20 kN/m at unloading, etc.)

6.2.1. Normal force

As for the comparison between scales, for this analysis no inner pressure in the pipe was considered, so the pipe is only subjected to the surface load and the action of the surrounding soil.

From Figure 6.6 and 6.7 it can be observed that the values of normal force, in the case of a loose sand, are included between 0 kN/m and -1 kN/m and for each phase they remain quite constant around the pipe. In the model with dense sand, a more important variability can be noted especially for higher loading phases.

In both models, greater stresses are recorded in the unloading path than the stresses recorded with the same loads in the loading phase. This is much more pronounced in the model with dense sand.

Considering the complexity of the soil model there are several factors that can lead to this behaviour. Surely its non-linear nature is the main cause and also the changes in the stiffness moduli that are stress dependent.

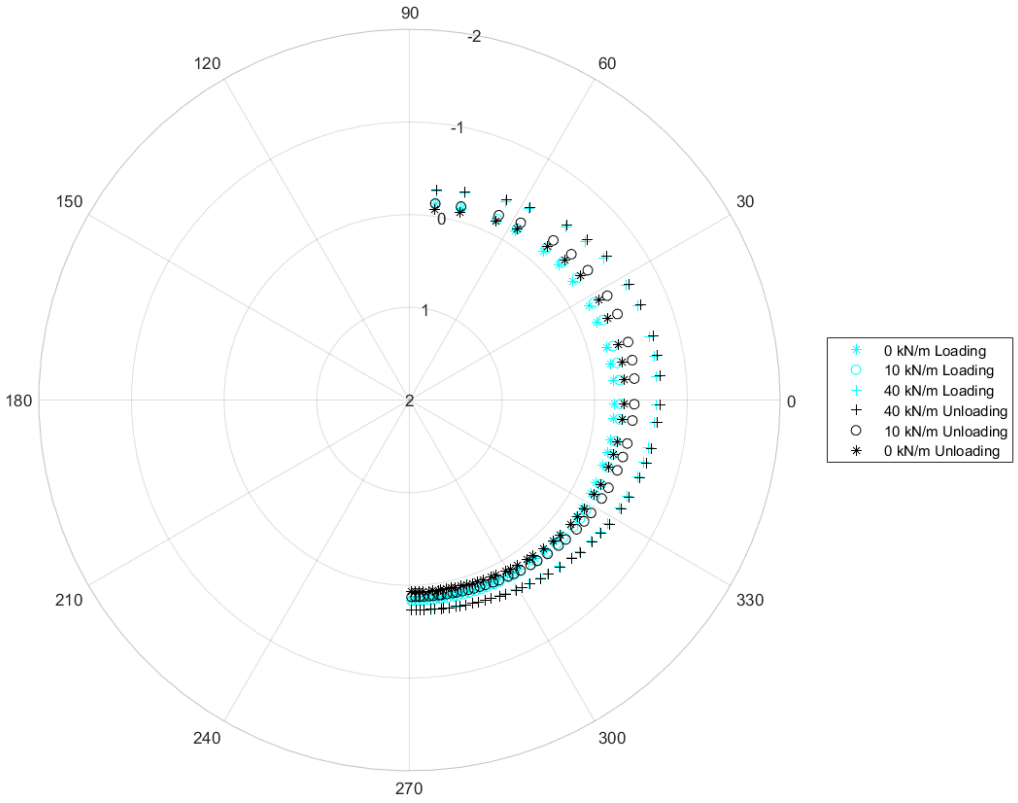

Figure 6.6: Normal force [kN/m] in the pipe under loading-unloading cycle in loose sand

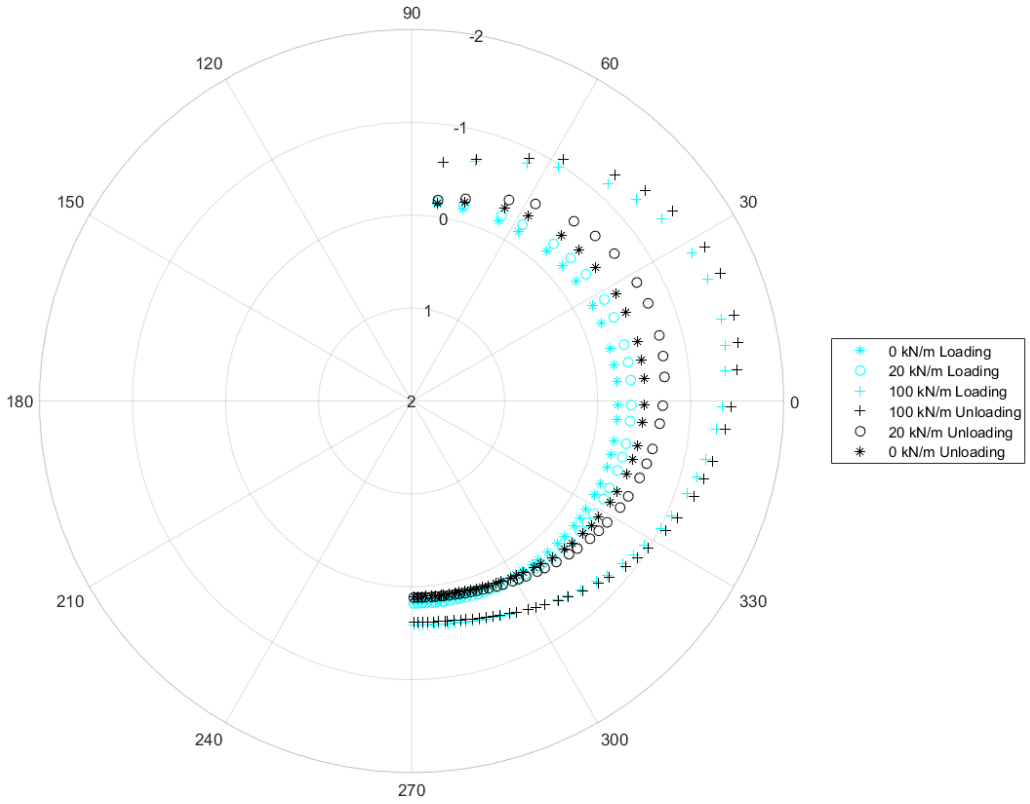

Figure 6.7: Normal force [kN/m] in the pipe under loading-unloading cycle in dense sand

6.2.2. Bending moment

The bending moment is the other important solicitation that was analysed, and the results obtained are reported in figure 6.8 and 6.9.

By first analysing the loading path, it can be noted that at low loading steps (0 kN/m, 10 kN/m and 0 kN/m, 20 kN/m) the values of the bending moment are almost null. Instead for the last step of loading and for all the unloading steps, the values are varying. At $\theta=\pm 90$ the values are still positive, but around $\theta=\pm 60$ they become negative.

The values of the bending moment are low, they are almost always included in the interval between 0.01 kN m/m and -0.01 kN m/m and the maximum admissible value is 0.08 kN m/m. It can also be observed that, apart from the last loading/unloading phase, there is quite a difference in the solicitation between the two paths. The hypothesis to try to understand this behaviour is the same as for the normal force and as before the pattern is more evident in the dense sand.

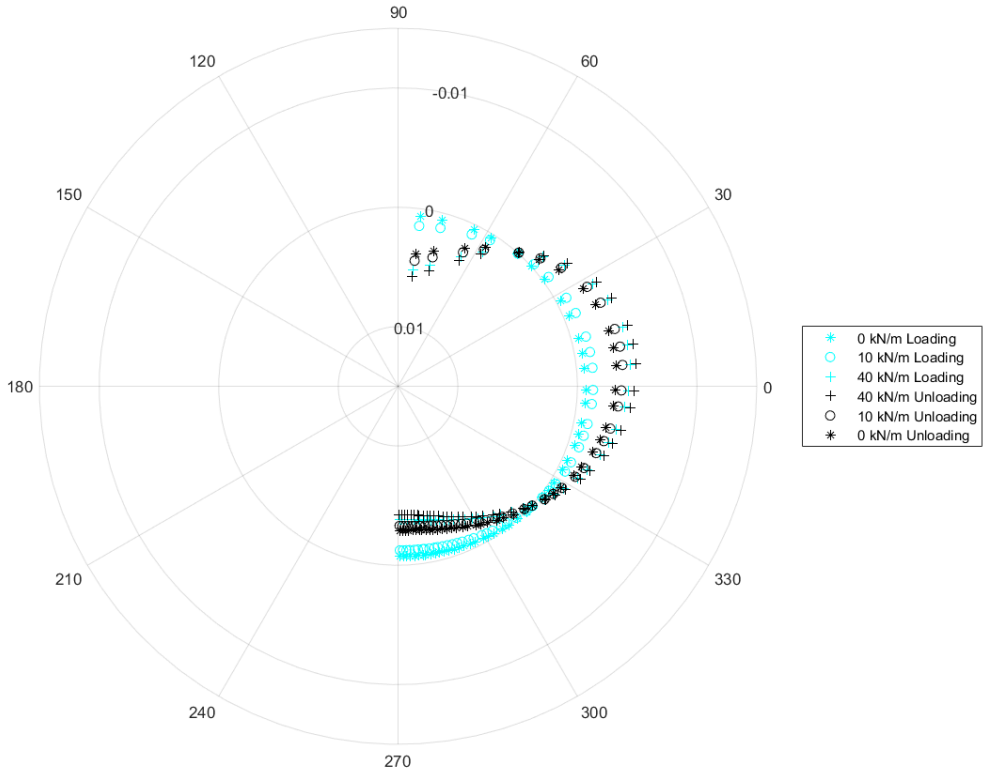

Figure 6.8: Bending moment [kN m/m] in the pipe under loading-unloading cycle in loose sand

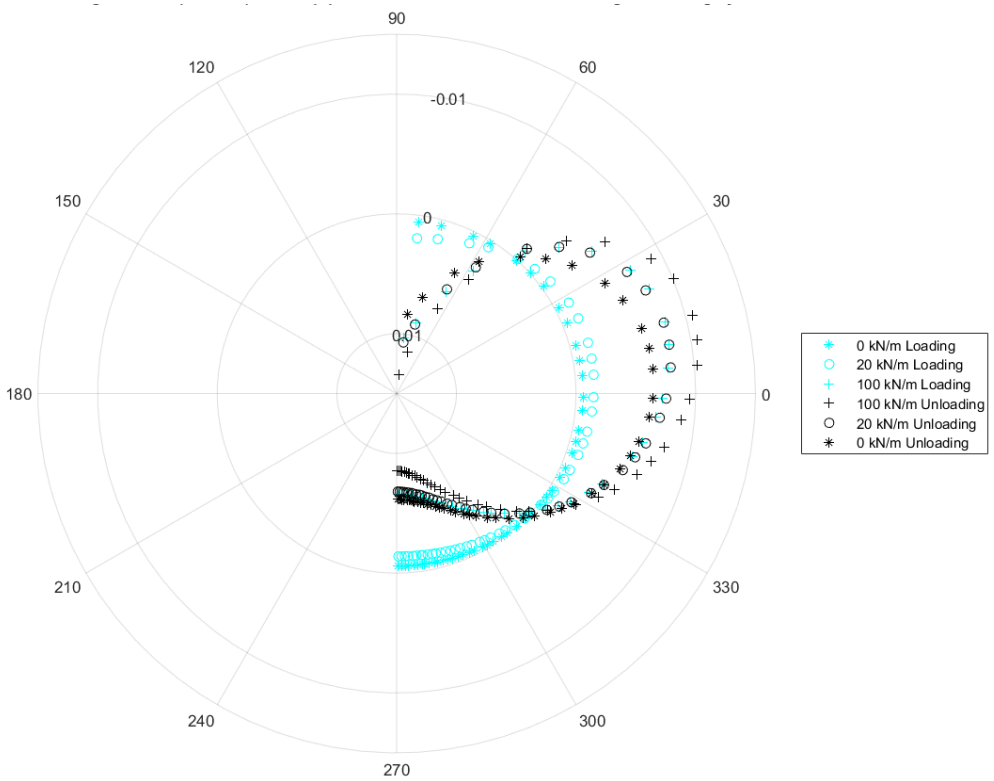

Figure 6.9: Bending moment [kN m/m] in the pipe under loading-unloading cycle in dense sand

6.3. Actions at the soil/pipe interface

In this section the action at the soil/pipe interface are analysed, in particular normal stress, shear stress and the stress ratio. The same convention and colour code adopted in the chapter before will be adopted for this section.

6.3.1. Normal stress at interface

The normal stress applied by the soil on the pipe at the different phases of loading and unloading is presented in figure 6.10 and 6.11.

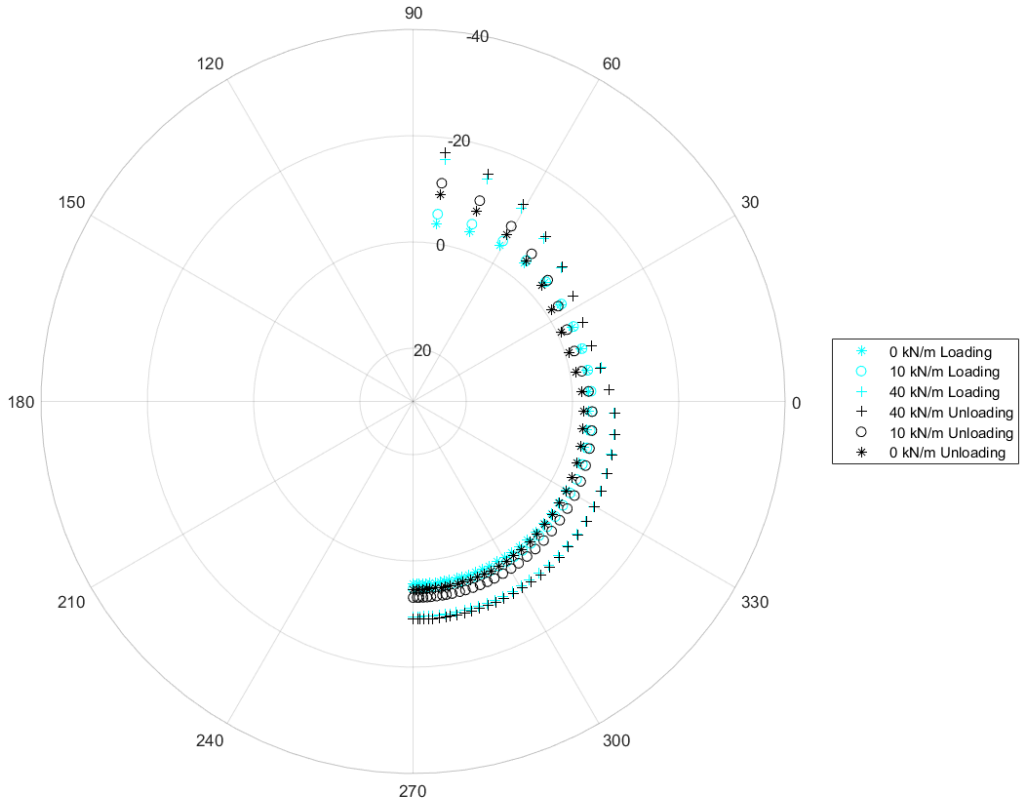

Figure 6.10: Normal stress [kPa] at interface soil/pipe under loading-unloading cycle in loose sand

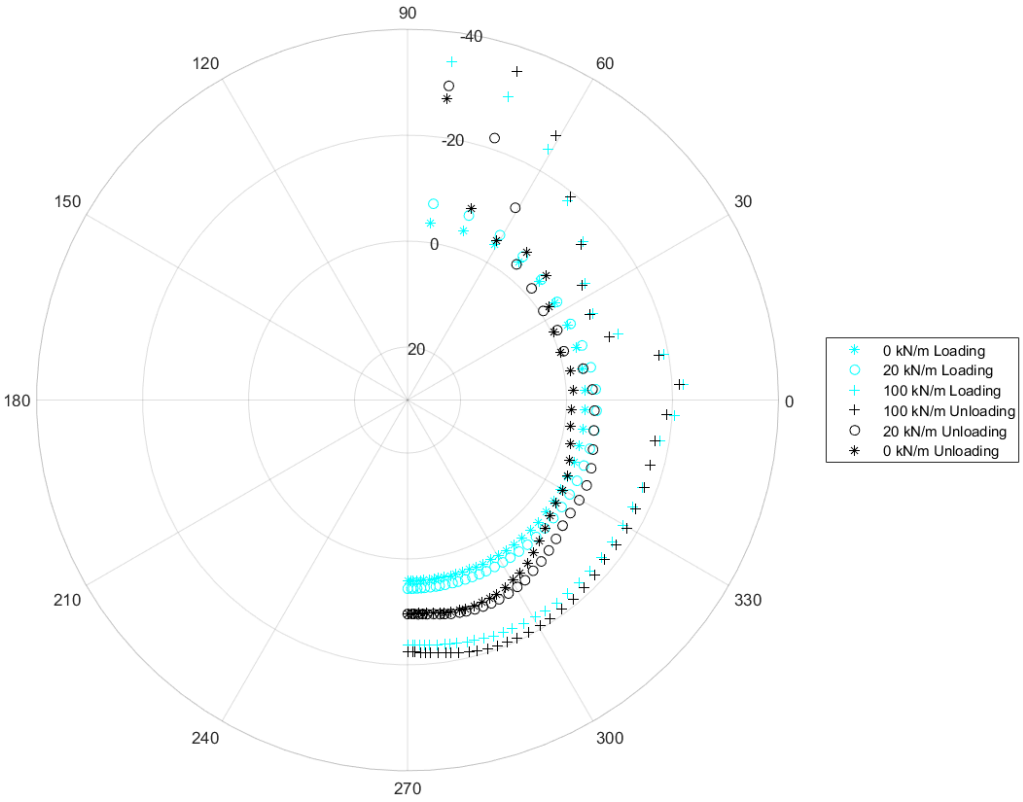

Figure 6.11: Normal stress [kPa] at interface soil/pipe under loading-unloading cycle in dense sand

The values of the normal stress are always negative, i.e. the soil is applying compression on the pipe, and quite constant for the initial phases of loading (0 kN/m and 10 kN/m for loose, 0 kN/m and 20 kN/m for dense). In the following phase of loading and in all the unloading phases, a variability in the values is registered especially at the top and bottom of the pipe. Here, in fact, the values are higher with respect to the initial phase and higher with respect to the values registered in the other parts of the pipe.

Concerning the differences between loading and unloading, it can be noted that there is quite a good agreement and less differences, as found for the solicitation. This is not true for points around $\theta=\pm 90°$ where the values are more scattered, this last behaviour is less evident in the model with loose sand, but in the dense sand is more evident. It can be noted, then, that in the unloading phase the stresses are higher.

Another area of variability is between $\theta=15°$ and $\theta=0°$ in the dense sand, where a sudden increase is registered, for 100 kN/m of loading.

6.3.2. *Shear stress at interface*

The other interesting action at interface extracted from the software is the shear stress (Figures 6.12-6.13).

In this case, the pattern followed by loose and dense sand is quite the same for what concern the sign of the values. They both present a shear stress at interface positive between θ=90° and θ=30° and after that negative or almost null in the other points of the pipe. Concerning the differences between loading and unloading, it can be noted that there are some differences between loading and unloading, especially for low loadings. This behaviour is anyway less pronounced in the normal stress compared to the bending moment and normal force plot. So also in this case it can be noted, then, that in the unloading phase the stresses are higher. This is not true for points around θ=90° where the values are inverted.

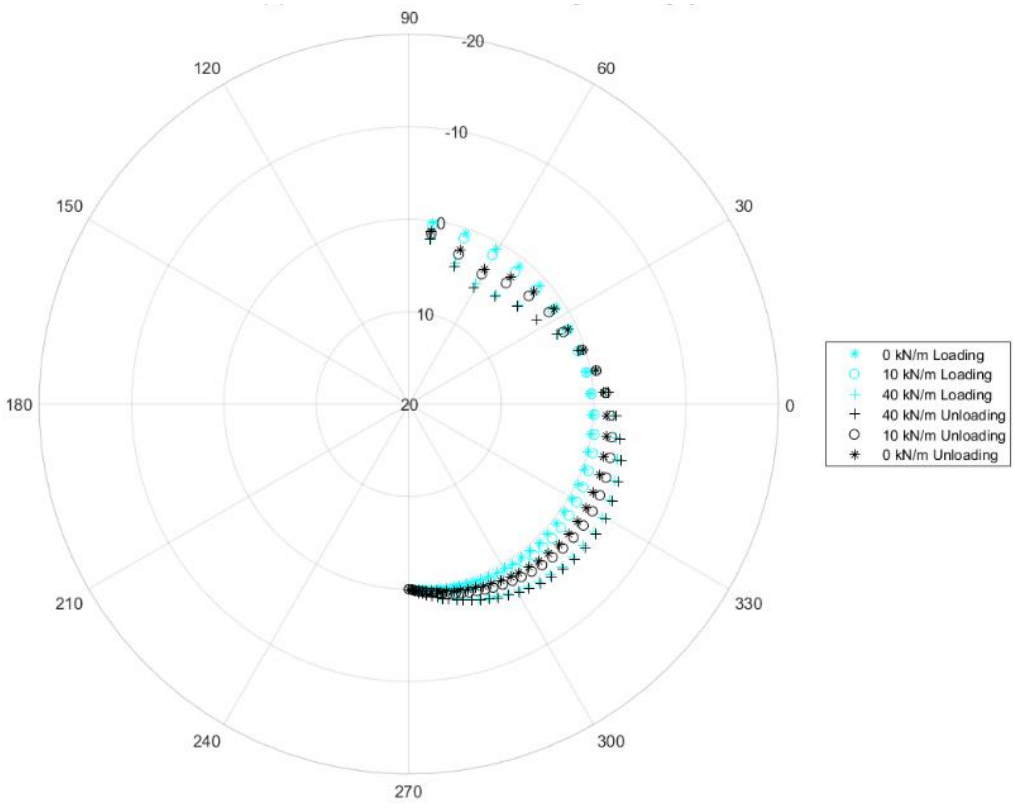

Figure 6.12: Shear stress [kPa] at interface soil/pipe under loading-unloading cycle in loose sand

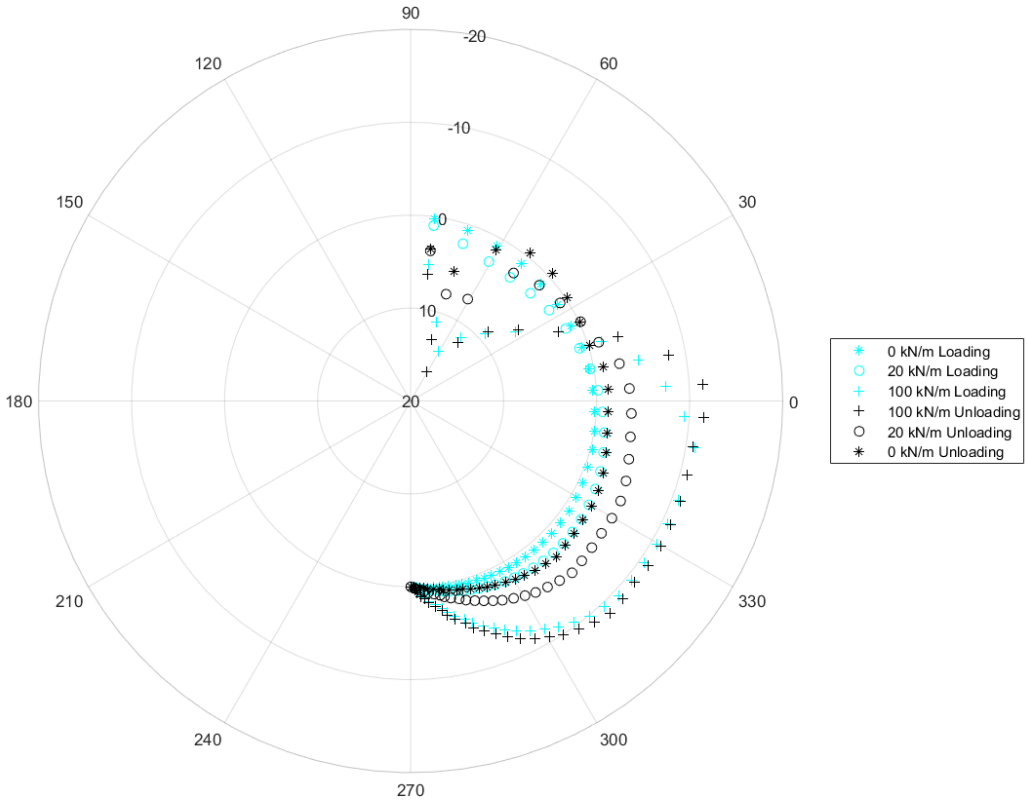

Figure 6.13: Shear stress [kPa] at interface soil/pipe under loading-unloading cycle in dense sand

6.4. Evolution of the stresses near the pipe

In this section, the evolution of the ratio between horizontal effective stress σ'_h and vertical effective stress σ'_v is presented.

Three interesting point are analysed -90°, 0° and 90° according to the convention expressed in figure 5.1.

In the following table 6.2, the loading-unloading path is reported according to the phase, in order to make Figure 6.14, 6.15 and 6.16 where the ratio is plotted with the phases.

Table 6.2: Complete loading-unloading path

Loose sand		Dense sand	
Initial phase	Phase 0	Initial phase	Phase 0

Loose sand		Dense sand	
Put in place 1	Phase 1	Put in place 1	Phase 1
Put in place 2	Phase 2	Put in place 2	Phase 2
Put in place 3	Phase 3	Put in place 3	Phase 3
10 kN/m	Phase 4	20 kN/m	Phase 4
20 kN/m	Phase 5	40 kN/m	Phase 5
25 kN/m	Phase 6	50 kN/m	Phase 6
40 kN/m	Phase 7	60 kN/m	Phase 7
45 kN/m	Phase 8	80 kN/m	Phase 8
U 40 kN/m	Phase 9	100 kN/m	Phase 9
U25 kN/m	Phase 10	120 kN/m	Phase 10
U 20 kN/m	Phase 11	130 kN/m	Phase 11
U 10 kN/m	Phase 12	U 120 kN/m	Phase 12
U 0 kN/m	Phase 13	U 100 kN/m	Phase 13
		U 80 kN/m	Phase 14
		U 60 kN/m	Phase 15
		U 40 kN/m	Phase 16
		U 20 kN/m	Phase 17
		U 0 kN/m	Phase 18

The initial value of K0 is set to 0.5 in both models. From the following figure, we can see that in both models, the one with loose and the one with dense sand, the values of σ_h/σ_v remains around this value. This means that the soil is never fully in passive or active state, but neither at rest.

Table 6.3:Ka and Kp values for both sands

	Ka	Kp
Loose sand (φ=34°)	0.2827	3.5371
Dense sand (φ=41°)	0.2077	4.8150

Some variability can be noted in the initial phase where the model is put in place and the soil is only subjected to gravity, but the major changes are in the unloading phases. At point 0° a sudden increase can be noted, instead in the other points (top and bottom of the pipe). The increase starts with the unloading. One hypothesis to try to understand this behaviour could be that some points of the soil, during the loading and unloading cycle, have reached plasticity.

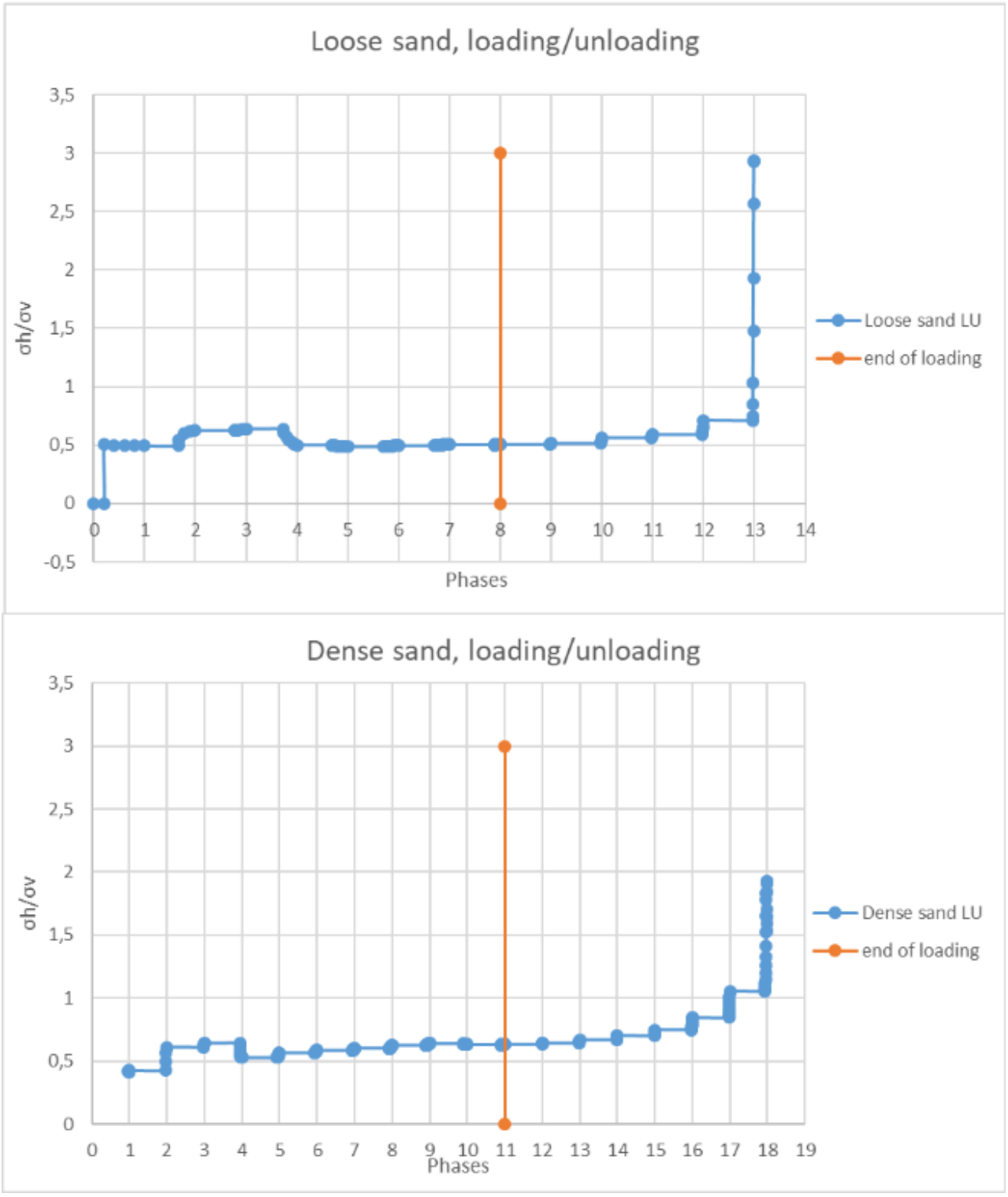

Figure 6.14:Evolution of σ_h/σ_v at point 0°

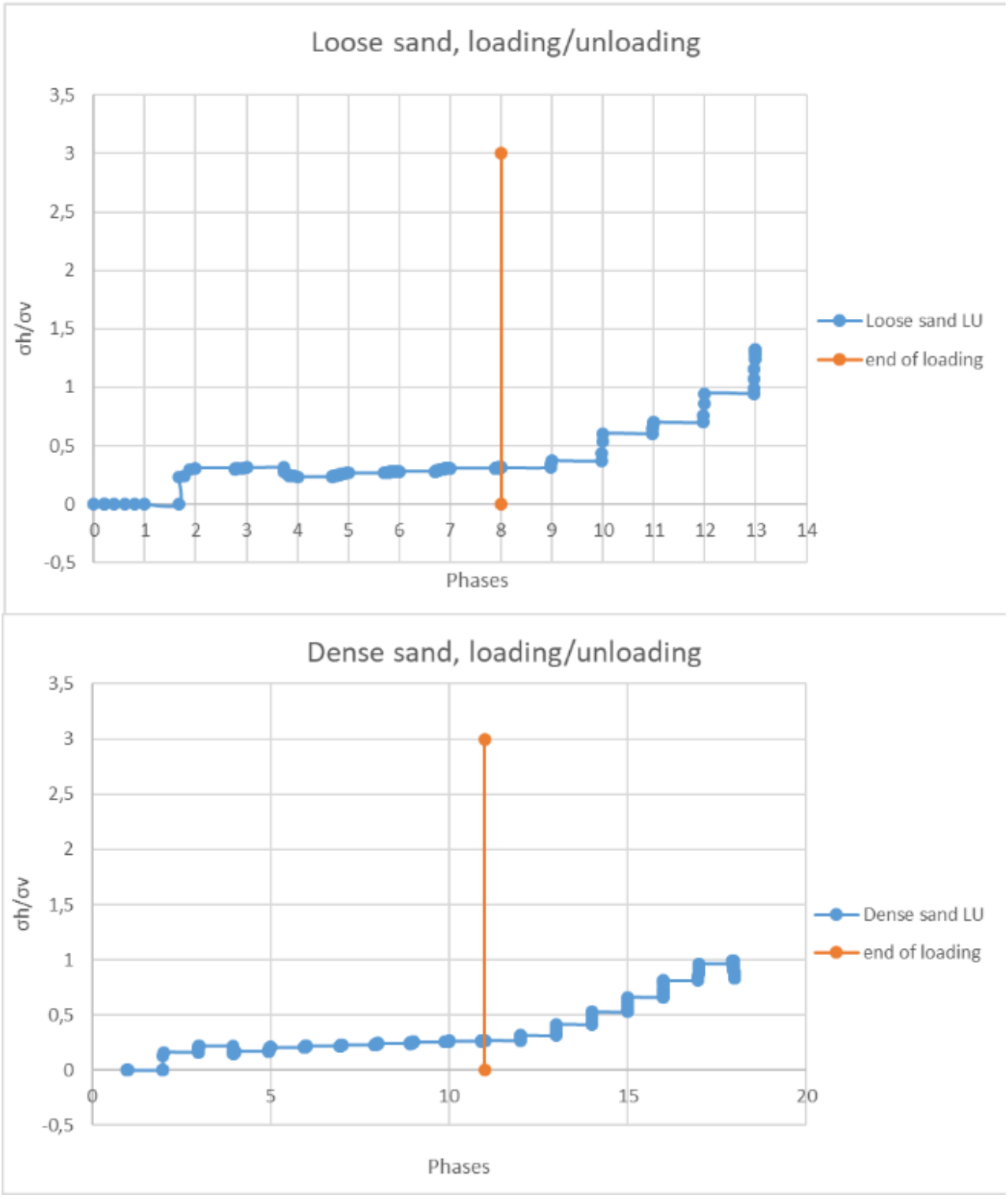

Figure 6.15: Evolution of σh/σv at point 90°

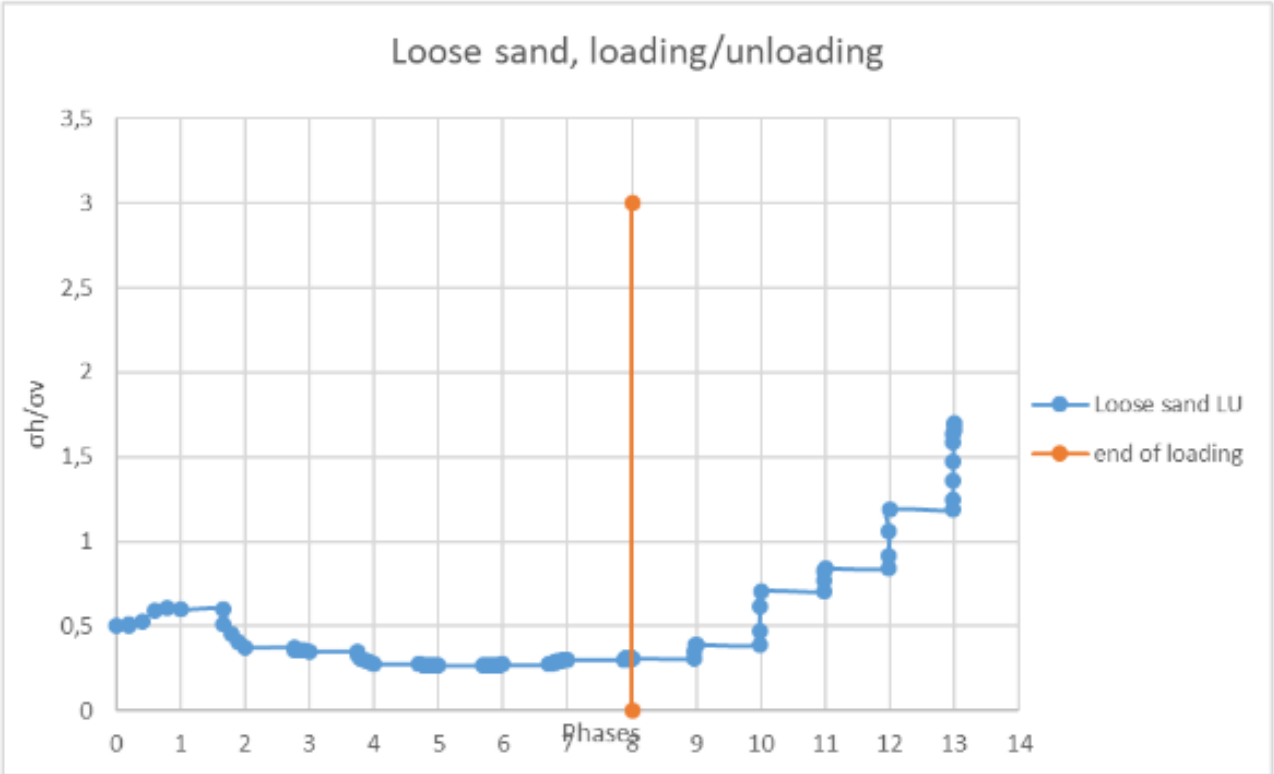

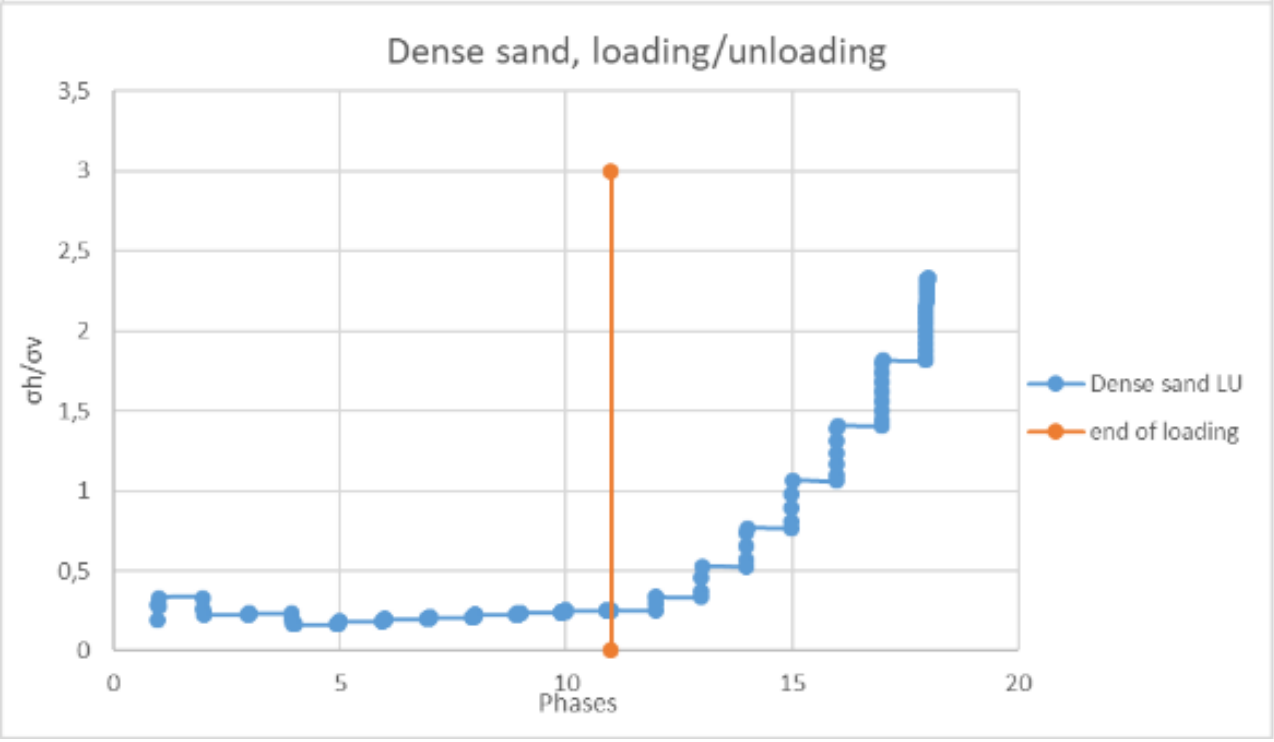

Figure 6.16: Evolution of σ_h/σ_v at point -90°

6.5. Ovalisation of the pipe

As said before, ovalisation is an important metric to be considered for pipes. In Figure 6.17 and 6.18, the resulting ovalisation from the model with loading-unloading cycle is reported.

The oriented ovalisation is again computed as illustrated in paragraph 5.4 and the results are again expressed in percentage.

By first analysing the behaviour with 0 kN/m of loading, we can see that in the unloading phase we still have a higher ovalisation with respect to the one at 0 kN/m in loading path. This result can be also found at 40 kN/m and 100kN/m. In general, in both models, the top and bottom of the pipe are subjected to negative values of ovalisation, instead the part of the pipe between $\theta = \pm 30°$ is subjected to positive values of ovalisation. In this section higher loading phases were considered with respect to the one analysed in the paragraph 5.4, and here it can be noted that higher ovalisation is reached. The maximum values for the model with loose sand is -0,16% at $\theta=90°$, instead in the model with dense sand the maximum value is -0.34% again at $\theta=90°$. Also in this case the ovalisation remains low.

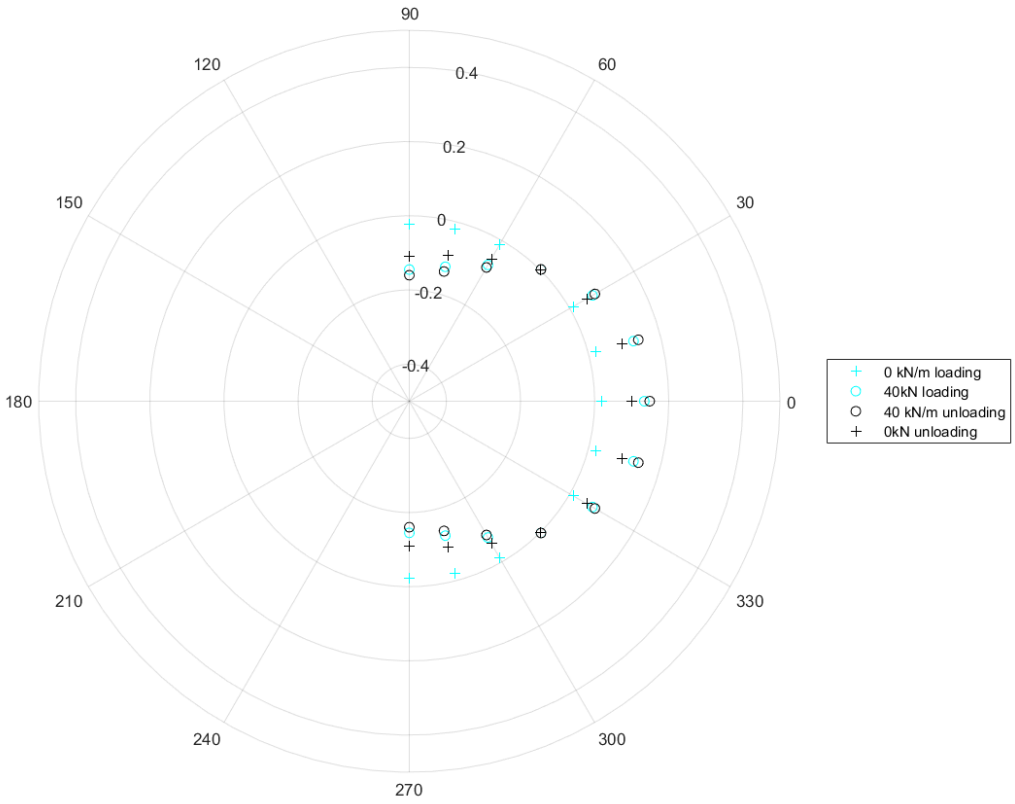

Figure 6.17: Ovalisation (%) in the pipe under loading-unloading cycle in loose sand

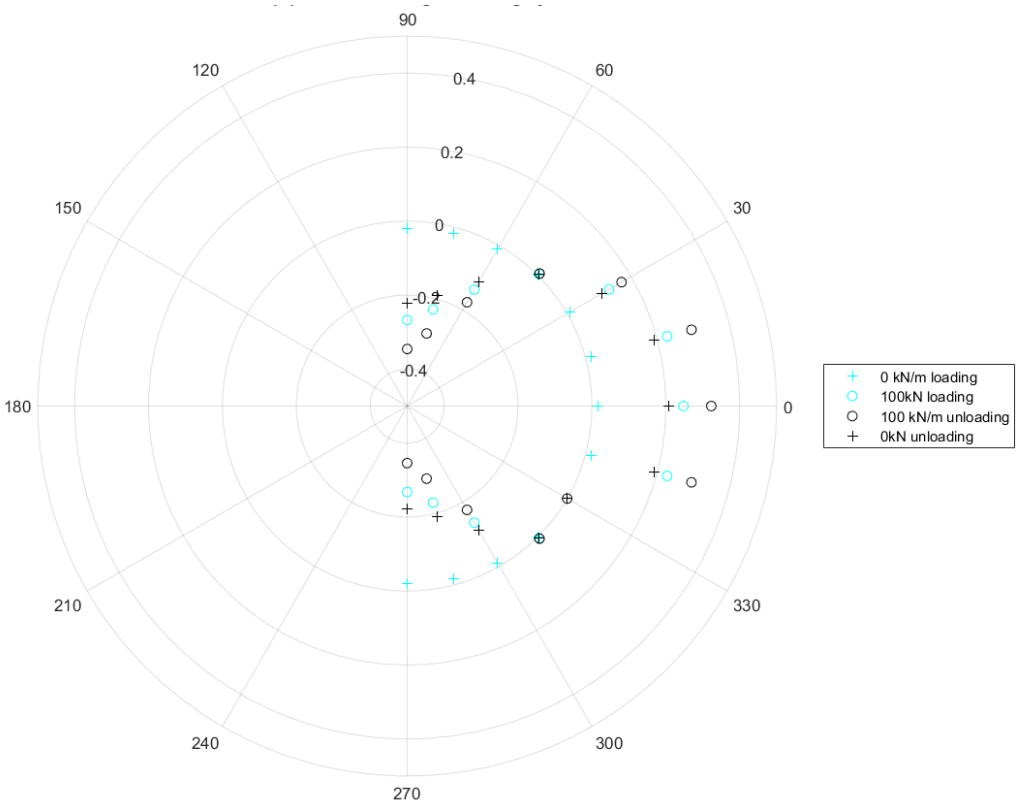

Figure 6.18:Ovalisation (%) in the pipe udder loading-unloading cycle in dense sand

7. Numerical study at model scale with different thicknesses of the pipe

This chapter presents the results obtained by modelling the problem, which is being studied, on a small scale, by changing the thickness of the pipe. It was decided to do this analysis since GRTgaz presents an extensive catalogue of pipes, so it is interesting to investigate the changes in solicitations and actions due to the use of different pipes.

The characteristics of the pipes used in the models are reported previously in tables 4.2 and 4.4, instead the reference catalogue is table 4.1.

The loading steps considered for this analysis are reported in a scheme in figure 7.1

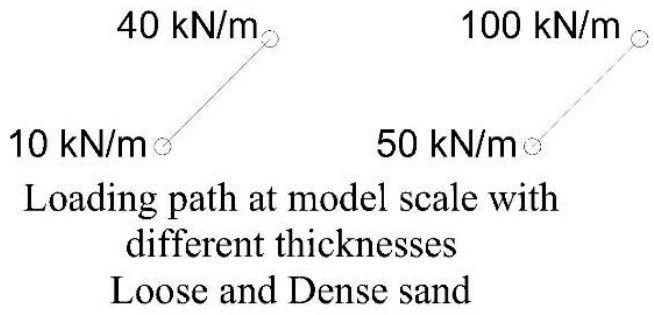

Figure 7.1: Loading path extracted for the case of different thicknesses

As in the previous chapter, the results presented in this section are just at model scale, for this reason they are "raw" data. The normalization was not necessary because no comparison with results from other scale was done.

Again, the same convention on angles (Figure 5.1) and sign (continuum mechanics) was adopted.

For this section all the plots have the same colours: BLACK results from pipe with thickness 2mm, MAGENTA for results from pipe with thickness 1.33mm and GREEN results from pipe with thickness 1mm.

To have a more facilitated reading the same marker (*, o) between related loading phase has been used. (for example, 10 kN/m model with 1st thickness, 10 kN/m model with 2nd thickness and 10 kN/m model with 3rd thickness, etc…)

7.1. Bearing capacity

During the modelling of the problem with the three different thicknesses it was noted that this parameter influences the bearing capacity. The maximum load reached in each model are summarized in the table 7.1.

Table 7.1: Bearing capacity with different pipes

	MAX load (loose sand)	MAX load (dense sand)
Model with pipe 2mm thickness	45 kN/m	130 kN/m
Model with pipe 1.33mm thickness	40 kN/m	125 kN/m
Model with pipe 1mm thickness	40 kN/m	110 kN/m

This is an interesting result because it means that the pipe contributes to the bearing capacity of the soil, in fact in the case of thicker pipe the bearing capacity is higher, in both sands.

7.2. Solicitation and stresses on the pipe

The solicitation analysed in this section are, again, normal force, bending moment and hoop stress.

7.2.1. Normal force

Also in this case no inner pressure was considered, but just the empty pipe subjected to the surface load and the weight of the soil. In Figure 7.2 and 7.3 are plotted the values of normal force in pipes with different thicknesses. The resulting pattern is the same found in the previous analyses, constant for low loads and more variable for higher loads, in all the three types of pipes and in the sands.

What is interesting is that at θ=± 90°, for 40 kN/m in loose sand and 100 kN/m for dense sand, the thinner pipe is subject to a higher solicitation, in this case normal force, but after θ=± 30° this behaviour is inverted, in fact the thicker is subjected to a higher normal force.

At lower loading phases, 10 kN/m in loose sand and 50 kN/m for dense, this behaviour is not really pronounced, and it can be said that the values are almost the same between the different pipes.

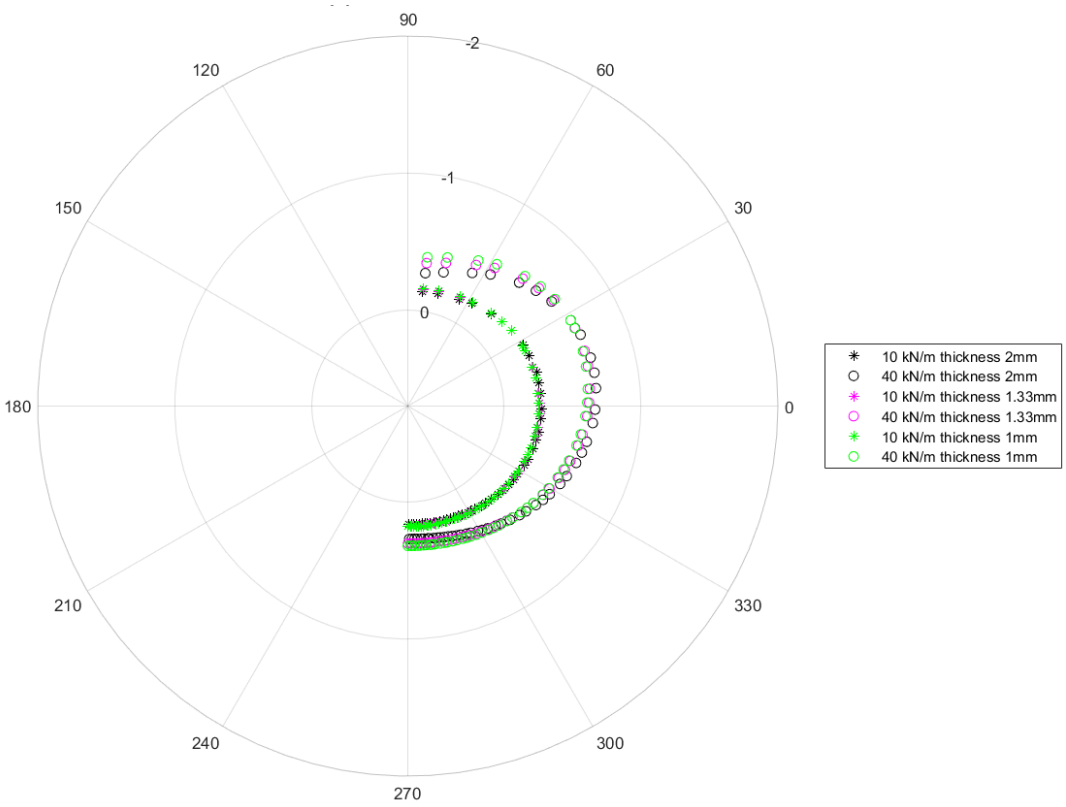

Figure 7.2: Normal force [kN/m] in different pipes in loose sand

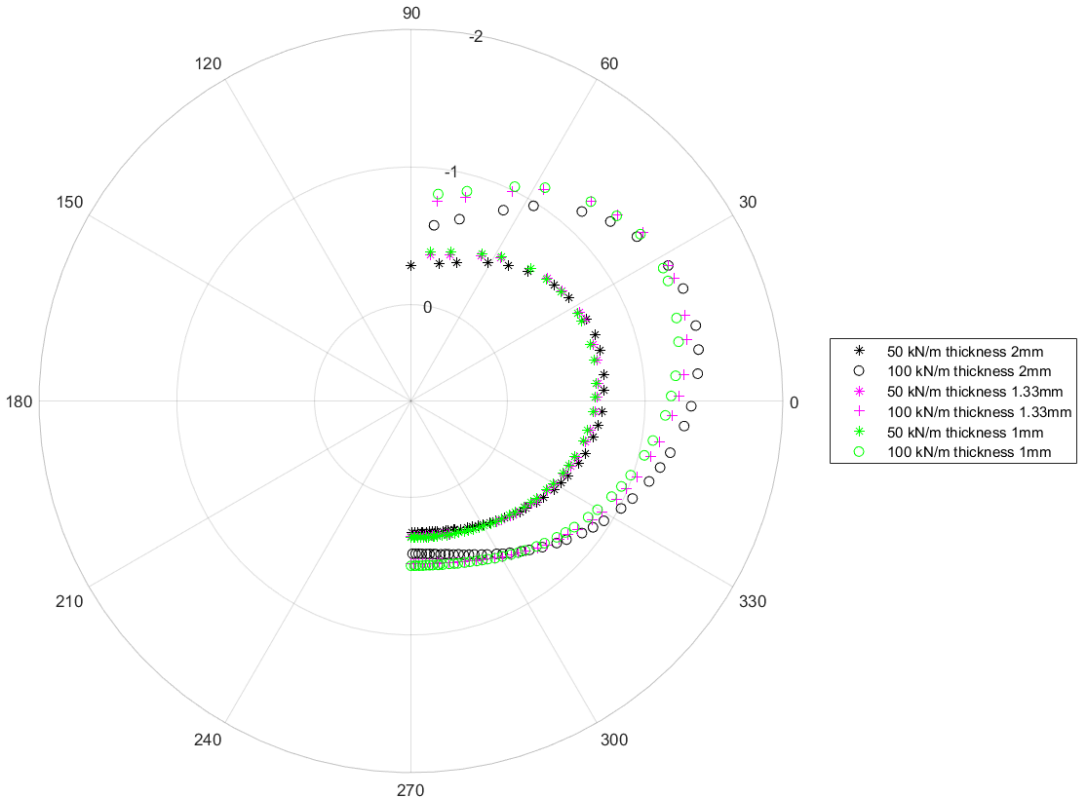

Figure 7.3:Normal force [kN/m] in different pipes in dense sand

7.2.2. Bending moment

The results of the bending moment of the three pipes with different thicknesses are reported in figures 7.4 and 7.5 and the resulting pattern is again the one found in the previous analyses.

Values around 0 kN m/m for the initial loading phases and more variability at 40 kN/m in the loose sand and 100 kN/m for the dense sand. Between $\theta=\pm$ 90° and $\theta=\pm$ 60° the values are positive, after this interval, they change sign and becomes negative for all the loading phases. Again, this behaviour is more evident for higher loading phases. Concerning the comparison between thickness, the thicker pipe is subject to higher solicitation, in absolute value, all around the pipe.

Note the pattern of the solicitation is always almost symmetric between top and bottom of the pipe.

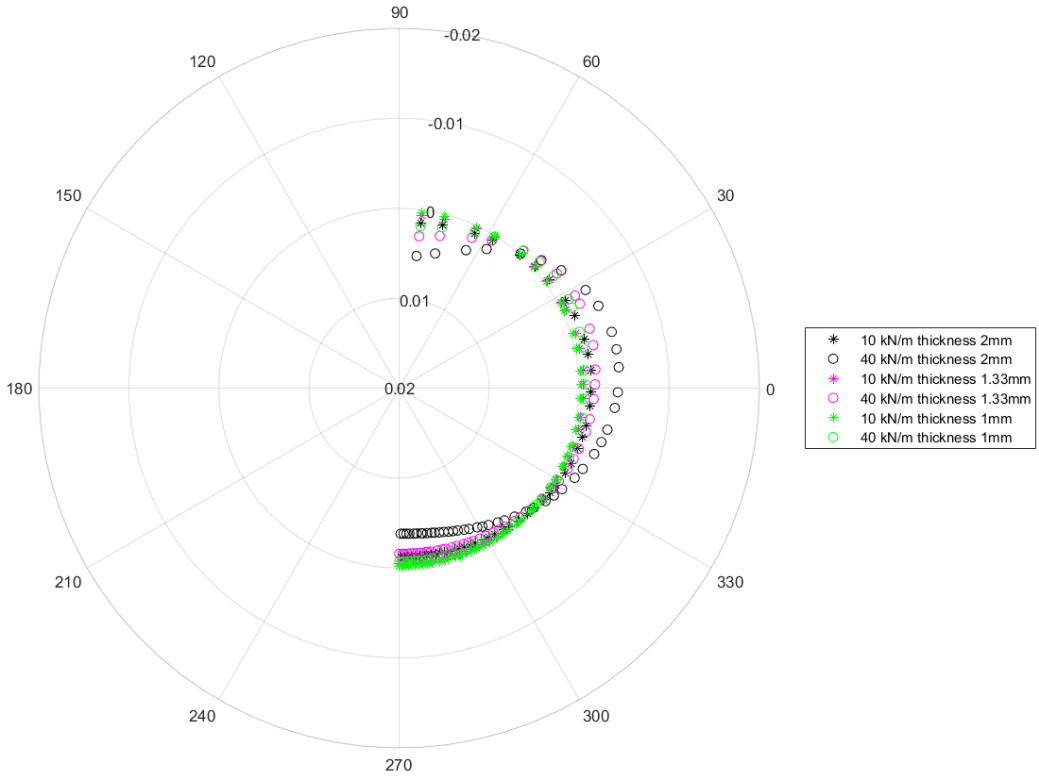

Figure 7.4: Bending moment [kN m/m] in different pipes in loose sand

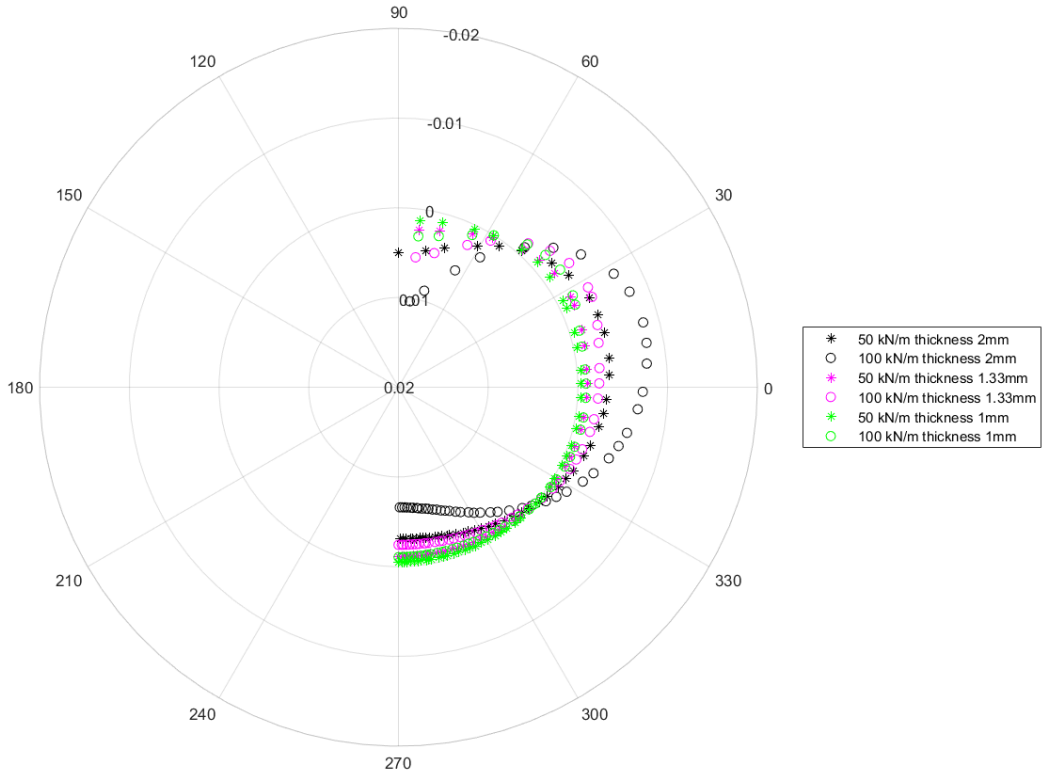

Figure 7.5: Bending moment [kN m/m] in different pipes in dense sand

7.2.3. Hoop stress

In figure 7.5 and 7.6 are reported the results of the hoop stresses in the three pipes with different thicknesses.

The distribution of the stress in the pipe is similar to the one found and analysed in paragraph 5.2.3 but with some differences. These changes can come from the normalization that in this case was not performed since not necessary. It can be observed that the values are always negative but around θ=± 60° the values of the hoop stress tend to 0 kN/m. For bending moment and normal force the response from the different pipes at different angles was more distinct, in fact the same behaviour can be noted between θ=± 90° and θ=± 60° but after these angles the diagrams of the different pipes are inverted several times, so that conclusions cannot be drawn, as done before, on which pipe is most stressed. In this case the stress at top and bottom of the pipe is totally asymmetric.

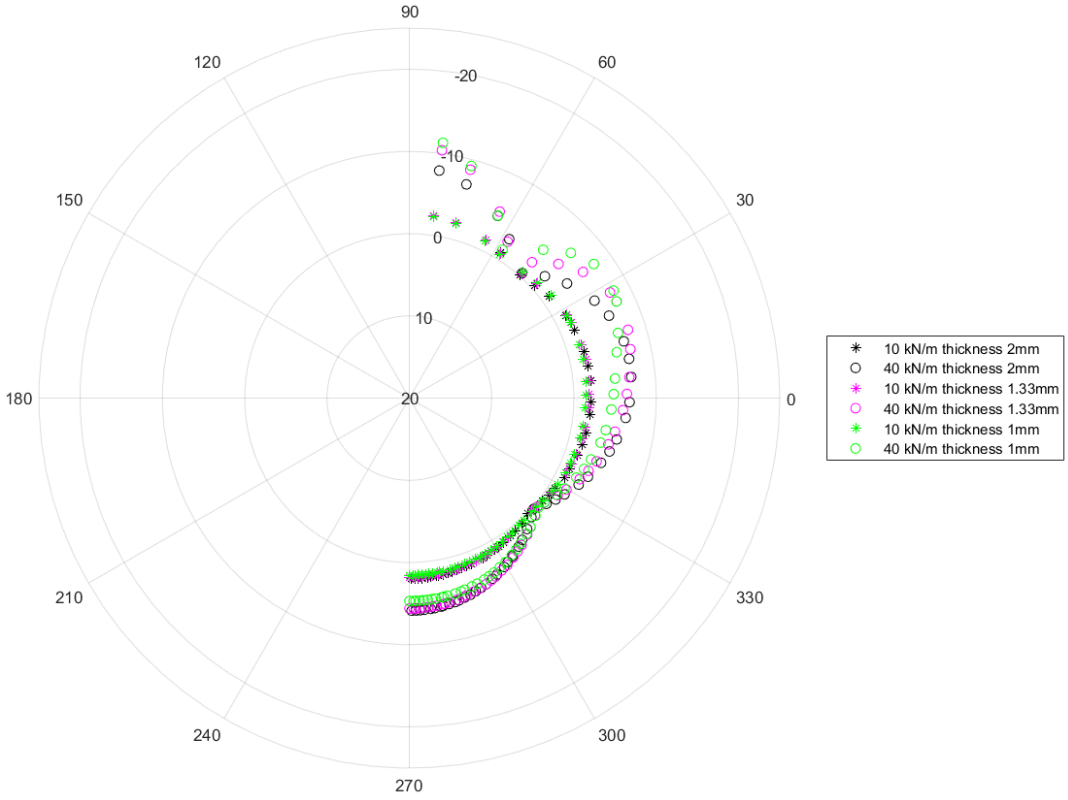

Figure 7.6: Hoop stress [kPa] in different pipes in loose sand

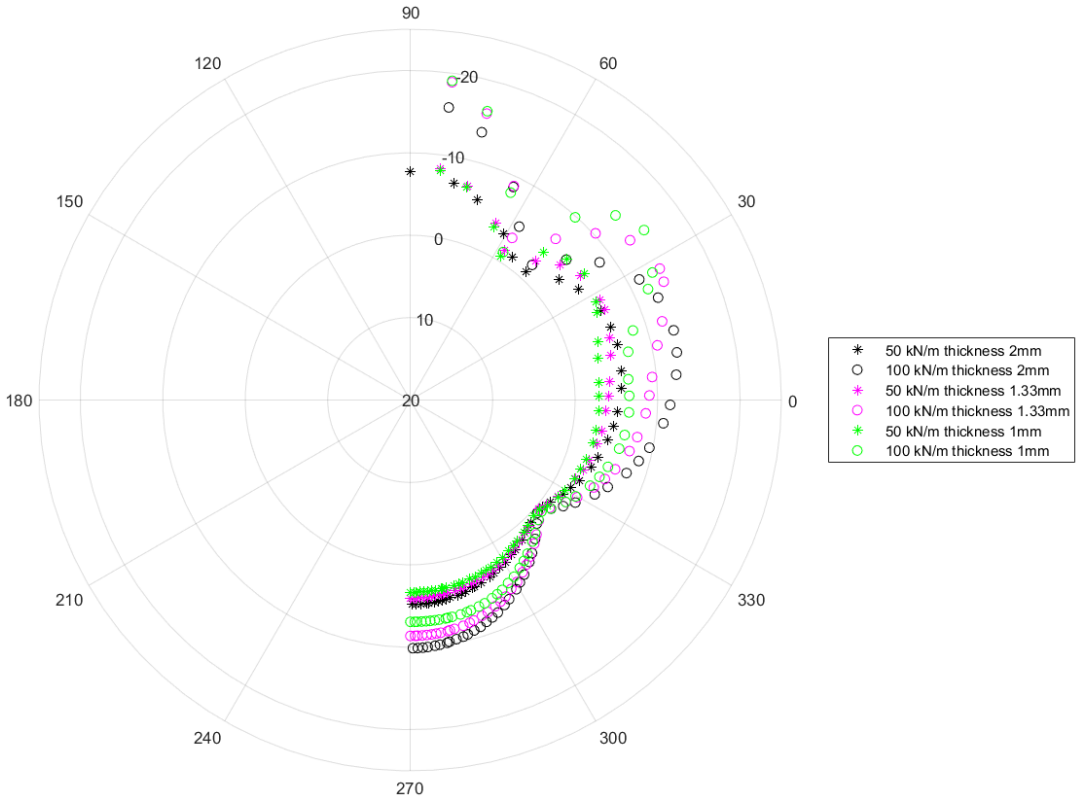

Figure 7.7: Hoop stress [kPa] in different pipes in dense sand

7.3. Actions at the soil/pipe interface

In this section are reported the resulting diagrams for normal stress and shear stress acting at the interface between pipe and soil.

7.3.1. Normal stress at interface

In figure 7.8 and 7.9 is presented the normal stress applied by the soil on the pipe at the different phases of loading of the model with the two sands with three different pipes.

In this case, the values of the stresses are always negative, meaning that the soil is applying compression at every points of the soil. The values aren't applied symmetrically around the pipe with a particular increase between θ=30° and θ=0°. This behaviour is consistent at high loading phases and for all the pipes.

In the loose sand, there is not much difference in the stresses between the different pipes, apart from the interval previously noted were the thinner pipe seems to attract more stress. In the model with dense sand instead, it can be noted that the thicker pipe is the most stressed all around the pipe apart from the interval θ=30°-0° were the thinner one is more stressed.

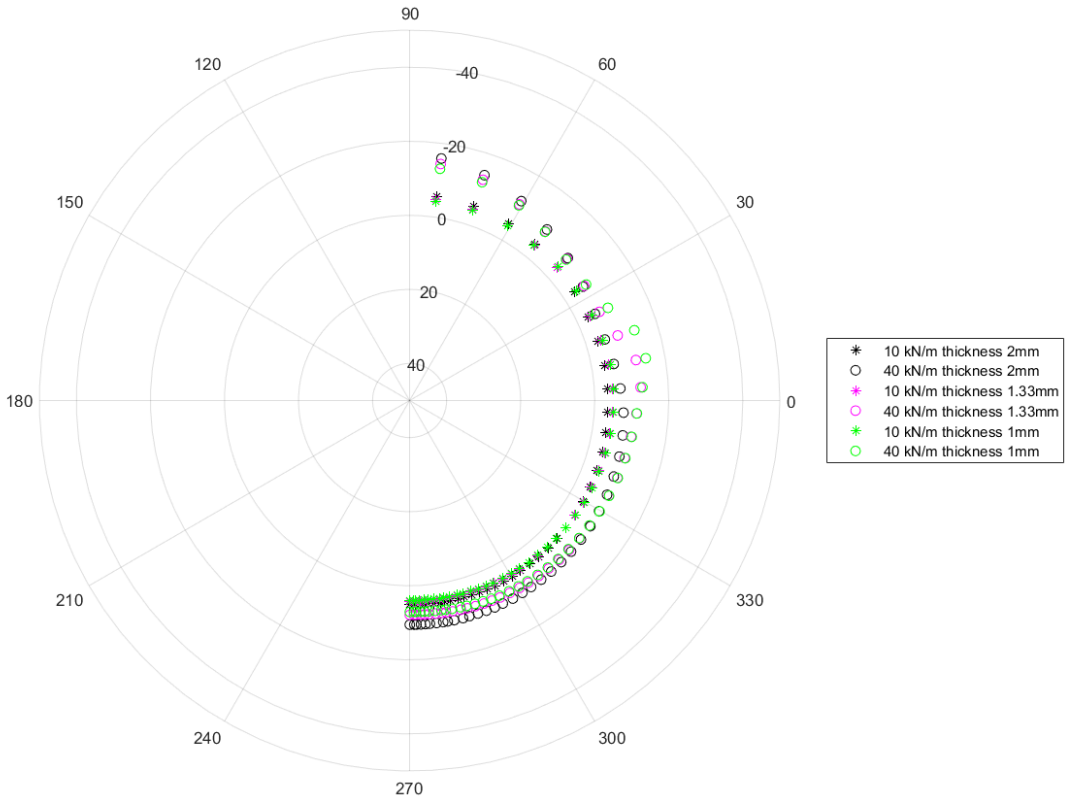

Figure 7.8: Normal stress [kPa] at interface pipe/soil in loose sand

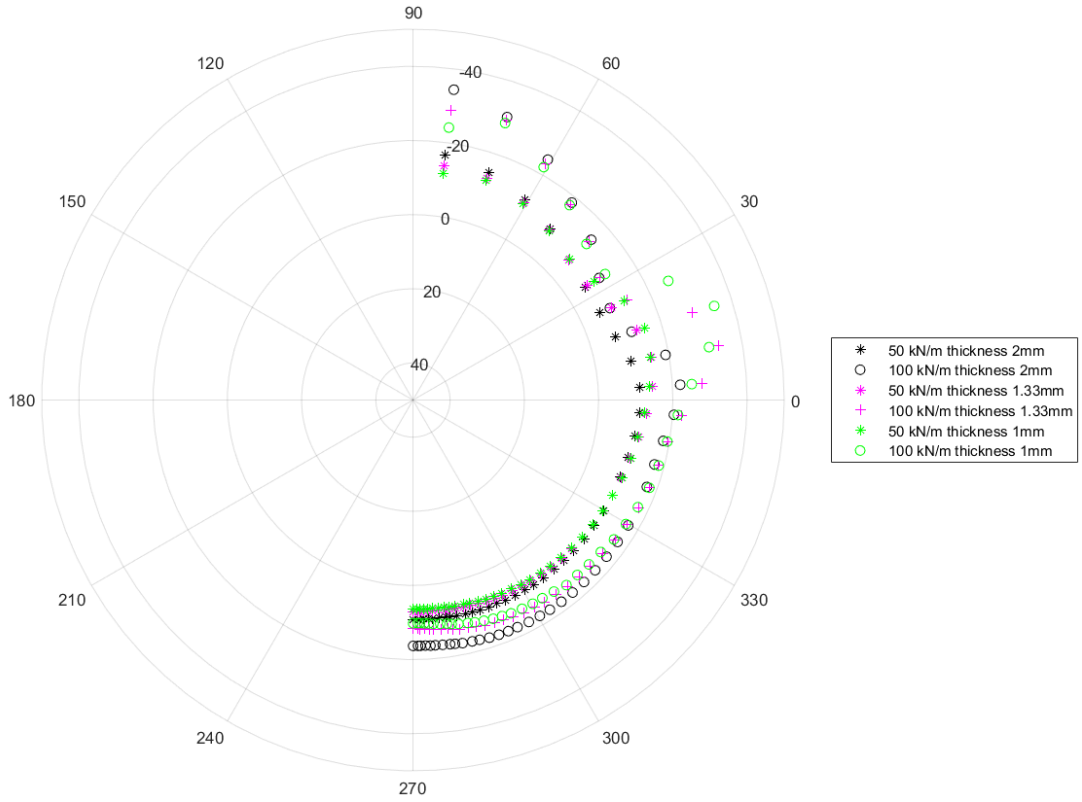

Figure 7.9: Normal stress [kPa] at interface pipe/soil in dense sand

7.3.2. Shear stress at interface

Also the values of shear stress at interface were extracted from the software and in figure 7.10 and 7.11 are plotted the diagrams in polar coordinates. In the loose sand the values are almost constant with small variation for high loading phases, instead in the dense there is some variability. It can be observed that from the top to θ=30° the values are positive and after are negative and again the variability is more evident at loading of 100 kN/m. There is a good agreement between the response obtained from the different pipes so the conclusion that can be draw is that the shear stress at interface is not affected much by the annular stiffness of the pipe.

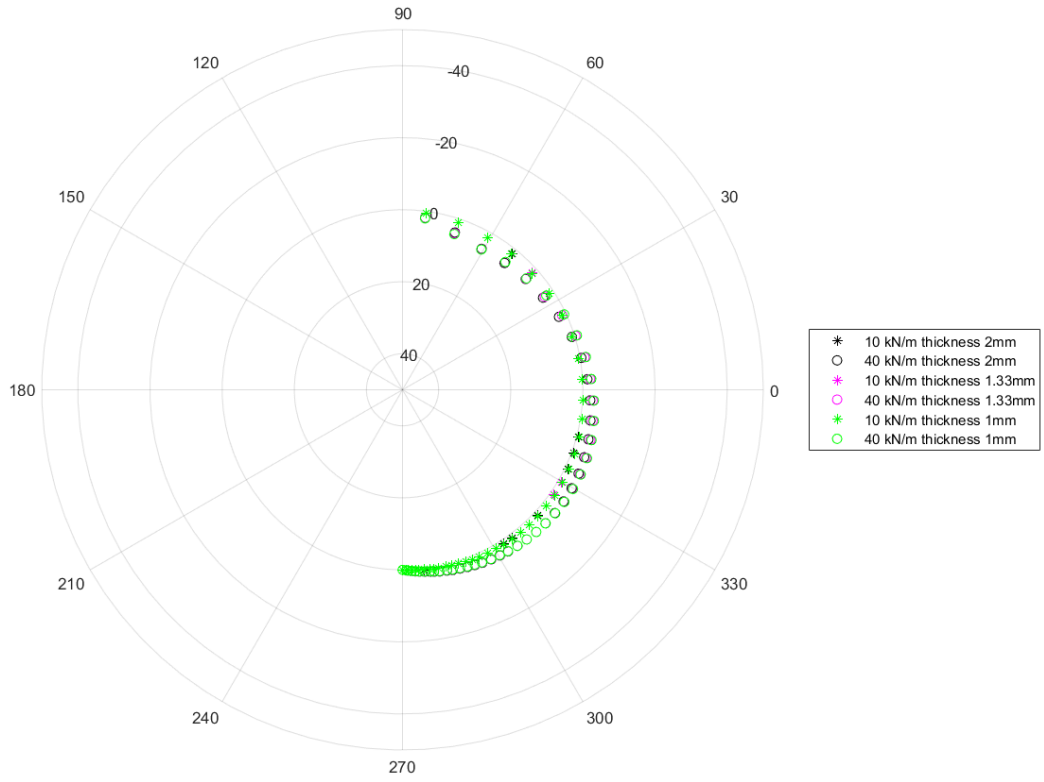

Figure 7.10: Shear stress [kPa] at interface pipe/soil in loose sand

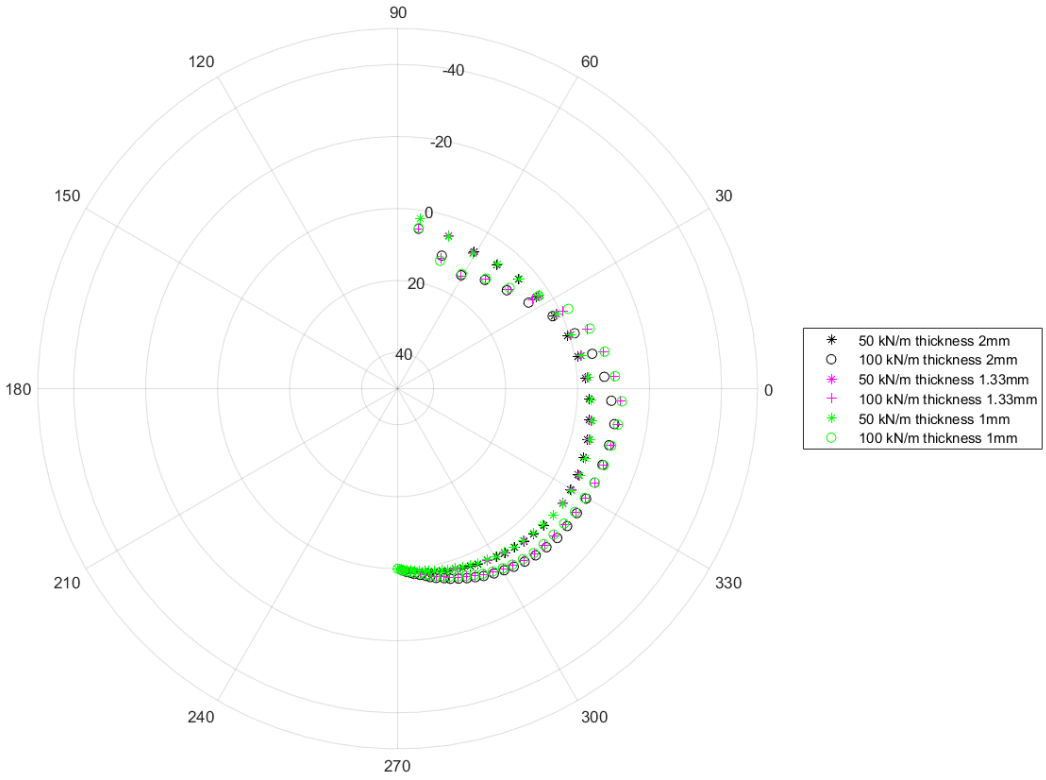

Figure 7.11: Shear stress [kPa] at interface pipe/soil in dense sand

8. Conclusions

The aim of this research project is to create numerical models to study the problem of pipes buried into sand subjected to surface loads. The project has examined several aspects of this problem. First of all, it focused on analysing the effects of scale. Two models were then created, one at the scale of the model, the other at the scale of the prototype. The models were loaded with static loads increasing until failure. Then data on the main solicitations acting on the pipe, actions acting at the soil/pipe interface and other relevant data were extracted. These results were normalized in order to compare them between two scales. One of the main conclusions drawn from these analyses is that there is no perfect similitude between the models due to the soil scale effect. This in fact remains unchanged between the two models and therefore leads to an underestimation of the small-scale results. This underestimation could also be caused by the normalization. For this reason, for the future work, it could be interesting to better understand the effect of the normalization and find a method to normalize the results by also taking into account the ratio between pipe stiffness and soil stiffness. In this way the effect of scale should have less impact.

The second analysis was carried out only on a small scale, since future experiments will be carried out at the model scale. In this case the soil/pipe structure was solicitated with a loading-unloading cycle (under static conditions). The loading and unloading cycle was composed by the same loading steps in both paths (loading and unloading one), in order to have comparable phases in both of them. It was found that the stresses and solicitations are greater in the unloading phase, these results are coming from the non-linear behaviour of sand.

The last analysis was again made only on a small scale. In this case, three different tubes were modelled, by varying the tube wall thickness. It has been noted that this parameter affects the response of the tube but also influences the load-bearing capacity of the soil/tube model.

Concerning the future of this project, the main objective is the experimental campaign, in order to better understand and calibrate the numerical models. Instead for the numerical part of the work many other simulations could be done in the future. For example, create a model where both sands (dense and loose) are present. This would in fact better reflect the VisuCuve situation, where around the pipe the sand does not maintain the same density due to the installation of the latter. Another possibility that could be explored is to include in the models the road, to check the influence of this structural element on the diffusion of the loads in the soil and on the pipe.

References

Adams, D. (1989). *Polyethylene pipe under high fill*. In Transportation research record (p. 89-95). National research council, Washington DC.

Andria-Ntoanina, I., Canou, J., & Dupla, J.-C. (2010). *Caractérisation mécanique du sable de Fontainebleau NE34 à l'appareil triaxial sous cisaillement monotone.* PROJET DE RECHERCHE SOLCYP (ANR + PN)

Atkinson, J., & Sallfors, G. (1991). *Experimental determination of soil properties.* General Report to Session 1. Proc. 10th ECSMFE, Florence, Vol.3.

Bardet, J. (1990). *Lode dependences for isotropic pressure-sensitive elastoplastic materials.* Journal of Applied Mechanics. Vol.57

Benz, T. (2007). *Small-strain stiffness of soil and its numerical consequences.* Institut für Geotechnik der Univertät Stuttgart

Boulon, M. (2018). *Modélisation numérique de l'enfouissement en cuve à sable et du chargement en surface d'une conduite modèle de 50 mm de diamètre.* Internal report, 3SR lab, xx p.

Brinkgreve, R. (2013). Validating geotechnical finite element models. In *Computational Geomechanics.* International centre for computational engineering.

Buckingham, E. (1914). *On physically similar system; Illustrations of the use of dimensional equations.*(p. 345-376) Bureau of Standards

Crabb, G., & Carder, D. (1985). *Loading tests on buried flexible pipes to validate a new design model.* Transport and road research laboratory.

Dano, C. (2019). *Experimentation su tube creux en cuve à sable.* Internal report, 3SR laboratory, xx p.

Dano, C., & Boulon, M. (2018). *Condition de similitude appliquees aux problemes de conduites enterrees.* Internal report, 3SR lab, xx p.

Essentiel GRTgaz. (2020). Chiffres clés: Périmètre GRTgaz France.

European Commission. (2015). *Safety of buried steel pipelines under ground-induced deformations (GIPIPE).*

Fernando, N., & Carter, J. (1998). *Elastic analysis of buried pipes under surface patch loadings.* J.Geotech.Geoenviron.Eng.

GRTgaz. (s.d.). Tratto da http://www.grtgaz.com/.

Hejazi, Y., Dias, D., & Kastner, R. (2008). *Impact of constitutive models on the numerical analysis of underground constructions.* Acta Geotechnica.

Hoeg, K. (1968). Pressure distribution on underground structural cylinders. In *Tecnical report AFWL-TR-65-98.* Research and technology division, Kirkland air force base.

Lancellotta, R. (2008). *Geotechnical Engineering.* Taylor & Francis.

Liu, J., Tian, X.-y., & Gao, X.-m. (2017). *Study on calculation model of culvert soil pressure.* IOP Conference Series: Materials Science and Engineering

Marston, A. (1930). The theory of external loads on closed condiuts in the light of latest experiments. Iowa State College Bulletin 96.

Marston, A., & Anderson, A. (1931). The theory of loads on pipes in ditches, and tests of cement and clay drain tile and sewer pipe. Iowa State College Bulletin 31.

Moore, I. (1987). *The elastic stability of shallow buried tubes*. Géotechnique 37, No.2, p. 151-161.

Moore, I., & Booker, J. (1985). *Behaviour of buried flexible cylinders under the influence of nonuniform hoop compression.* International Journal of Solids and Structures, Volume 21, Issue 9.

Mosandegh, A., & Nikraz, H. (2017). *Buried pipe response subjected to traffic load experimental and numerical investigations.* International Journal of GEOMATE.

PLAXIS. (2019). PLAXIS CONNECT edition V20 (manuals).

Randeniya, C., Robert, D., Li, C.-Q., & Kodikara, J. (2020). *Large-scale experimental evaluation of soil saturation effect on bahavoiur of buried pipes under operational loads.* Canadian Geotechnical Journal.

RICE GRTgaz. (2018). *Imagining solutions for the gas of tomorrow.*

Sargand, S., & Masada, T. (2003). *Soil arching over deeply buried thermoplastic pipe.* Transportation Research Board.

Schanz, T., & Vermeer, P. (1998). *On the stiffness of sands.* Pre-failure deformation behaviour of geomaterials, 383-387

Schanz, T., Vermeer, P., & Bonnier, P. (1999). *The hardening soil model: Formulation and verification.* Beyond 2000 in computational geotechnics - 10 years of PLAXIS

Sheil, B., & McCabe, B. (2016). *Biaxial loading of offshore monopiles: numerical modelling.* International Journal of Geomechanics.

Spangler, M. (1941). The structural design of flexible pipe culverts. Iowa State College.

Terzaghi, K. (1943). *Theoretical soil mechanics*. Chapman and Hall.

Tian, Y., Liu, H., Jiang, X., & Yu, R. (2015). *Analysis of stress and deformation of a positive buried pipe using the improved Spangler model.* Soils and Foundation*s*, 485-492.

Viggiani, G. (2020). *The hardening soil model*. Personal communication

Voronin, E. (2016). *Il mercato di trasporto del gas naturale in Italia.* Università degli studi di Padova.

Watkins, R. (1957). *Characteristics of the modulus of passive resistance of soil.* Iowa State College.

Zhu, B., Jardine, R., & Foray, P. (2009). *The use of miniature soil stress measuring cells in laboratory applications involving stress reversals.* Soils and Foundations.